Phil. Trans. R. Soc. Lond. A **306**, 291–345 (1982) [291]
Printed in Great Britain

MUD DRAPES IN SAND-WAVE DEPOSITS: A PHYSICAL MODEL WITH APPLICATION TO THE FOLKESTONE BEDS (EARLY CRETACEOUS, SOUTHEAST ENGLAND)

By J. R. L. ALLEN, F.R.S.
Department of Geology, The University, Reading RG6 2AB, U.K.

(*Received* 17 *December* 1980 – *Revised* 15 *June* 1981)

[Plates 1–8]

CONTENTS

PAGE

1. Introduction 293

A. A MODEL FOR MUD DRAPES

2. Sand-wave characteristics 294

3. Transport and deposition of sand and mud in tidal environments 295
   (*a*) Sand transport 295
   (*b*) Mud deposition 295
   (*c*) Mud erosion 296

4. Tidal streams and their implications for sand transport and mud-drape deposition 297
   (*a*) Tidal height and stream velocity 297
   (*b*) Rotary tidal streams 297
   (*c*) Reversing tidal streams 298
   (*d*) Effects due to longer-term tidal periodicities 302
   (*e*) Summary of controls on mud drapes under ideal tidal conditions 308

5. Factors distorting or suppressing drape formation 309
   (*a*) Sand-wave shape 309
   (*b*) Flow separation 310
   (*c*) Bedform relative movement 310
   (*d*) Wind waves 311
   (*e*) Some combined currents 312
   (*f*) Feedback arising from mud deposition 313

B. APPLICATION OF THE MODEL TO THE FOLKESTONE BEDS

6. Introduction to the Folkestone Beds 313
   (*a*) Lower Greensand 313
   (*b*) Folkestone Beds and correlatives 315
   (*c*) Facies groups of the Folkestone Beds in the Weald 315

 [Published 27 August 1982

PAGE

7. Cross-bedded sand units with mud drapes: methods of study 318
(*a*) Localities 318
(*b*) Field methods 318
(*c*) Presentation and analysis of results 322

8. Hog's Back Sandpit 323
(*a*) Unit A 323
(*b*) Unit B 324
(*c*) Unit C 326
(*d*) Comparison of units 329

9. West Heath Common Sandpit 329
(*a*) Unit A 329
(*b*) Unit B 329
(*c*) Unit C 330
(*d*) Unit D 331
(*e*) Comparison of units 331

10. Pendean Sandpit 331
(*a*) Unit A 331
(*b*) Unit B 331
(*c*) Unit C 333
(*d*) Unit D (north and south) 335
(*e*) Comparison of units 336

11. Interpretation of cross-bedded units with mud drapes 336
(*a*) Tidal origin 336
(*b*) Nature of tidal régime 337
(*c*) Time-scale of cross-bedded units 339
(*d*) Regional implications 340

12. General conclusions 340

13. References 341

Large-scale cross-bedded units with mud-draped bottomsets and foresets occur in several shallow-marine sand formations attributed to tidal sand waves.

The deposition and preservation of mud drapes on sand waves are favoured by a large sand-wave asymmetry, a high bottom concentration of suspended mud, large time–velocity asymmetry and low strength of tidal currents, and a high eccentricity of the tidal-current ellipse. The deposits formed on a strongly asymmetrical sand wave beneath a strongly asymmetrical current during one semidiurnal or diurnal tidal cycle will be a distinctive couplet composed of (i) a compound mud drape, with an internal silt–sand parting formed by the subordinate tidal stream, overlain by (ii) a group of sandy foresets and bottomsets deposited by the dominant stream. As the tides wax from neaps towards springs, and subsequently wane toward the next neaps, the spacing of drapes between sandy foresets will at first increase and then decline, whence a bundling or clustering of mud layers, and a periodicity in the streamwise arrangement

of drapes and sandy foresets, will appear within the cross-bedding set. Tidal régime and the bed-material erodibility determine the character of these spring–neap depositional cycles, or bundles. The number of sand layers, their accumulated thickness, and their range in thickness within a spring–neap depositional cycle all increase as the tidal currents grow in strength relative to the threshold speed for sand erosion. Non-tidal factors may modify the tidally dependent spring–neap pattern of drapes and foresets, among which wave action seems most important. Mud deposition is suppressed at times of heightened wave-activity, with the result that spring–neap depositional cycles become abbreviated in the number of identifiable sedimentary episodes while acquiring an exaggeratedly large range in drape spacing. Long term changes of tidal régime, such as occur between equinoxes and solstices, should be detectable as gradual changes through a long sequence of spring–neap bundles.

The Folkestone Beds of the western and northeastern Weald include many thick cross-bedded units with mud drapes often visibly bundled. At three western sites, the sands are fine to medium grained, with some coarse-grade and even pebbly material. The drapes there, consisting of fine- to very-fine-grained kaolinitic silt, range in thickness mainly between about 0.002 mm and 0.02 m. The spacing between groups of sandy foresets and bottomsets changes in an orderly way along the cross-bedding sets, varying from as little as about 0.01 m to several metres. With reference to the model, and with the help of time-series and Fourier analysis, the character of the drapes themselves, and the nature of the depositional cycles to which they contribute, it seems likely that the Folkestone Beds were deposited from diurnal tidal currents of spatially changing strength assisted by a strong unidirectional current. The limitation of drapes to western and northeastern areas is consistent with the restriction of the more eccentric tidal currents to nearshore areas, even though the currents seem to have been strongest nearest to shore. The length of the depositional cycles in the Folkestone Beds – proposed to record spring–neap tidal cycles – is consistent with the slightly longer year (in terms of solar days) inferred for early Cretaceous times on various independent grounds.

1. Introduction

Pioneering work by Lüders (1929, 1936) and Van Veen (1935, 1936) has led to the recognition today that sand waves are a common mesoscale bedform in estuaries and shallow tide-swept seas. Although sand-wave deposits are increasingly being claimed from the stratigraphic record (Allen & Narayan 1964; De Raaf & Boersma 1971; Narayan 1971; Pryor & Amaral 1971; Johnson 1975; Anderton 1976; Nio 1976; Button & Vos 1977; Hobday & Tankard 1978; Levell 1980; Allen 1981), the strength of these claims is uncertain, as we know so little for comparison of the internal features of present-day sand waves. Few workers have either trenched or cored active sand waves (Reineck 1963; Houbolt 1968; Klein 1970; Dalrymple *et al.* 1975; Kirby & Oele 1975; Hine 1977; Wunderlich 1978) and in no instance was the full range of sand-wave forms examined. Progress on this empirical front will continue to be slow and uncertain, on account of the severe technical problems associated with sedimentological work in tidal environments.

For some years to come our attempts to identify sand-wave deposits in the stratigraphic record will therefore rest to a marked extent on models of sand-wave internal features, based rather on the form, hydraulics, and inferred or perceived movement of modern forms than on what little is directly known of their internal character. Stride (1965) and Allen (1968) speculated briefly on the nature essentially of formations due to sand waves. Reineck (1963) and Hine (1977), from modern environments, modelled the internal structure of sand waves of near-perfect cross-sectional symmetry. Models for strongly asymmetrical forms are offered by McCave (1971), from work in the North Sea, and by Nio (1976) from an Eocene sandstone. The dangers of circularity in the latter's reasoning are clear. A survey of modern sand waves (Allen 1980*a*)

confirmed Van Veen's (1935) finding that there exists a very wide spectrum of forms, from symmetrical through moderately asymmetrical to strongly asymmetrical, and gave further proof that sand-wave cross-sectional shape depends on the extent to which tidal currents are themselves asymmetrical (or, better, the bedload transports caused), the floood and ebb streams normally differing in both peak speed and duration. The nature of this spectrum of sediment transports and external forms suggested a strictly related and parallel continuum of sand-wave internal bedding (Allen 1980*a*, *b*), within which earlier models (Reineck 1963; McCave 1971; Nio 1976; Hine 1977), after modification, represent specific points.

A distinctive feature of some sand-wave deposits is the presence of mud drapes, recording pauses in bedload movement (Allen & Narayan 1964) such as might occur at slack water after ebb or flood tides (Terwindt 1971*a*), or during neap conditions (Allen & Friend 1976). Such drapes occur in some modern sand waves (Houboult 1968; Wunderlich 1978) and in at least three ancient shallow-marine formations assigned a sand-wave origin (Allen & Narayan 1964; Nio 1976; Allen 1981; Homewood 1981; Homewood & Allen 1981).

Here the mud-drape theme is pursued in detail. I show in part A how the scale (thickness and lateral extent) and spacing (particularly a clustering or bundling) of drapes reflect the character of tidal currents, in particular, the degree of asymmetry and rotariness, and the spring–neap fluctuations of peak strength. Part B of the paper sees the deductions (or model) applied to the Folkestone Beds (Upper Aptian–Lower Albian) in the Lower Greensand (Lower Cretaceous) of southeast England. This sand-dominated shallow-marine formation, locally yielding ammonites and bivalves, was formed near land, to judge the contained driftwood. Much of it consists of well sorted (Humphries 1956) and well rounded quartz sand in cross-bedded units generally 0.5–2.5 m thick, a feature early noted and exploited by Sorby (1858). A distinctive facies is formed by those units in which the foreset and bottomset surfaces support mud drapes (Topley 1875, p. 139; Allen & Narayan 1964) which, in the field, are strikingly clustered streamwise along the sets (Allen 1980*b*, 1981). In these drapes and their bundling we can glimpse some of the quantitative features of early Cretaceous tides in southeast England as well as measure the length of the Cretaceous year.

A. A MODEL FOR MUD DRAPES

2. Sand-wave characteristics

Sand waves are large grouped transverse bedforms found in estuaries (Reineck 1963; Daboll 1969; Ludwick 1970; Ulrich 1972), in restricted tidal seas and gulfs (Gibson 1951; Stride 1963; McCave 1971; Terwindt 1971*b*; Ozasa 1974; So *et al.* 1974; Dalrymple *et al.* 1975, 1978; Bokuniewicz *et al.* 1977; Bouma *et al.* 1978), in straits (Keller & Richards 1967; Boggs 1974), on shallow platforms (Jordon 1962; Drapeau 1970; Hine 1977), and to depths of 165 m on open continental shelves (Cartwright 1959; Hunt *et al.* 1977). The features scale on water depth (unstratified seas) or flow thickness (stratified waters), the height (less than 25 m) being generally a small fraction of thickness or depth, and a very small fraction of the wavelength. Transverse vertical profiles range from symmetrical-trochoidal, with sharp crests and broad troughs, to strongly asymmetrical with one slope very much longer than the other. Dune bedforms an order of magnitude smaller in scale adorn many sand waves (Reineck 1963; Klein 1970; McCave 1971; Terdwindt 1971*b*; Langhorne 1973; Boothroyd & Hubbard 1974; Ludwick & Wells 1974; Dalrymple *et al.* 1975 1978; Kirby & Oele 1975; Bouma *et al.* 1977*a*, *b*, 1978; Hine 1977). Current ripples, sometimes without dunes, have also been seen.

What is the origin of sand waves? Cartwright's (1959) and Furnes's (1974) 'internal wave' hypotheses are hard to apply generally, for most sand waves occur in well mixed waters. McCave's (1971) application to sand waves of Kennedy's (1969) potential flow model of bedforms in one-way flows is appealing qualitatively, but ignores the special features of oscillatory boundary-layer flows wherein may lie an explanation for sand waves in terms of bed instability promoted by stationary recirculating mass-transport currents related to tidal boundary-layer thickness changes (Allen 1980*a*, *c*).

3. Transport and deposition of sand and mud in tidal environments

(*a*) *Sand transport*

In the absence of any generally agreed formula, the spatially averaged rate of sand (bedload) transport by a tidal current traversing sand waves is assumed to be described by

$$J(t) = k(Re, H/h, D)\,[U(t) - U_{ces}(D)]^n, \quad U \geqslant U_{ces}, \tag{1}$$

in which $J(t)$ is the dry mass rate varying with time t, k a dimensional coefficient, $U(t)$ the overall mean speed of the tidal current, U_{ces} the speed at the threshold of sand movement, and $n = 3$ an exponent. The transport coefficient k, in the general order of 1 kg s^2 m^{-4}, varies with the Reynolds number Re, the height H of superimposed bedforms compared with the mean flow depth h, and the bed-material calibre D. The coefficient as quoted is consistent with Colby's (1964) river data, and the experimental results of Guy *et al.* (1966), also adapted to the marine environment by Gadd *et al.* (1978). Equation (1), although entirely kinematic, is equivalent through the quadratic stress law to entrainment and transport formulae based on force or stream power (see for example Bagnold 1941, 1956, 1966). With reference to Bagnold's (1966) threshold curve, and with a Darcy–Weisbach friction coefficient $f = 0.06$ as representative of estuaries and tidal seas (Sternberg 1968, 1972; McCave 1973; Ludwick 1975), $U_{ces} \approx 0.2$ m s^{-1} for medium-grained quartz sands and $U_{ces} \approx 0.4$ for coarse to very coarse sands. The exponent $n = 3$ is representative of flume data and sand-bed rivers at the sediment-transport stages implied by the dunes superimposed on sand waves (Colby 1964; Maddock 1969; Guy *et al.* 1966). Flow unsteadiness (Bowden *et al.* 1959; Gordon 1975; Anwar & Atkins 1980), and delayed responses by superimposed dunes (McCave 1973), may limit equation (1) in a tidal setting.

The speed $U_b(t)$ of a sand wave of height H and triangular profile is then given by

$$U_b(t) = 2J(t)/H\gamma \tag{2}$$

where γ is the sediment dry bulk density (Bagnold 1941). This equation with a realistic $J(t)$ substituted from equation (1), leads to the horizontal separation between mud drapes in sand-wave cross-bedding sets.

(*b*) *Mud deposition*

The extent to which a mud drape forms over a sand wave reflects the degree of mud deposition during slack water(s) and the amount of mud scour before substantial sand transport recommences and leads to burial. The dispersed mud is in the form of highly porous flocs (see for example Zabawa 1978) whose characteristics vary with turbulence (Owen 1971), mud concentration and composition, and salinity. On deposition the flocs cohere, the bed fairly quickly becoming denser and stronger as it ages (Owen 1970). Mud behaviour is therefore less predictable than is sand behaviour.

The general equation (Krone 1962; McCave 1970; Odd & Owen 1972; McCave & Swift 1976) for mud deposition in a tidal current, written kinematically, is

$$R(t) = \sigma C(t)\, W(t)\,[1 - U^2(t)/U_{\mathrm{cdm}}^2], \quad U \leqslant U_{\mathrm{cdm}}, \tag{3}$$

in which $R(t)$ is the mass deposition rate per unit area and time, σ the solids density, $C(t)$ the fractional volume concentration of near-bed mud solids, $W(t)$ their falling velocity, and U_{cdm} the threshold speed for mud deposition.

Mud concentration in tidal waters varies regionally as well as locally, with the seasons, and with time (current speed) and height above the bed. The concentration is normally greatest at the bed, but because of lag effects, may not be a maximum when the tidal current is strongest (Joseph 1954; NEDECO 1961; Delft Hydraulics Laboratory 1962; Schubel 1969; Visser 1970). The concentration peaks during times (autumn and winter in North Sea) of storms and high winds, often exceeding the fair-season value by a factor of two or more (Eisma & Kalf 1979). The general level of dispersed matter declines with decreasing current speed and lateral constraints on tidal streams, and with increasing water depth (Postma 1954, 1961; Van Andel & Postma 1954; Inglis & Allen, 1957; Inglis & Kestner 1958; NEDECO 1961; Delft Hydraulics Laboratory 1962; Allen 1965*a*; Terwindt 1967; Sheldon 1968; Schubel 1969; Allen *et al.* 1974; Gallenne 1974; Migniot 1974; Wells & Coleman 1977, 1978; Eisma & Kalf 1979; Parker *et al.* 1980). Typical near-bed concentrations are: (i) estuaries, 10^{-5}–10^{-3} with local values as high as 10^{-2} or even greater; (ii) open seas near shore, 10^{-5} with local values as great as 10^{-4} or even 10^{-3}; (iii) open seas offshore, generally less than 10^{-5}. The largest values seem to occur in tropical waters and in areas into which large rivers drain.

Empirically, W in equation (3) is a linear to steeply increasing function of C up to $10^{-3} < C < 10^{-2}$ (Delft Hydraulics Laboratory 1962; Migniot 1968; Kendrick 1972). Up to this limit W typically ranges from 0.001 m s^{-1} to 0.01 m s^{-1}, implying that floc size, and therefore falling velocity, are greatly enhanced by increasing mud concentration. Size also depends on mineralogy and salinity and, so Kendrick (1972) finds, on turbulence effects related to tidal phase.

The mud deposition threshold speed U_{cdm} is poorly known, but appears to lie between 0.05 m s^{-1} and 0.11 m s^{-1}, with reference to empirical or empirically based estimates of the equivalent dynamic threshold (a boundary shear stress value) (Krone 1962; Partheniades *et al.* 1969; Kendrick 1972; McCave & Swift 1976; McCave 1978) and $f = 0.06$ in the quadratic stress law.

Concentration appears to be the dominant control on mud deposition. It not only appears explicitly in equation (3) but also strongly influences floc falling-velocity and as well affects the deposition threshold-criterion. Drape formation is therefore greatly favoured by large near-bed concentrations.

(*c*) *Mud erosion*

Since $U_{\mathrm{cdm}} < U_{\mathrm{ces}}$ there could be intervals during the tidal cycle when the stream scours up mud but does not entrain sand. Raudkivi (1976) gave a formula for mud erosion which can be written

$$R(t) = -k[U^2(t)/U_{\mathrm{cem}}^2 - 1], \quad U \geqslant U_{\mathrm{cem}}, \tag{4}$$

in which $R(t)$ is the mass erosion rate per unit area and time, k a new dimensional coefficient, and U_{cem} the threshold speed for erosion. The value of k cannot yet be predicted but must be obtained empirically. The Delft Hydraulics Laboratory's (1962) work indicates that U_{cem} for a mud bed immediately after its deposition in sea water is about 0.1 m s^{-1}, the threshold increasing fairly steeply as the bed subsequently ages. Migniot's (1968) findings agree with this estimate and,

together with the work of Kendrick (1972), Raudkivi & Hutchinson (1974), and Fukuda & Lick (1980), point to a rapid increase in the threshold with bed yield strength (a function of ageing). In view of the similarity between U_{cdm} and U_{ces} for a zero-age mud bed, and the significant strengthening of such beds even after the elapse of so short a period as one hour (Delft Hydraulics Laboratory 1962), I conclude that scour is unlikely to reduce a drape significantly in thickness once deposited. Observations by Reineck & Wunderlich (1967, 1969), Wunderlich (1969), and Terwindt & Breusers (1972) provide confirmatory evidence.

4. Tidal streams and their implications for sand transport and mud-drape deposition

(*a*) *Tidal height and stream velocity*

The real tide is multiperiodic but its most striking fluctuation is that associated with the semidiurnal tide (period approximately 12.5 hours, so two high and two low waters daily) and, in some localities, the diurnal tide (period approximately 25 hours, so one high and one low water daily). If the tide is modelled as a free progressive wave (Doodson & Warburg 1941), the velocity V of the tidal stream at a site is

$$V = cy/(h+y), \tag{5}$$

in which c is the celerity of the tidal wave, y the elevation of the water surface (positive upward) relative to the undisturbed level, and h the undisturbed water depth. When the tidal amplitude cannot be ignored compared with depth, the flood (positive) stream noticeably exceeds in maximum velocity the ebb (negative). However, should $y_{max} \ll h$, a good approximation is $V = cy/h$, the ebb and flood peak speeds then being equal. The above relations require modification for reflected or standing waves and for the tide being forced into a restricted area.

(*b*) *Rotary tidal streams*

The open-water real tide is rotary (see for example Marmer 1926; Göhren 1971; Sager & Sammler 1975), owing to such influences as lack of confinement by land masses, Coriolis force, and superimposed non-tidal currents (thermohaline, wind-driven, meteorological). The rotary tide shown in figure 1*a* has a principal component of the wave-motion advancing in the positive x-direction and at any instant a magnitude (speed) U making an angle α with the positive z-direction. The flow is therefore described by $U = f_1(\alpha)$ and $\alpha = f_2(t)$. As the vector representing the stream rotates, its tip describes the ideally closed tidal ellipse. A practical characterization of this loop is afforded by the *eccentricity* (X_1), *major-axis asymmetry* (X_2), and *minor-axis asymmetry* (X_3), as follows

$$X_1 = \frac{(U_2+U_4)-(U_1+U_3)}{(U_2+U_4)}, \quad X_2 = \frac{(U_2-U_4)}{(U_2+U_4)}, \quad X_3 = \frac{(U_1-U_3)}{(U_1+U_3)}, \tag{6a,b,c}$$

in which U_1 and U_3 are the speeds of the streams respectively in the positive and negative z-directions, and U_2 and U_4 are the corresponding x-direction flows. The eccentricity is zero for a vector tip describing a circle, but unity when the current reverses along a rectilinear path. The asymmetries range between zero and ± 1.

The amount and duration of sand transport and mud deposition depend on the magnitude and shape of the tidal current ellipse in relation to the thresholds U_{ces} and U_{cdm}. If $U(\alpha)$ is at all

times greater than U_{ces}, which in turn exceeds U_{cdm}, sand transport is continuous and no mud drapes arise (see figure 1*b*). But should $U_{ces} > U_1 > U_{cdm}$ and $U_{ces} > U_3 > U_{cdm}$, then sand transport is intermittent, although no drapes form because the speed does not fall below the threshold of mud deposition, though under-reaching the sand threshold (see figure 1*c*). In figure 1*d* we see a second case of intermittent sand transport, but the possible formation of a single drape, as U_1(or U_3) $\leqslant U_{cdm}$ but $U_{ces} > U_3$ (or U_1) $> U_{cdm}$. Sand transport in two episodes with the possible deposition of two drapes occurs when both U_1 and U_3 are smaller then U_{cdm} (see figure 1*e*). The stippled figure-of-eight area represents the sand transports in this case, the actual transports being yielded by integrating equation (1) after the introduction of $U(t) = f_1(f_2(t))$. Hence the practical characterization of the tidal ellipse is completed by evaluating its *strength*

$$X_4 = [\tfrac{1}{2}(U_2 + U_4) - U_{ces}]/\tfrac{1}{2}(U_2 + U_4) \qquad (6d)$$

ranging (in theory) between zero and unity. Reference to equation (1) shows that the total transports on each of the ebb and flood tides increase with the strength, whence by equation (2) the horizontal spacing of mud drapes should reflect the general magnitude and asymmetry of the tidal flow. To conclude, mud drapes can form beneath rotary tidal currents only where the tidal ellipse is relatively eccentric. Drape spacing should increase with tidal asymmetry and strength.

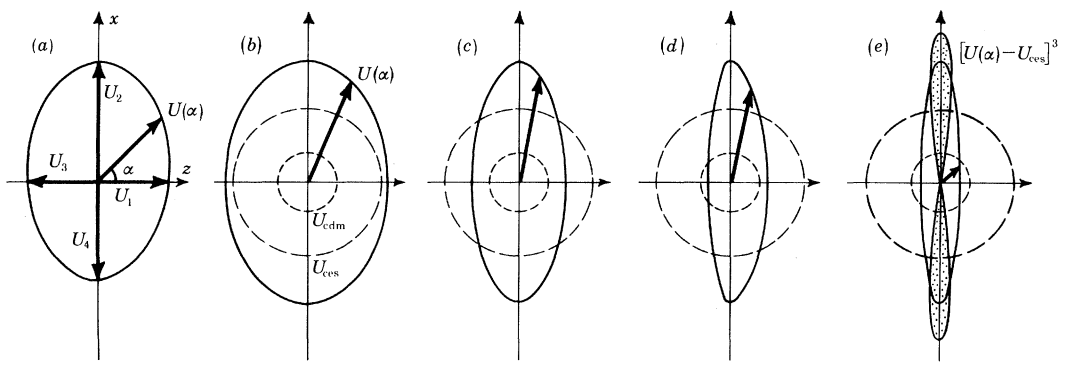

FIGURE 1. Rotary tides and their theoretical implications for sand transport and mud deposition. (*a*) Tidal current ellipse. (*b*) Continuous sand transport but no mud deposition. (*c*) Intermittent sand transport but no mud deposition. (*d*) Intermittent sand transport and mud deposition during one 'slack' water. (*e*) Intermittent sand transport and mud deposition during both 'slack' waters, the total sand transport being related to the stippled area under the curve for $[U(\alpha) - U_{ces}]^3$.

(*c*) *Reversing tidal streams*

The tidal ellipse increases in eccentricity with growing confinement by land masses until, in estuaries, between sand shoals, and close to shore, the streams for practical purposes reverse along a single path. Sand transport (see figure 2) occurs twice, during the flood between t_3 and t_4, and during the following ebb between t_7 and t_8. The percentage of time in each tidal semicycle represented by these episodes appears in figure 3 as a function of the simplified strength $X_4 = (U_{max} - U_{ces})/U_{max}$, in which U_{max} is the peak tidal current speed. Because the sand transport rate increases very steeply with the speed difference, the total semicyclic transport is highly sensitive to current strength, the value normalized by the total transport for a strength of unity decreasing over four orders of magnitude for a change of two orders in strength (U_{max} = constant assumed) (see figure 3).

Mud can be deposited (see figure 2) between t_1 and t_2 after the ebb and again between t_5 and t_6 after the flood. Hence the thickness d_m of the post-ebb drape is

$$d_m = \frac{\sigma}{\gamma}\int_{t_1}^{t_2} C(t)\, W(t)\left(1-\frac{U^2(t)}{U_{cdm}^2}\right)\mathrm{d}t, \quad U \leqslant U_{cdm}, \tag{7}$$

in which γ is the bulk density of the deposited mud (say 1800 kg m^{-3} at 50% (by volume) water content). As the currents shaping sand waves reach peak speeds of 1–2 m s^{-1}, 10–40 times U_{cdm},

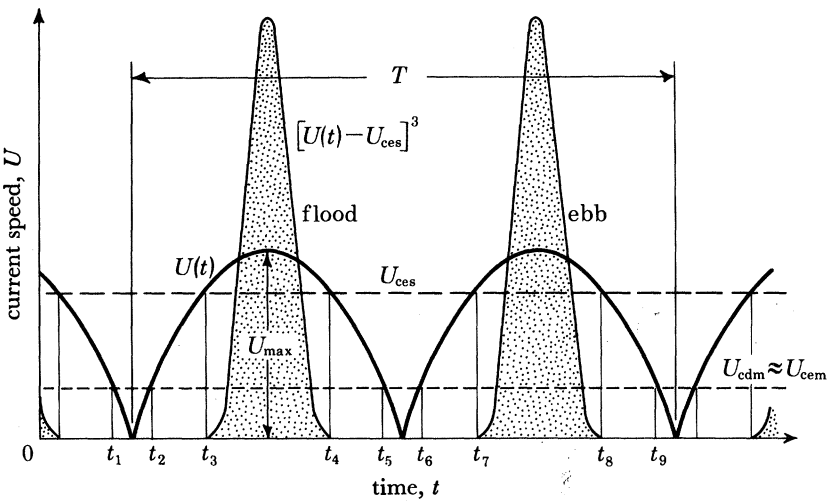

FIGURE 2. Sand transport and mud deposition during one cycle of a symmetrical reversing tide, the total sand transport being proportional to the stippled area under the curve for $[U(t)-U_{ces}]^3$.

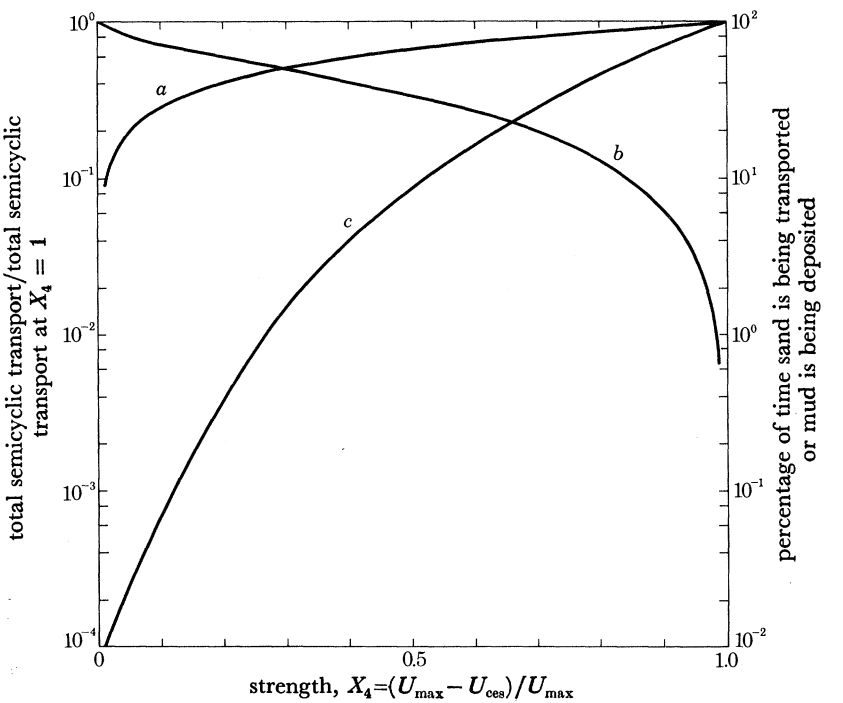

FIGURE 3. Quantitative features of sand transport and mud deposition during one semicycle of a symmetrical reversing tide. *a*, Sand transport; *b*, mud deposition; *c*, transport ratio. In reading the percentage of time during which mud is deposited, U_{cdm} should be substituted for U_{ces} in the strength index.

only a small percentage of the duration of each tidal semicycle is nominally available for mud deposition (see figure 3 with U_{cdm} substituted for U_{ces} in the strength index). For muds behaving quantitatively as described, d_m in the order of 0.02 m is likely at $C \approx 10^{-3}$ but a mere 0.0001–0.001 m at the lower concentration of 10^{-4}. Since most fossil drapes are 0.001–0.01 m thick, they must form either where bottom concentrations are great, or under local circumstances (see below) that heighten or prolong mud deposition.

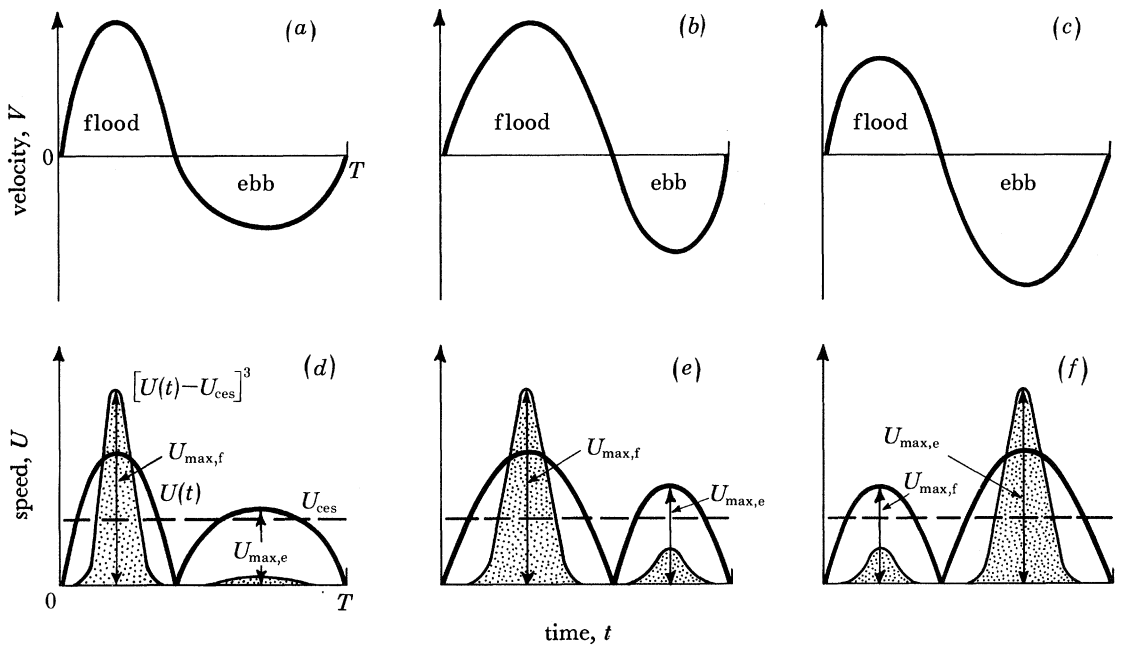

FIGURE 4. Sand transport during one cycle of an asymmetrical tide. (*a*), (*d*) Current velocity and sand transport where asymmetry results from shallow-water effects, there being a zero net flux of water but a finite net sand transport. (*b*), (*e*) Asymmetry with flood dominance, due to the presence of a steady current. (*c*), (*f*) Asymmetry with ebb dominance, due to the presence of a steady current. In (*d*)–(*f*) the total sand transport is proportional to the stippled area under the curve for $[U(t) - U_{ces}]^3$.

The symmetrical flow sketched in figure 2 can only shape stationary symmetrical sand waves. Asymmetrical sand waves and non-zero net bedload transports apparently are related to tidal streams differing between flood and ebb, that is showing a velocity asymmetry (Lüders 1929; Van Veen 1935; Stride 1963; McCave 1971; Allen 1980*a*). Most real tides reveal velocity asymmetry, notably those in confined waters (see for example Keller & Richards 1967; Daboll 1969; Farrell 1970; Ludwick 1970, 1971; Klein & Whalley 1972; Walton & Goodell 1972; Boothroyd & Hubbard 1974; Scott & Csanady 1976; Bokuniewicz *et al.* 1977; Hine 1977; Sternberg & Marsden 1979). In one kind of asymmetry (see figure 4*a*), the flood runs for less than the ebb but is the faster stream, the net fluid flux over the tidal cycle being zero. In the other (see figure 4*b*, *c*) there is a non-zero (residual) water transport, one stream exceeding the other in both speed and duration. Since the bedload transport rate depends on $U(t) - U_{ces}$, and U_{ces} is non-zero, *both* idealized kinds afford a net sediment transport in the direction of the faster stream (see figure 4*d*–*f*), increasing as the difference grows between flood and ebb maxima, respectively $U_{max,f}$ and $U_{max,e}$. Combined kinds of asymmetry are possible in real tides, when the net sediment transport may not be in the direction of the faster current. Kranck (1972) discusses other causes of net sediment transport.

Asymmetry in figure 4*a* reflects tidal-wave distortion in shallow water (Doodson & Warburg 1941), the flood having the shorter duration but greater height. The height and velocity patterns are no longer simple harmonic but can be modelled as the resultant of two simple-harmonic curves, one for the main tide (diurnal or semidiurnal) and the other, with one half its period, for the secondary tide (semidiurnal or quarter-diurnal), varying in amplitude roughly as the square of the amplitude of the main tide. In contrast, asymmetry in figure 4*b*, *c* depends on the combination of a unidirectional flow with the tidal current. Such residual flows record one or a combination of: (i) river currents, (ii) thermohaline currents (see for example Boggs 1974), (iii) wind-drift currents (see for example Keller & Richards 1967), and (iv) mutual evasion of flood and ebb tides in shoal areas (Van Veen 1936, 1950; Robinson 1956, 1960; Granat & Ludwick 1980), possibly an instability phenomenon. Currents of types (i) and, particularly, (iv) mainly affect estuarine tides, whereas open waters experience chiefly kinds (ii) and (iii). Wind-drift, thermohaline, and river currents are in practice unsteady, commonly with a seasonal periodicity.

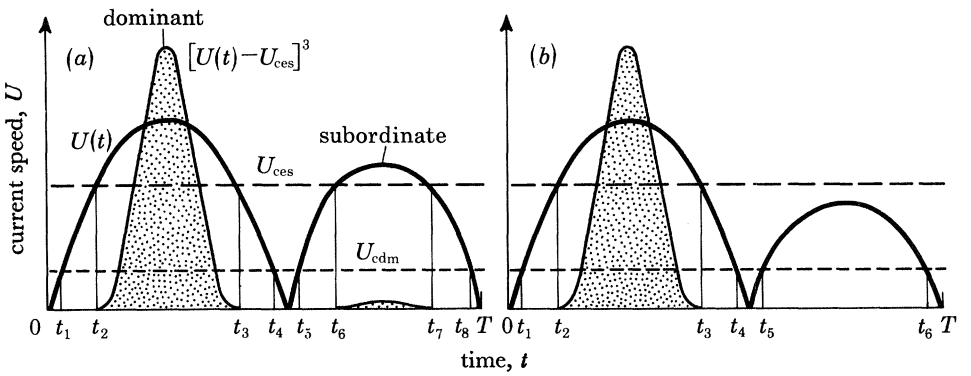

FIGURE 5. Sand transport and mud deposition during one cycle of a strongly asymmetrical tide. Total sand transport is proportional to the stippled area under the curve $[U(t)-U_{ces}]^3$. Note the negligible or non-existent sand transport during the weaker semicycle.

The total sand transports during flood and ebb become increasingly disparate as the currents sketched in figure 4 decline relative to the sand threshold. A particularly important case, apparently represented by sand waves of maximum cross-sectional asymmetry (Allen 1980*a*), occurs when the opposing total sand transports differ very greatly in amount, or when sand movement is limited to the dominant stream (see figure 5). Two long periods of mud deposition are now possible. The subordinate stream in figure 5*a* may cause little more than the rounding of the sand-wave crest, in which case a parting of sand or clean silt may be expected in any mud drape (a compound of two produced during t_5-t_4 and $T-t_8+t_1$) formed in the adjacent trough. Figure 5*b* illustrates even longer episodes of mud deposition, the compound nature of the drape (two episodes, t_5-t_4 and $T-t_6+t_1$) being possibly unrecognizable in the field since there is nominally no ebb sand transport, although silt alone may be deposited when $U \approx U_{max,\,e}$. The lengthening of mud-depositing episodes consequent on tidal asymmetry should promote thicker drapes, but not by more than a factor of perhaps two or three. As a practical proposition in the case of figure 5, the *horizontal streamwise spacing* d_s of the drapes can be regarded as fixed solely by the sand transport achieved beneath the dominant stream, by equations (1) and (2),

$$d_s = \frac{2k}{H\gamma}\int^{\text{dominant}} [U(t)-U_{ces}]^3\,\mathrm{d}t, \quad U \geqslant U_{ces}, \tag{8}$$

the spacing varying directly as the total sand transport and inversely as the sand-wave height. The product $d_s H$, the *sand-wave activity*, is the area swept forward by the sand wave during one tidal cycle; it is proportional to the total transport and a useful index of sand wave mobility.

How are mud drapes distributed within the sand waves representing the extremes of current asymmetry shown in figures 2 and 5? A symmetrical sand wave, adjusted to equal and opposite total semicyclic transports, should shift to and fro about a stable position, either bodily or, more probably, merely in terms of its upper slopes (see figure 6*a*). On account of the current pattern, the potentials for drape deposition and preservation are very low. The thickest drapes with the greatest preservation potential should form on asymmetrical sand waves adjusted to a bedload transport that is effectively one-way (see figure 6*b*). Such bedforms advance in steps of a length for each tide given by equation (8), a mud drape, compound and with a silt–sand parting, marking each pause. Not only are the drape-forming episodes much longer than for symmetrical sand waves, leading to thicker deposits, but also the associated stream never flows fast enough to carry much if any sand. Moreover, the first part of the drape has some hours in which to harden before the second portion is added, and so acquires a relatively high scour resistance.

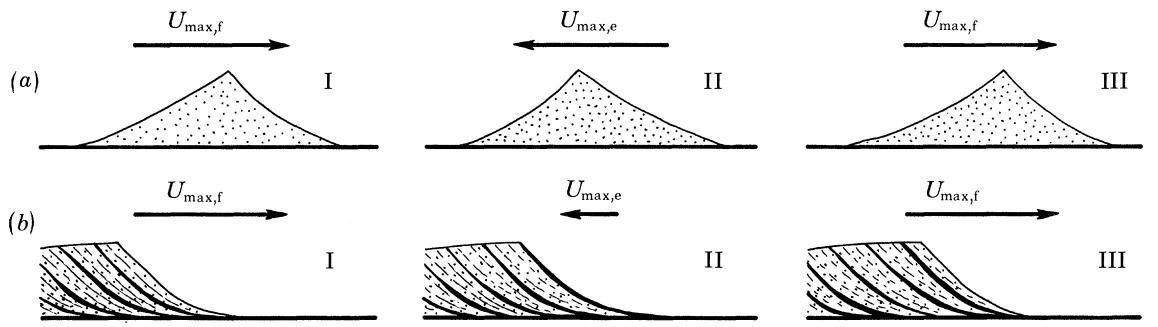

FIGURE 6. Three stages in the history of (*a*) a symmetrical sand wave adjusted to a symmetrical reversing tidal current, and (*b*) a strongly asymmetrical sand wave fashioned by a strongly asymmetrical tidal current. The symmetrical feature 'wavers' backwards and forwards about a stable position (tide-induced aqueous mass-transport neglected), whereas the strongly asymmetrical form advances by the addition of sandy foresets (stippled) during the more vigorous semicycle and a mud drape (black line) deposited in association with a a weaker stream. Peak streams are shown by the arrows (flood assumed dominant in (*b*)).

(*d*) *Effects due to longer-term tidal periodicities*

The spring–neap cycle will introduce patterns into the streamwise spacing of mud drapes in sand-wave deposits (Allen 1980*b*, 1981). Four harmonic constituents largely control the spring–neap tidal pattern (Doodson & Warburg 1941): M_2, the principal lunar semidiurnal constituent (period 12.42 mean solar hours); S_2, the principal solar semidiurnal constituent (period 12 hours); K_1, a lunar diurnal constituent (period 25.83 hours); and O_1, another lunar diurnal constituent (period 23.93 hours). Their relative magnitudes are characterized by the *diurnality* $X_5 = (K_1 + O_1)/(M_2 + S_2)$, in which the symbols now represent the respective amplitudes. The four kinds of pattern thereby recognized by Defant (1958) appear in figure 7. *Semidiurnal tides* ($X_5 < 0.25$) (figure 7*a*) have two high waters and two low waters of approximately the same height daily; for periods there is a noticeable diurnal inequality, successive high or low waters stepping either side of the mean high- or low-water curve. In a *mixed predominantly semidiurnal tide* ($0.25 \leqslant X_5 < 1.50$) (figure 7*b*) two high waters and two low waters appear daily but for periods with markedly different heights. A *mixed predominantly diurnal tide* ($1.50 \leqslant X_5 < 3.00$)

(figure 7*c*) has the high waters of the higher-ranging tides occurring only once a day, with otherwise two high waters and two low waters daily of considerably different heights. *Diurnal tides* ($X_5 \geqslant 3.00$) (figure 7*d*) have one high water and one low water per day, with the possibility of two high waters daily at neaps. Defant's patterns differ mainly by (i) the number of tides, (ii) the relative amplitude of spring and neap tides, and (iii) the degree and distribution of tidal inequalities. Difference (ii) is readily quantified for semidiurnal and mixed predominantly

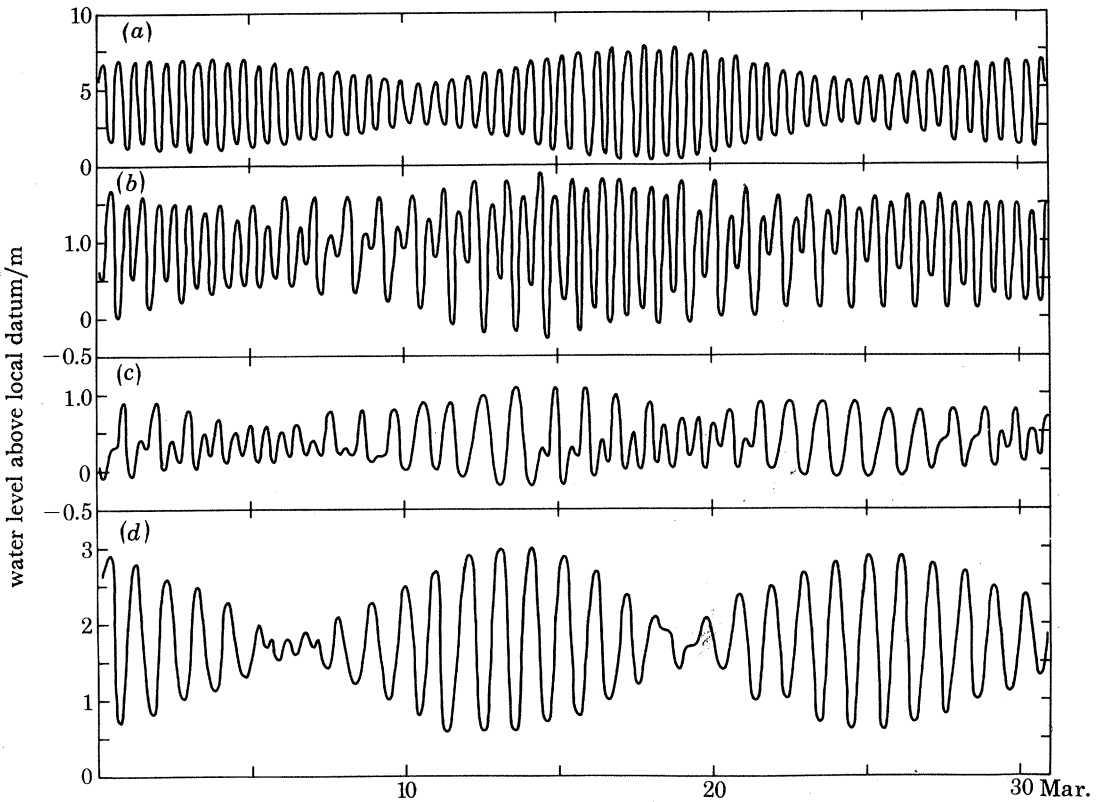

FIGURE 7. Tidal régimes as illustrated by predictions for March 1980 (Hydrographer of the Navy, 1979*a–c*). (*a*) Semidiurnal, Immingham, east coast of England. (*b*) Mixed predominantly semidiurnal, San Francisco, Pacific coast of U.S.A. (*c*) Mixed predominantly diurnal, Manila, Philippine Islands, Pacific Ocean. (*d*) Diurnal, Cua Cam (Hon Dau), Gulf of Tong-King.

semidiurnal tides as $X_6 = (M_2 + S_2)/(M_2 - S_2)$, the ratio of the mean spring to the mean neap tidal amplitudes. Figure 8 shows the present-day distribution and frequency (195 standard ports) of the four tidal patterns, together with the distribution of amplitude ratios (167 standard ports) for semidiurnal and mixed semidiurnal tides (Hydrographer of the Navy 1979*a–c*). Semidiurnal and mixed semidiurnal tides predominate on open coastlines and in many confined waters, but diurnal and mixed diurnal tides typify several restricted subtropical and tropical seas.

What implications for mud-drape distribution have Defant's patterns? To restrict the discussion, consider either pure semidiurnal or pure diurnal tides that are asymmetrical in the manner of figure 5. The current speed therefore varies as in figure 9, on the simplifying assumption that there are exactly 14 diurnal and 28 semidiurnal tidal cycles in each spring–neap cycle. The envelope containing the sand-transporting semicycles is described to a good approximation by

$$U_{\mathrm{env}} = \tfrac{1}{2}(U_{\mathrm{e,\,max}} + U_{\mathrm{e,\,min}}) + \tfrac{1}{2}U_{\mathrm{e,\,max}} - (U_{\mathrm{e,\,min}}) \sin(2\pi t/nT) \qquad (9)$$

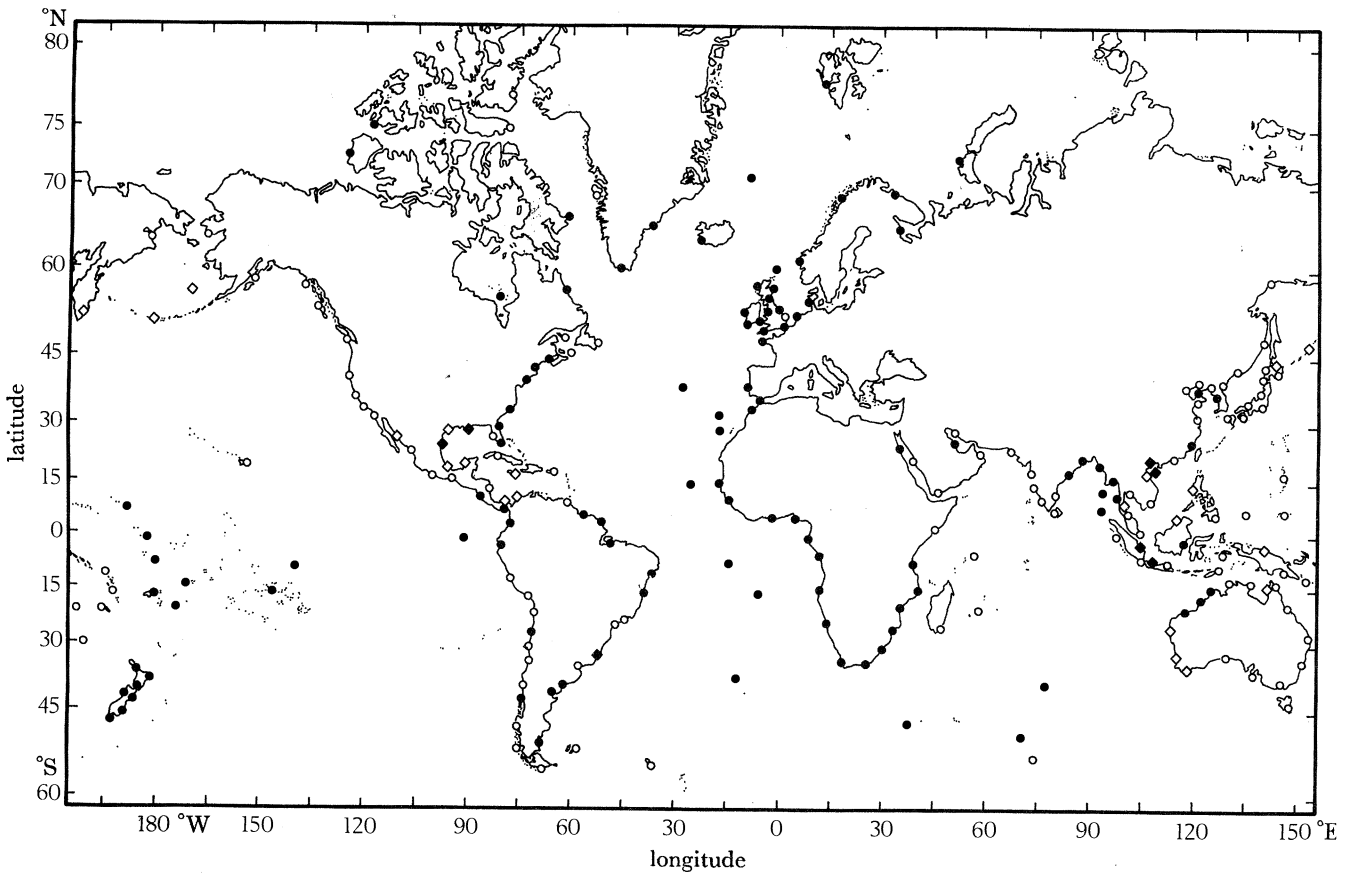

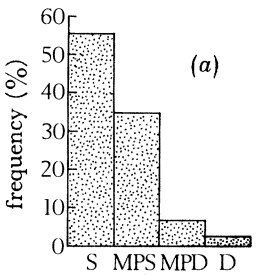

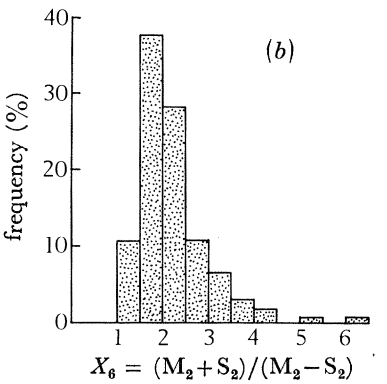

FIGURE 8. World distribution of tidal régimes, based on standard ports and a sampling of secondary ports listed by the Hydrographer of the Navy (1979*a–c*). Key to régimes: ●, semidiurnal; ○, mixed predominantly semidiurnal; ◇, mixed predominantly diurnal; ◆, diurnal. (*a*) Distribution of régimes between 195 standard ports. Key to régimes: S, semidiurnal; MPS, mixed predominantly semidiurnal; MPD, mixed predominantly diurnal; D, diurnal. (*d*) Distribution of the tidal amplitude ratio between 167 standard ports where the régime is either semidurnal or mixed predominantly semidiurnal.

in which $U_{e,\max}$ and $U_{e,\min}$ are respectively the maximum (spring) and minimum (neap) peak speeds during these cycles, T is the tidal period, and $n = 14$ or 28 according as the tide is diurnal or semidiurnal. The spring–neap cycle is characterized by the *neap–tide strength* (X_7) and *spring–neap strength* (X_8), combining into the *spring–neap speed ratio* (X_9):

$$X_7 = \frac{U_{e,\min}}{U_{ces}}, \quad X_8 = \frac{U_{e,\max} - U_{ces}}{U_{e,\max}}, \quad X_9 = \frac{U_{e,\max}}{U_{e,\min}} = X_7(1 - X_8), \qquad (10a, b, c)$$

the last corresponding to the spring–neap speed ratio X_6.

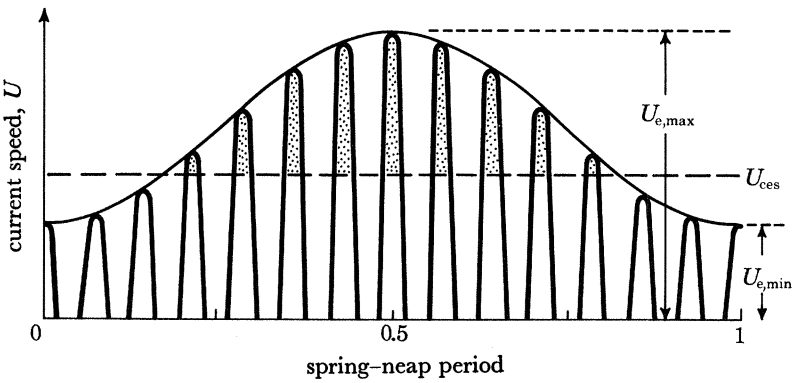

FIGURE 9. Idealized distribution of current speed in the dominant part of a strongly asymmetrical diurnal tidal cycle, over one full spring-neap cycle (exactly 14 tides assumed). The current speeds that give rise to sand transport are shown by the stippled portions of the graph.

The mud drapes and sand layers (groups of sandy foresets) numbering N in total produced during a spring–neap cycle constitute a *bundle* of layers, of which there are two classes. In the absence of disturbing influences, spring–neap tidal patterns occupying the triangular field bounded by $X_7 = 1$ and $X_9 = 1$ in figure 10*a* will create bundles of either 14 mud drapes added to 14 groups of sandy foresets (diurnal tides), or of 28 drapes combined with 28 sand layers (semidiurnal tides), one pair for each tide (i.e. $\frac{1}{2}N$ tides in total). When $X_7 < 1$, however, sand transport is restricted to the stronger tidal cycles, which decline in number as the neap-tide strength falls, whence $N < 28$, 56. No matter what the actual size of a bundle, however, the extent to which the drapes are clustered, that is their range in spacing, may be expressed by the *bundling strength* $X_{10} = d_{s,\max}/d_{s,\min}$ involving the maximum and minimum streamwise separation distances between consecutive drapes. Values for N (see figure 10*b*) and for bundling strength (see figure 10*c*) were calculated by using equations (8) and (9) for (i) a diurnal tide divisible into semicycles of equal duration, and (ii) a simple-harmonic variation of the sand-driving stream. Representative patterns of relative drape spacing $d_s/d_{s,\max}$ as a function of the tidal sequence (semidiurnal tides) appear in figure 11. The envelopes enclosing the bars representing drape sapcing tend to an inverted trochoidal form.

What of tidal patterns neither purely diurnal (see figure 10) nor purely semidiurnal (see figure 11)? A semidiurnal tide like that at Immingham (see figure 7*a*) yields a pattern in which the bars representing drape spacing step either side of the mean envelope (see figure 12*a*, *b*). A more complex pattern results from tides of mixed predominantly semidiurnal type (for example at San Francisco, see figure 7*b*), the bars forming two interdigitating series (see figure 12*c*). Mixed predominantly diurnal and diurnal tides (for example at Manila and Cua Cam, see

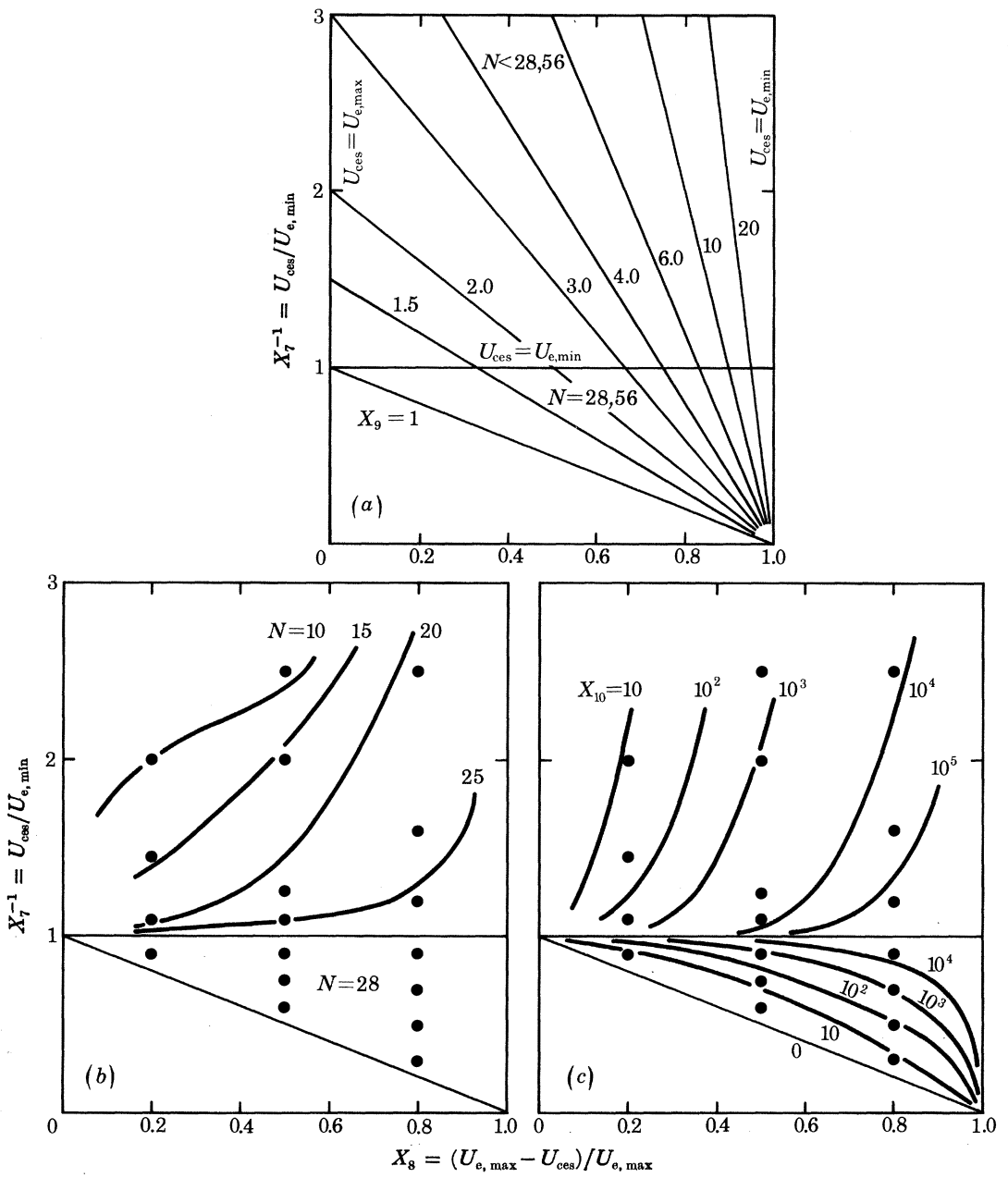

FIGURE 10. Summary of a quantitative model for the interpretation of spring–neap depositional cycles preserved in strongly asymmetrical sand waves adjusted to strongly asymmetrical semidiurnal or diurnal tidal currents. (*a*) The relation between the neap–tide strength (X_7), the spring–neap strength (X_8), and the spring–neap speed ratio (X_9). It is assumed that either exactly 14 diurnal tides or 28 semidiurnal tides occur in each spring–neap tidal cycle. The number of depositional episodes N which can be represented (two per tidal cycle) is dependent on the value of X_7. (*b*) Approximate distribution of values of N on the assumption of a diurnal régime. (*c*) Approximate distribution of values for the bundling strength (X_{10}) on the assumption of a diurnal régime. ●, Calculated points in (*b*) and (*c*).

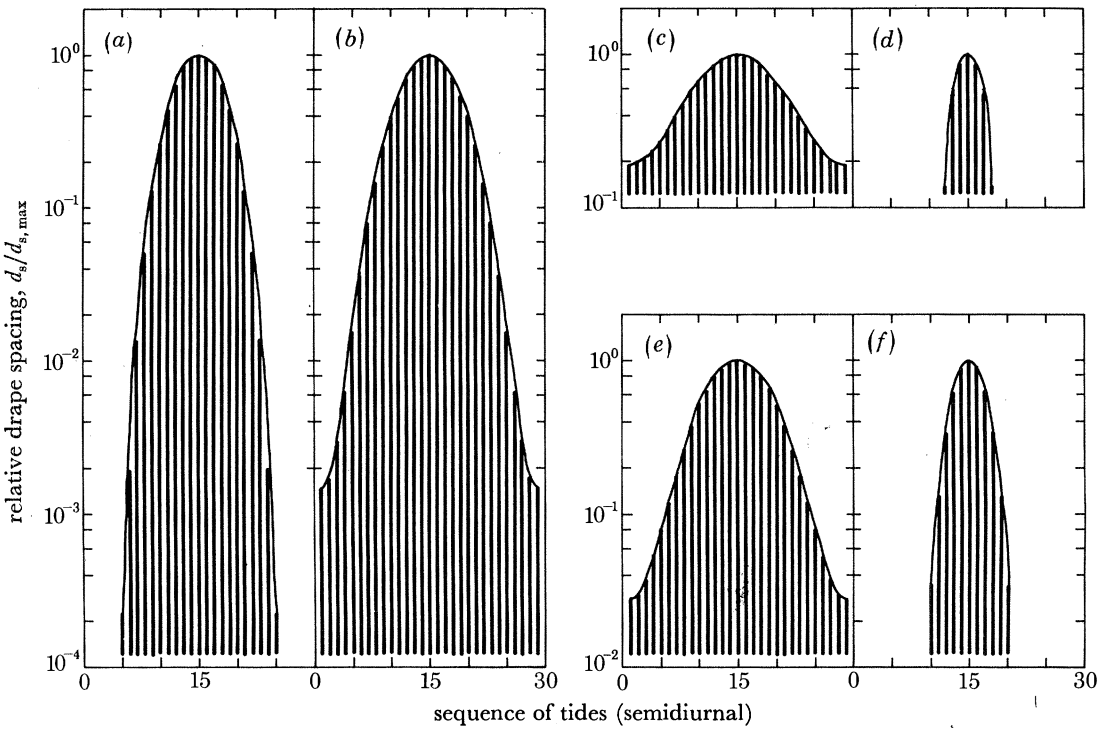

FIGURE 11. Representative temporal patterns of drape spacing in one spring–neap depositional cycle (bundle), as predicted by the model for a semidiurnal régime. (*a*) $X_8 = 0.5$, $X_7^{-1} = 1.25$. (*b*) $X_8 = 0.5$, $X_7^{-1} = 0.9$. (*c*) $X_8 = 0.8$, $X_7^{-1} = 0.3$. (*d*) $X_8 = 0.5$, $X_7^{-1} = 2.5$. (*e*) $X_8 = 0.5$, $X_7^{-1} = 0.5$. (*f*) $X_8 = 0.2$, $X_7^{-1} = 1.49$. Note that patterns (*a*), (*d*) and (*f*) are abbreviated, containing fewer groups of sandy foresets than there were tidal cycles in the spring–neap tidal cycle.

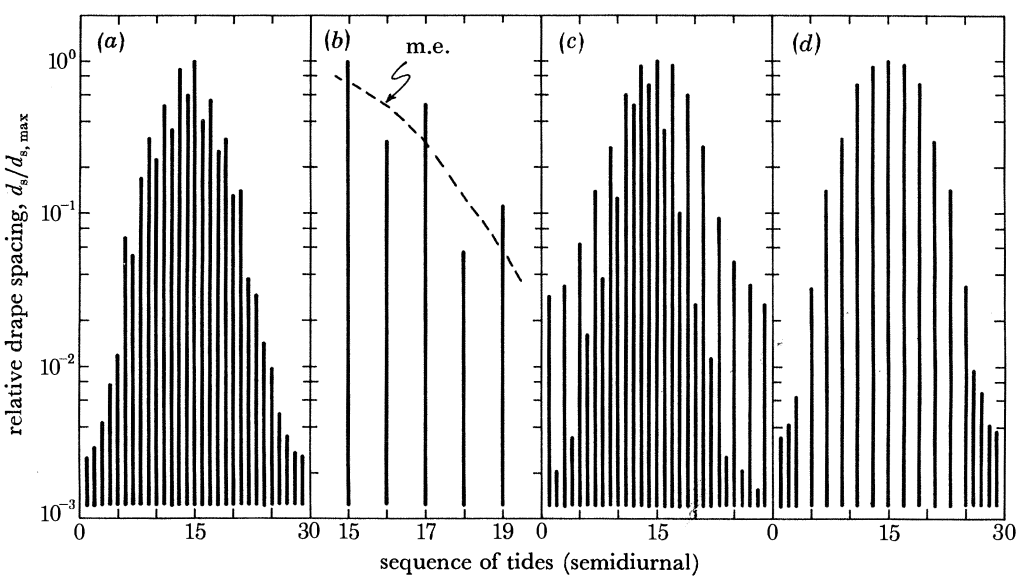

FIGURE 12. Schematic temporal patterns of drape spacing in complete spring–neap depositional cycles (bundles) due to (*a*) semidiurnal tides (note diurnal inequality), (*c*) mixed predominantly semidiurnal tides, and (*d*) mixed predominantly diurnal or diurnal tides.
(*b*) Deviation from mean envelope due to diurnal inequality in semidiurnal régimes (m.e., mean envelope).

figure 7*c*, *d*), afford a return to simpler patterns, but with appropriately fewer drapes and sand layers.

The 'six-monthly' tidal cycle will be detectable only in particularly long sequences of drapes and sand layers. By the above reasoning there should be sequences of bundles in which the ratio $d_{s,\max}/d_{s,\min}$ gradually increases as the springs grow in range toward an equinox, interspersed with sequences in which the ratio declines on the approach of a solstice.

(*e*) *Summary of controls on mud drapes under ideal tidal conditions*

To summarize, drape production in tidal environments is under complex controls, but three factors – tidal-current eccentricity, asymmetry, and strength – seem paramount (see figure 13). The availability of dispersed mud in significant concentrations is subsumed under eccentricity, since both eccentricity and mud content tend to increase shoreward, with maxima in estuaries. Drape production is favoured by high eccentricity, high asymmetry and low strength. High eccentricity and high asymmetry as factors favouring drape development point to estuarine and inshore waters as perhaps the most likely in which to find mud drapes within sand-wave deposits. Offshore sand waves are unlikely to have drapes, since tidal-current eccentricity and mud concentrations are seldom great enough, although the current strength, favouring drapes, tends to be low.

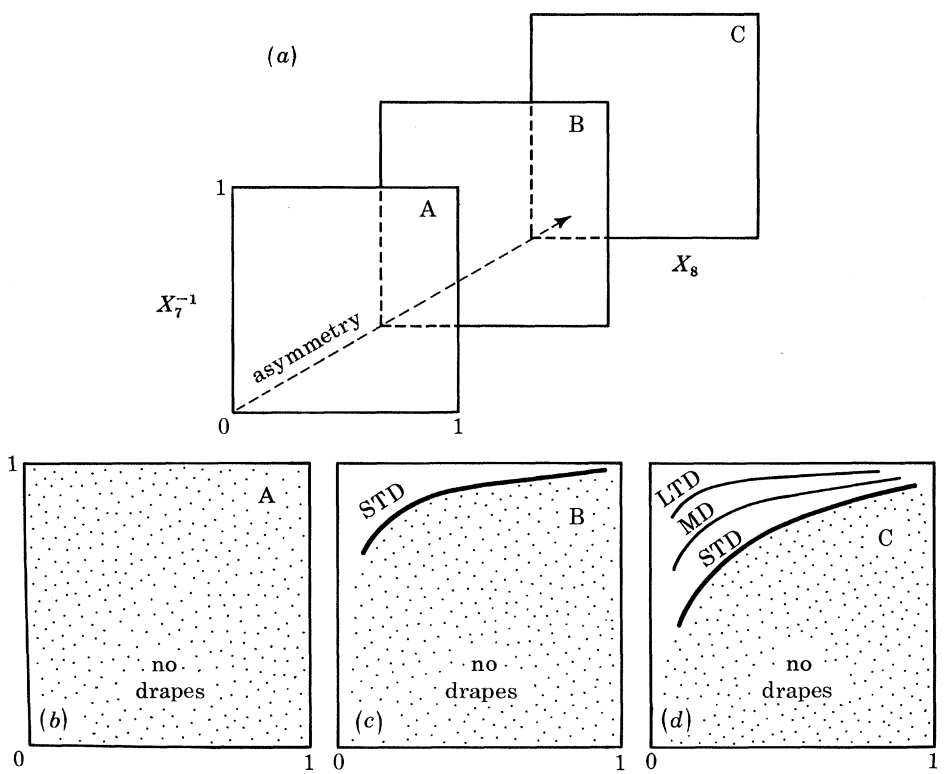

FIGURE 13. Summary of main controls on development (thickness and length) of mud drapes under ideal tidal conditions: STD, short thin drapes; MD, medium drapes; LTD, long thin drapes.

5. Factors distorting or suppressing drape formation

(*a*) *Sand-wave shape*

To see the influence of this so-far neglected factor, consider in figure 14 a sand wave not so asymmetrical that it promotes flow separation. If two-dimensional conditions are assumed, continuity demands that the mean flow speed U_y at a station of depth y varies as $U_y = h(t)\,U(t)/y$, in which $h(t)$ is the mean water depth and $U(t)$ the overall mean flow speed. The stream therefore remains for a longer period in excess of U_{cdm} at the sand-wave crest than in the trough, whence by equation (7) the drape should be thickest in the trough. A drape can form beneath a rotary tide only where $U_y < U_{\mathrm{cdm}}$, and so may arise in a trough, where the depth is relatively great, but not on an adjacent crest.

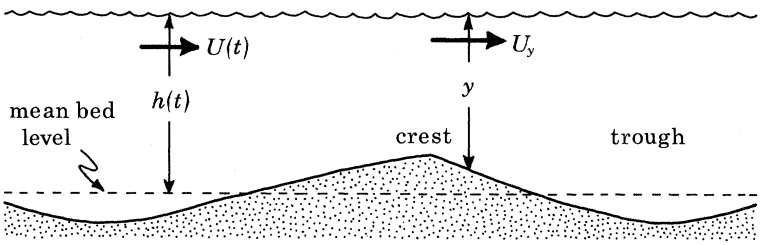

Figure 14. Definition diagram for tidal flow over a near-symmetrical sand wave.

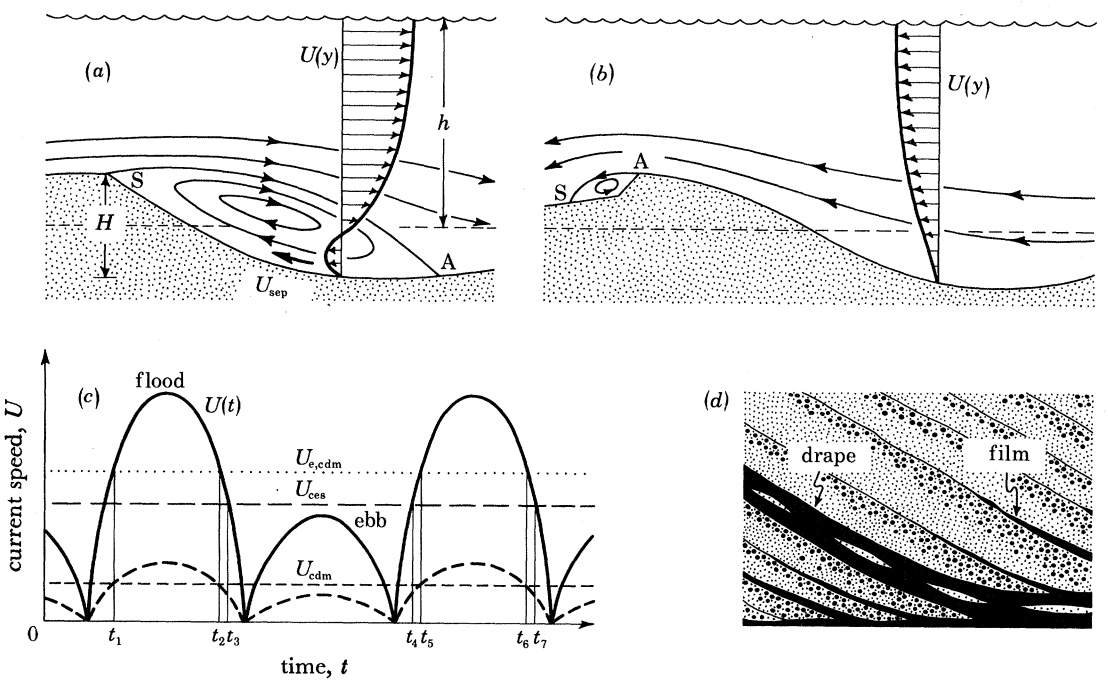

Figure 15. Implications of flow separation for drape development on strongly asymmetrical sand waves. (*a*) Separation downstream of sand-wave crest during flow of dominant tidal stream (say, flood). (*b*) Rounding and reversal of crest and creation of nearly separated flow in trough during flow of subordinate tidal stream (say, ebb). (*c*) Periods during a tidal cycle when sand can be transported past the sand-wave crest and mud can be deposited in association with the separation bubble. (*d*) Schematic representation of mud drape formed by the subordinate stream and the weaker currents of the dominant stream, together with the accompanying mud films produced between episodes of sand avalanching on the steeper slope of the sand wave.

(*b*) *Flow separation*

Many sand waves are so asymmetrical and with one face so steeply graded that the separation of the tidal streams is inevitable (Allen 1980*a*), compounding the shape effect already noted. For the sand wave depicted in figure 15*a*, the separation streamline SA isolates from the external flow a separation bubble formed to lee (flood tide) of the crest. Two boundary layers start at the attachment point A, one within the separation bubble and the other on the bed below the external stream. Mud deposition beneath the bubble therefore depends on the character of the *local* boundary layer, and occurs under the conditions

$$U_{\mathrm{sep}} = k(H/h, Re)\, U, \quad U \leqslant k^{-1} U_{\mathrm{cdm}} = U_{\mathrm{e,\,cdm}}, \tag{11}$$

in which U_{sep} is the mean speed in the boundary layer within the bubble, k a new numerical coefficient, H the sand-wave height, h the mean water depth, Re the Reynolds number and $U_{\mathrm{e,\,cdm}}$ the effective threshold speed for mud deposition, i.e. the speed of the external stream when mud can theoretically be deposited beneath the separation bubble. The coefficient k should from experimental studies lie between 0.15 and 0.3 with the relative roughness exerting the main control (Allen 1968; Karahan & Peterson 1980), whence $U_{\mathrm{e,\,cdm}}$ may range between approximately 0.17 and 0.65 $\mathrm{m\,s^{-1}}$. Hence when the tidal stream separates on a sand wave, substantially longer periods are available for drape deposition than with an unseparated flow. Drape thickness could be increased by a factor of two or more in consequence of separation.

The subordinate stream created by the reversal of the tide over the sand wave shown in figure 15*a* is unlikely to become fully separated upstream of the crest, particularly if the flow compressed over the crest is strong enough to round off the crest and temporarily reverse it. Nevertheless, at the same time as a reactivation surface is being formed by the rounding of the crest, the deposition of a mud drape in the trough will be favoured by the relative sluggishness of the subordinate stream over the deeper-lying parts of the sand wave (see figure 15*b*). The nearly separated subordinate stream may therefore be almost as effective as the fully separated dominant one in promoting mud deposition over the trough.

The speed pattern shown in figure 15*c* (see also figure 5) suggests that multiple drapes may in consequence of separation arise during a single tidal cycle, although only one drape is normally expected. During the intervals $t_2 - t_1$ and $t_6 - t_5$ only sandy foresets and bottomsets can form in the lee of the sand wave, whereas mud alone is deposited during the period $t_4 - t_3$. In the intervals $t_3 - t_2$ and $t_5 - t_4$, however, mud can accumulate in the sand-wave trough at the same time as sand is passing the crest toward the trough. If the sand transport rate is comparatively low, as it will be in view of the near-threshold conditions, avalanches of grains should spill into the trough at widely separated instants (Allen 1965*b*, 1970). A thin mud layer could therefore form over the surface of one avalanche-deposited sand layer in the long interval before the arrival of the next, adding to the main drape one or more branch-like companions in the shape of subordinate impregnations or films (see figure 15*d*).

(*c*) *Bedform relative movement*

One possible cause of distortion in drape-spacing patterns is the relative movement of neighbouring sand waves and associated bedforms, for each individual feature both influences its neighbours, and in turn is influenced by them, through its effect on the *local* flow and sediment

transport, while in the assemblage as a whole there operates a slow process of bedform creation–destruction. That neighbouring bedforms of the same one-way species affect each other's shape and movement through their influence on local flow and sediment transport is now widely accepted (Nordin & Algert 1966; Nordin 1971; Allen 1973). In sand waves, mutual interference is likely to have a comparatively long-term effect, apparent only on the scale of the bundle of drapes and sand layers. A distortion on much smaller temporal and spatial scales is likely to result from the comparatively rapid migration of any superimposed dunes. Experimentally, a sand wave should experience some erosion and lowering of its (usually upper) leeward slope as each dune advances to its crest (Allen 1973; McCabe & Jones 1977). In consequence, a convex-upward discontinuity or reactivation surface (Collinson 1970) will be preserved within the sand wave, the extent and slope of the surface respectively increasing and decreasing as the superimposed bedforms approach closer to the sand wave in size. Reversal of the tide (see figures 4, 5), however, can also produce such surfaces (Boersma 1969), and the two kinds may not in practice be distinguishable.

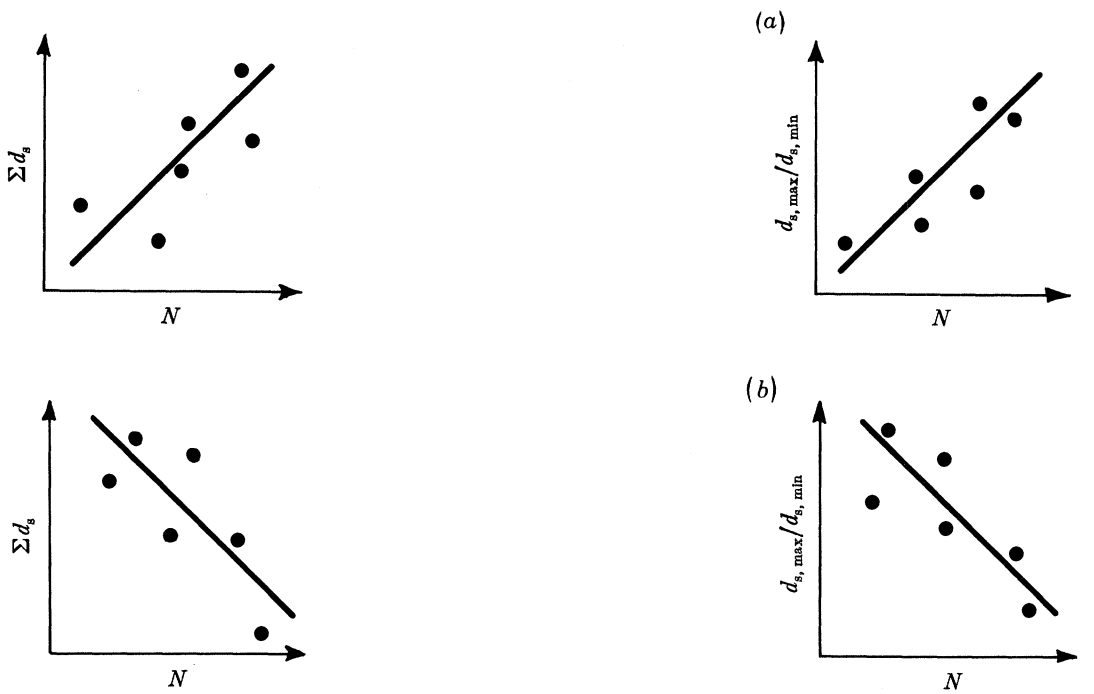

FIGURE 16. Expected correlations of Σd_s with N and $d_{s,\max}/d_{s,\min}$ with N under (*a*) sand omission and (*b*) mud suppression.

(*d*) *Wind waves*

Bottom currents due to wind waves (period 1–15 s) invariably accompany tidal streams and during windy or stormy weather may significantly inhibit if not totally prevent mud deposition. Waves create an oscillatory either laminar or turbulent bottom boundary layer in which the velocity and mean boundary shear stress vary on the same period as the waves. With reference to small-amplitude wave theory (Wiegel 1964), and laboratory work on wave boundary layers (Sleath 1974, 1975, 1976; Kamphuis 1975; Jonsson & Carlsen 1976; Knight 1978), a 50% reduction in drape thickness is theoretically possible when $U_{\max} = U_{\mathrm{cdm}}$, where $U_{\max}$ is the amplitude of the wave-induced near-bed oscillatory current. The reductions are 68% and 78% for respectively

$U_{max}/U_{cdm} = 2$ and $U_{max}/U_{cdm} = 4$. Since mud flocs settle very slowly, and therefore cannot sink far during one wave period, it is probable because of the consequent settling-lag effect that these nominal reductions are highly conservative. A practical criterion for the total suppression of drape formation during wave action may therefore be $U_{max}/U_{cdm} = 1$. At the depths where sand waves are most common, between 10 and 50 m, a moderate degree of wave action could significantly suppress drape formation. Perhaps only during comparative calms at sea, and in the more sheltered parts of estuaries, will waves have a negligible influence on mud deposition. The above process of *mud suppression* lowers the number of drape–sandy foreset pairs which might otherwise have formed during the spring–neap cycle.

How can we distinguish abbreviation of the spring–neap depositional cycle caused by mud suppression from the reduction of bundle size by *sand omission*, the process exemplified by the upper field in figure 10*a*? In a spring–neap depositional cycle abbreviated by sand omission (see figures 10, 11) the values of $d_{s,max}/d_{s,min}$ and of Σd_s are positively correlated with N, the total of mud drapes and groups of sandy foresets in the bundle (see figure 16*a*). Under mud suppression, however, drapes fail to be deposited, whence two or more groups of sandy foresets that would otherwise be separated by drapes become inseparable in the field, with the further consequence that the drapes that limit the complex assume an abnormally large spacing. Hence in bundles affected by mud suppression $d_{s,max}/d_{s,min}$ and Σd_s are either independent of or negatively correlated with N (see figure 16*b*).

(*e*) *Some combined currents*

Storm winds significantly affect sea level at the coast, and offshore induce surface currents with a speed of 3–4% of the wind speed measured at 10 m height. Near-bed storm-related currents in shelf seas measure centimetres to decimetres per second, occasionally reaching over $1\,m\,s^{-1}$, and may persist for many hours (Murray 1970, 1972; Smith & Hopkins 1972; Gienapp 1973; Caston 1976; Forristall *et al.* 1977). These currents in tidal seas must significantly distort the normal tidal streams, and either sharply reduce or increase, depending on their strength and relative direction, the extents of mud deposition and net sand-wave movement (i.e. drape spacing).

The movement of large-scale atmopsheric pressure systems across the surface of the sea creates currents by the direct action of the accompanying winds and as a consequence of the induced changes in sea level. These currents should significantly influence sand transport and mud deposition where land masses apply constraints, as in an archipelago or in a strait connecting substantial seas. The archipelago between the Kattegat and western Baltic Sea provides an excellent example of such currents (Wyrtki 1953, 1954*a*, *b*). Tidal streams reach maximum speeds of only $0.1–0.2\,m\,s^{-1}$, but the inflowing or outflowing depression-related currents attain peak strengths of up to $1\,m\,s^{-1}$ and can last for up to ten days. Large so-called sand waves have been generated by these currents (Werner & Newton 1970, 1975; Werner *et al.* 1974). For long periods these forms are stationary and, given other circumstances, could become mud-draped in addition to being bioturbated. Any accumulated drapes will be randomly distributed, however, on account of the aperiodicity of the currents. The same inflows and outflows may be partly responsible for the 'sand waves' occurring in an area of weak tidal flows on the south side of the Skagerrak (Stride & Chesterman 1974).

(*f*) *Feedback arising from mud deposition*

The increasing tendency for mud to accumulate as tides wane from springs to neaps has two possibly important implications for sand-wave behaviour when the tides subsequently increase: (i) sand transport may occur at below full capacity until encrusting mud is freed from a sufficient proportion of the bed area, and (ii) the presence of mud impregnations and films over the nominally sandy parts of the surface may significantly enhance U_{ces} compared with the same mud-free sand, as Allen & Friend (1976) found in an East Anglian estuary. A spring–neap depositional bundle could reflect these effects in two ways. Firstly, a larger value of U_{ces} for waxing than for waning tides should make the pattern of $d_s/d_{s,max}$ asymmetrical, with the ratio increasing more rapidly than it falls (a small time lag with peak current speed may be detectable). Secondly, because of the erosional modifications likely to accompany the waxing of the tides, maximum drape development should slightly precede the minimum in $d_s/d_{s,max}$.

B. APPLICATION OF THE MODEL TO THE FOLKESTONE BEDS

6. Introduction to the Folkestone Beds

(*a*) *Lower Greensand*

The Folkestone Beds lie in the upper part of the Lower Greensand (late Upper Aptian to early Lower Albian), accumulated according to Casey (1961) in two depressions (see figure 17), the Northern Basin and the Southern Basin, separated by the London Platform. Resting on an unconformity, the Lower Greensand in the north is represented by the Carstone (Lincolnshire–Norfolk Province) and Woburn Sands (Cambridge–Bedford Province). In the south the Lower Greensand is as thick as 240 m on the Isle of Wight (Vectian Province), passing up from the Wealden Shales, but declines westward to 50–60 m near Swanage, where there is possibly a basal non-sequence. The Wealden Province comprises the Weald proper together with the western outliers of Abingdon, Faringdon, Seend, and other places ranging toward the English Channel. The Wealden Lower Greensand rests mainly disconformably on the Wealden Beds and is thickest (160–210 m) near Farnham. It thins drastically eastward along its north crop (*ca.* 85 m in the Folkestone–Hythe area), but more modestly southward toward Petersfield and Midhurst. A dramatic reduction and eventual elimination occur eastward along the south crop (Young & Monkhouse 1980). The 'Aptien Marin' of the Bas-Boulonnais (reviews in Narayan 1971; Mégnien & Mégnien 1980) is a natural extension of the Wealden Lower Greensand, consisting of thin sands and clays, apparently with non-sequences. The western outliers of the Wealden Province reveal thin and incomplete developments of the Lower Greensand.

Of the uplifts thought by Casey (1961) to have controlled Lower Greensand sedimentation, the most important is the Paris-Plage–Portsdown Axis (Kent 1949; King 1954; Casey 1961) separating the Vectian and Wealden Provinces. It appears from mainly borehole evidence (Taitt & Kent 1958; Falcon & Kent 1960; Young & Monkhouse 1980) to have underlain an east–west zone of reduced deposition, which may at times have been either land or a scoured sea floor.

(*b*) *Folkestone Beds and correlatives*

The formation in the Weald consists mainly of sands which overlie various sandy and clayey beds and in turn graduate up, with local non-sequences, into the Gault clays. The thickness pattern (see figure 17 inset) resembles that for the Lower Greensand as a whole. A threefold

internal division is recognizable from Reigate and Dorking as far as Haslemere and Petersfield (White 1913; Dines & Edmunds 1929, 1933; Hayward 1932; Humphries 1964; Thurell *et al.* 1968), thin ferruginous and often pebbly quartz sands being succeeded by rose-pink to white sands (silver sands) in turn overlain by generally thick and ferruginous locally pebbly coarse sands. From Sevenoaks eastward to Folkestone, silver sands appear irregularly at the base of the

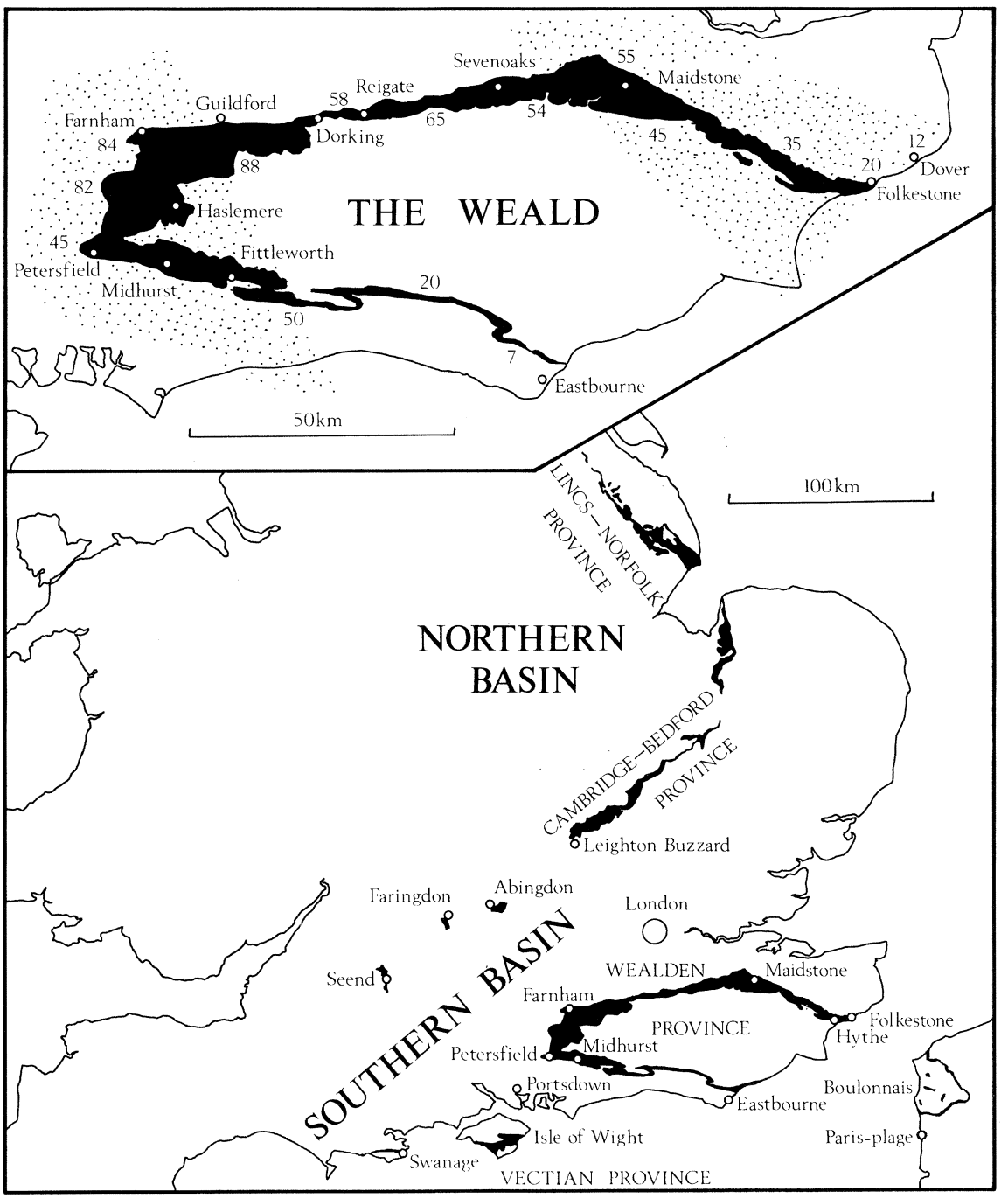

FIGURE 17. Outcrops (shown in black) of the Lower Greensand (main map) in England and the Bas-Boulonnais, and in the Weald (inset map). Thickness in metres of Folkestone Beds shown as numbers by outcrop. Distribution of facies with mud layers and drapes shown by stippling. Partly after Casey (1961).

Folkestone Beds as well as higher up (Dewey *et al.* 1924; White 1928; Dines *et al.* 1954, 1969; Worssam 1963; Smart *et al.* 1966). Silver sands are comparatively rare and also unevenly distributed between Midhurst and Eastbourne (Reid 1898, 1903; White 1924, 1926; Humphries 1964; Young & Monkhouse 1980). These Wealden Folkestone Beds reach from the *Hypacanthoplites rubricosus* Subzone (topmost Aptian) up to the *Hypacanthoplites milletioides* Subzone (lowermost Albian) (Casey 1961). The thickly cross-bedded quartz sands and thin clays of the Aptien Marin range from mid Upper Aptian to late Lower Albian, and seem partly correlated with the Folkestone Beds (Narayan 1971; Mégnien & Mégnien 1980).

Correlatives elsewhere in Britain are few (Casey 1961). None exist in the western outliers, except for perhaps the ill-exposed and unfossiliferous red sands of Uffington in Berkshire. The most important in the Vectian Province is the series of the pale-coloured to ferruginous sands (35–57 m) called the Sandrock; this is not separately distinguished in the reduced Dorsetshire Lower Greensand, although there are quartz sands at the expected horizon. Around Woburn and Leighton Buzzard, in the Cambridge–Bedford Province, the Folkestone Beds are represented by the Woburn Sands, roughly 65 m of white to yellow or ferruginous cross-bedded quartz sands. The Carstone of the Lincolnshire–Norfolk Province is a khaki-coloured ill-sorted quartz sandstone some metres thick possibly of Albian age but without indigenous fossils.

(*c*) *Facies groups of the Folkestone Beds in the Weald*

There are two broad textural groupings: (i) facies involving very-fine- to fine-grained quartz sands, either white, pale grey or rose-pink (silver sands), and (ii) facies dominated by medium- to very coarse-grained often pebbly sands, generally ferruginous but locally pale grey. Both facies in southwestern and northeastern localities normally include plentiful drapes and seams of almost white, pink, or blue-grey kaolinitic silty mud (see figure 17 inset). Such seams and drapes are rare to absent in a central northwest–southeast zone.

The facies of grouping (i) involve (*a*) cross-bedded sands in thin sets with reactivation surfaces, (*b*) parallel-laminated sands infilling broad shallow scours, and (*c*) cross-laminated sands associated with incompletely to fully preserved wave and wave-current ripples. Accompanying muds (for example British National Grid Reference SU 783 229, SU 890 200) appear as drapes and seams on the foresets and bottomsets of the cross-bedded sands, at the bottoms of or within the scour-fills, and as layers, locally extending for several tens of metres, that bury rippled surfaces. Ripple wavelengths range between 0.1 and 0.25 m, increasing with grain size, and cross-sectional shapes from trochoidal to round-crested and moderately asymmetrical. Mud clasts are locally plentiful, especially in the cross-bedded sands. Several of the parallel-laminated and rippled sands are intensely bioturbated (for example SU 866 473). Certain thick mud seams extend over planar surfaces for some hundreds of metres (for example SU 890 200). Sedimentary structures can be difficult to see where mud drapes and seams are lacking (for example TQ 223 505) but are not significantly different from those where there are lithological contrasts to guide the observer.

Cross-bedding locally in compound sets dominates the second facies grouping. Most sets (thickness 0.5–3 m) have an uncomplicated internal geometry and can be described as 'simple'. These can be traced for distances as great as 150 m parallel with the cross-bed dip azimuth and, beginning upstream as down-cutting scoops, are bounded above and below by largely planar erosion surfaces. Foresets typically are reverse-graded and either rest acutely on the basal erosion surface or pass downward and laterally into long tangential bottomsets, which locally form as

much as one-third to one-half of the set thickness. Mud, where present, appears as frequently spaced drapes either mantling ripple-marked bottomsets or ranging up on to the foresets (for example SU 784 229, SU 821 839, SU 866 473, SU 890 200, TQ 824 544). Reactivation surfaces (Collinson 1970), commonly mud-draped toward the base, are frequent in some cross-bedding sets, as Narayan (1971) noted, but in many others are undetectable. Locally such surfaces are picked out by concentrations of sand-size limonite grains. The absence of mud drapes and seams makes little difference to the character of these simple cross-bedded units (for example TQ 418 535, TQ 425 537, TQ 432 539).

Here and there simple cross-bedding sets 0.25–1.5 m thick are arranged in large compound sets (see figure 18*a*) (for example, mud drapes present, SU 784 229, SU 866 473; mud drapes absent, TQ 432 539). These complex sets resemble the downcurrent-dipping cross-bedding of Banks (1973), the aeolian cross-bedded sandstones of Brookfield (1977, 1979), and some of Levell's (1980) inferred sand-wave deposits. As many as three orders of erosional contact are noticeable: (i) a markedly planar surface below and another above the compound set, (ii) the surfaces between simple sets, inclined at a few degrees to the base of the compound set, and (iii) reactivation

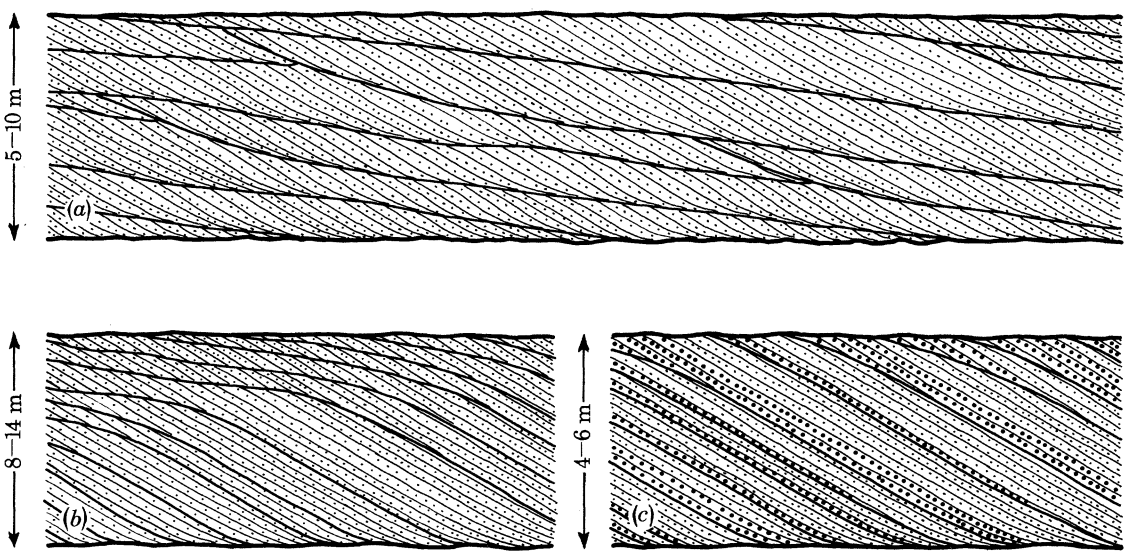

FIGURE 18. Schematic vertical sections of types of large scale compound cross-bedding preserved in the Folkestone Beds.

surfaces within simple sets. Figure 18*b* shows another kind of complex set (for example TQ 418 535). The upper part, composed of simple sets, generally without mud drapes, resembles an incompletely exposed compound set of the previous kind, but the bounding surfaces between the simple sets gradually steepen downward, truncating long foresets, and finally merge with those foresets. The erosion surfaces between the simple sets are perhaps reactivation surfaces with respect to the complex set. Figure 18*c* sketches a possibly severely truncated form of this kind of complex set (for example SU 821 389, SU 890 200). Characteristically 4–6 m thick, these sets show reactivation surfaces 0.5–1.5 m horizontally apart and, locally, zones of foreset-parallel bioturbation (Middlemiss 1962). The coarsest-grained sands are those first to appear above a reactivation surface.

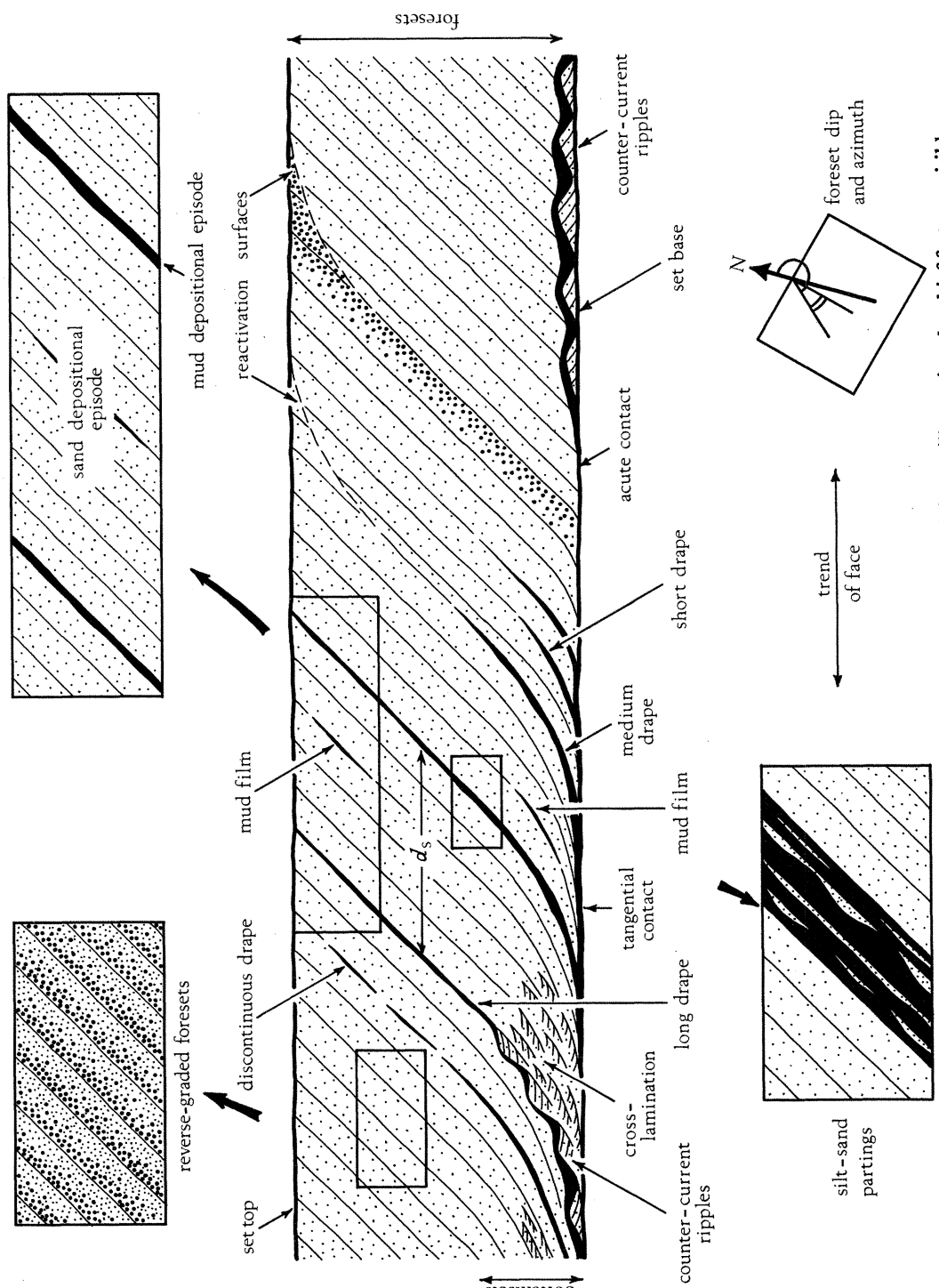

FIGURE 19. Schematic vertical section of cross-bedding unit with mud drapes illustrating the chief features visible or measurable in the field.

7. Cross-bedded sand units with mud drapes: methods of study

(*a*) *Localities*

Three sites in the western Weald exemplify the range of drape development met in the cross-bedded sands of the Folkestone Beds (see figure 17 inset). The sets are exposed on practically vertical quarry faces and for ease of reference are coded A, B, C etc. at each site. In the southern part of their Hog's Back Sandpit (SU 866 473), some 2 km east-northeast of Farnham, Ebenezer Mears (Sand Producers) Ltd work muddy silver sands sharply overlain by ferruginous cross-bedded sands with generally occasional but locally frequent drapes. Three sets were analysed. The West Heath Common Sandpit (SU 784 229) of S.E. Borrow Ltd lying 4 km east of Petersfield shows pale grey to rose-pink silver sands with frequent mud drapes, underlain by cross-bedded ferruginous sands with common to abundant drapes. Four cross-bedded units were examined here. The third site is the Pendean Sandpit (SU 890 200) of Hall Aggregates (South Coast) Limited, lying 1.5 km southeast of Midhurst. Four cross-bedding sets were measured, one (D) in two parts, mud drapes being abundant and mud layers numerous and extensive.

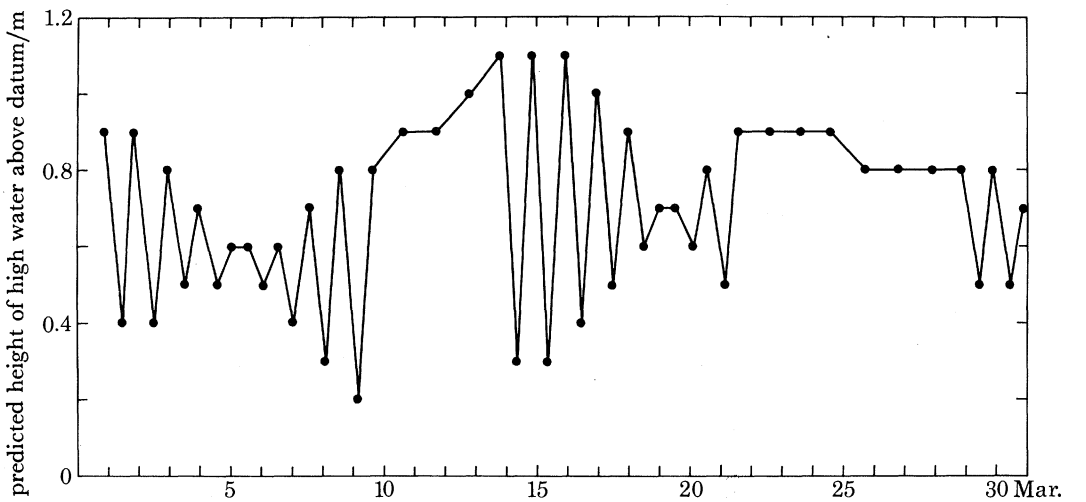

Figure 20. The predicted height of high waters above datum at Manila (Philippine Islands) during March 1980 (Hydrographer of the Navy 1979*c*). A line connects the points merely to emphasize their pattern.

(*b*) *Field methods*

Figure 19 summarizes the character of, and measurements made on, each cross-bedded unit with mud drapes. The *base* and *top* are erosional and in most cases planar; in some instances a row of cross-laminated *countercurrent ripples* overlies the base. Between the base and top range sandy *foresets*, which may pass down into *bottomsets*, interspersed with *mud drapes* spread over foreset or bottomset surfaces or both. The foresets dip steeply enough to have been emplaced by avalanching and typically are *reversely graded*, coarse sand overlying fine sand. Foresets meet set bases in an *acute basal contact* where bottomsets are lacking, and can locally be traced upward into convex-up *reactivation surfaces*. Bottomsets meet set bases *tangentially* and commonly are internally cross-laminated or reveal further *countercurrent ripples*. The mud drapes, either continuous or discontinuous, are described as *long* where they range from the top to the bottom of the set, but as *short* where confined to the lower one-third, covering either a bottomset or reaching only a

little way up a foreset surface. A *medium* drape ranges up into the middle parts of a set. Most drapes are of the order of several millimetres thick but some exceed a thickness of 0.02 m and others are thinner than 0.002 m. Internally, nearly all drapes possess one or more centrally or symmetrically arranged continuous or discontinuous *partings* of quartz silt or sand (a parting is defined as a layer thinner than the adjoining mud layers), in many instances having a flat

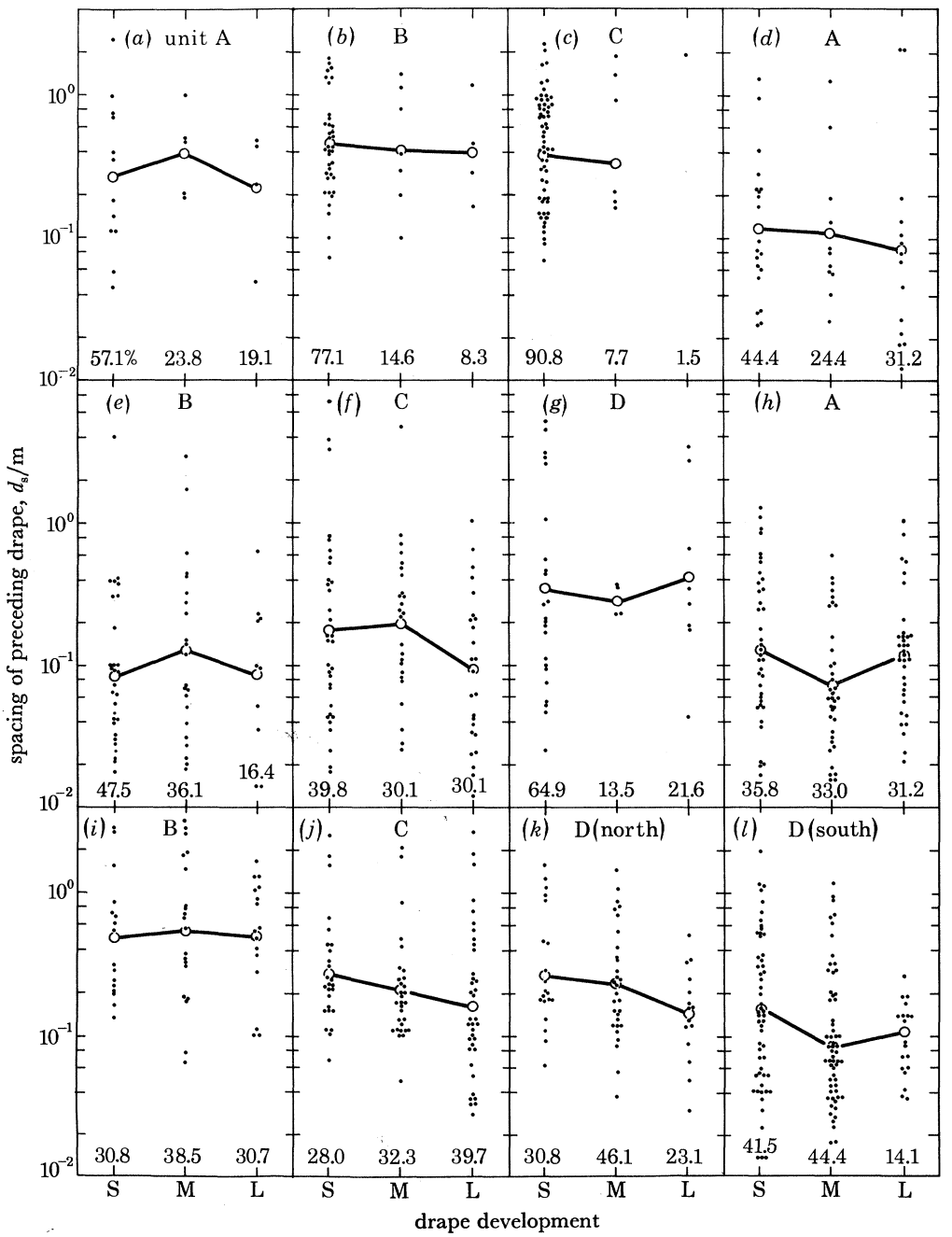

FIGURE 21. Correlation between drape development (length) and the spacing of the immediately preceding drape. (*a*)–(*c*) Hog's Back Sandpit. (*d*)–(*g*) West Heath Common Sandpit. (*h*)–(*l*) Pendean Sandpit. Heavy line joins logarithmic mean drape spacing (shown as open circles) at each degree of drape development. S, short; M, medium; L, long drapes.

lenticular cross section resembling a ripple mark, together with an internal cross-lamination. Many partings are mere wisps of grains revealed only on careful dissection with a clean knife. Locally, *mud films* are developed on foreset and bottomset surfaces. These films range for 0.05–0.3 m over the bedding and are seldom thicker than 0.001 m, silty or sandy partings being conspicuously absent. They favour two locations: (i) high up on foreset surfaces, close to the set top, and (ii) where foresets flatten out into bottomsets. Saucer-shaped mud films mantle the troughs of the current and wave-current ripple marks among the bottomsets.

Each cross-bedded unit records a series of not necessarily simple sedimentary events or episodes. Every mud drape is evidence of a *mud depositional episode*, the internal partings suggesting variable conditions during the episode, silt or sand transport having occurred during one or more intervals within its course. The group of foresets and bottomsets contained between any two consecutive

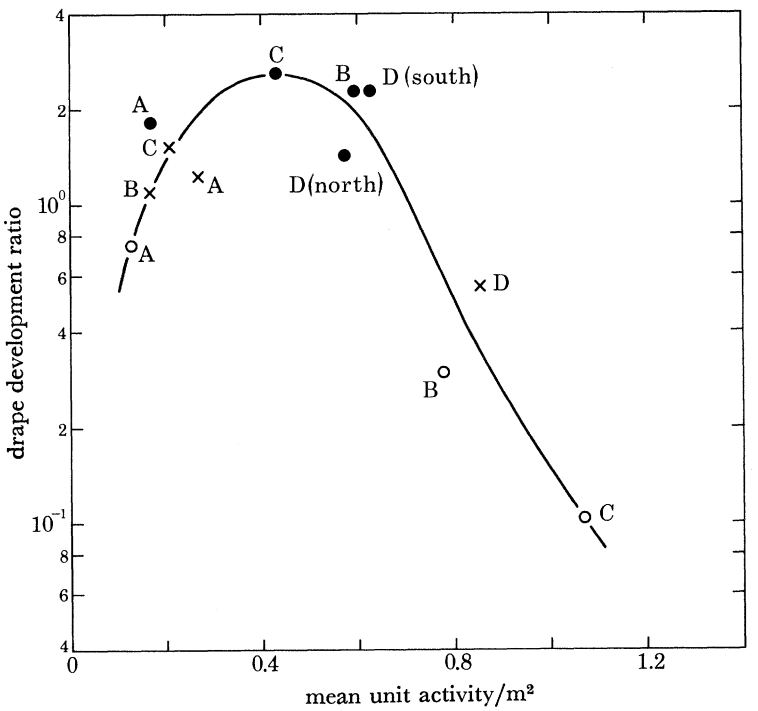

FIGURE 22. Correlation between drape development ratio and mean unit activity. Key to symbols; o, Hog's Back Sandpit; ×, West Heath Common Sandpit; ●, Pendean Sandpit. Individual units identified by code letters.

mud drapes records a *sand depositional episode*, a change in sand movement being manifested by any reactivation surface preserved within the group. Here and there, a drape partly covers a foreset surface which can be traced upward into a reactivation structure, whence reactivation in such a case occurred either toward the close of the sand episode or during the ensuing episode of mud emplacement.

The mud drapes and the groups of sandy foresets and bottomsets were carefully excavated and dissected with spade, trowel and knife. As far as possible mid-way up each set, the horizontal distance separating successive drapes (or their foreset-parallel upward projections) was measured along the smoothed quarry face between thin metal pins inserted into the deposit. This measurement was corrected to the true horizontal streamwise spacing d_s (see § 4*c*) with the help of the

TABLE 1.

locality	mean diameter of foreset sand (φ units†)	length of record: episodes	length of record: true horizontal distance (m)	mean unit thickness (m)	mean horizontal drape separation (m)	mean unit activity (m²)	drape separation patterns: runs test probability	drape separation patterns: turning points test probability	drape development: development ratio	drape development: runs test
Hog's Back Sandpit										
unit A	1.21	43	9.88	0.273	0.471	0.129	0.126‡	0.183†	0.752	0.460
unit B	1.35	97	28.3	1.32	0.589	0.777	0.418	0.175	0.298	0.0012
unit C	1.42	131	40.2	1.73	0.619	1.07	0.254	0.275	0.102	0.204
West Heath Common Sandpit										
unit A	1.22	91	12.0	0.986	0.266	0.262	0.224	0.168	1.25	0.110
unit B	1.96	123	16.8	0.610	0.276	0.168	0.0254	0.0255	1.10	0.0698
unit C	1.20	167	36.6	0.468	0.442	0.207	0.218	0.0582	1.52	0.364
unit D	1.19	75	32.1	0.985	0.866	0.853	0.199	0.0107	0.541	0.175
Pendean sandpit										
unit A	1.68	219	21.3	0.874	0.196	0.171	< 0.0001	0.0287	1.80	< 0.0001
unit B	1.56	105	42.5	1.40	0.425	0.595	0.164	0.186	2.25	0.0618
unit C	1.52	187	34.7	1.15	0.373	0.429	0.0083	0.254	2.58	0.0041
unit D (north)	1.32	131	21.5	1.88	0.331	0.622	0.0294	0.0501	2.25	0.0221
unit D (south)	1.65	271	29.2	2.64	0.217	0.573	0.0003	0.473	1.41	< 0.0001

† φ unit = $-\log_2$ (particle diameter/mm).
‡ Dichotomized relative to long-term trend.

foreset dip azimuth and face trend. The normal thickness H of the cross-bedding set was determined at frequent intervals along the exposure. From each set examined a composite sample of sand was assembled by collecting a uniformly small quantity every few metres laterally at about set mid-height. Representative bottomset sands and drapes were sampled, but not systematically.

(*c*) *Presentation and analysis of results*

Presentation is mainly in the form of time-series of (i) d_s-values and (ii) drape development (short, medium, long), with time measured (loosely) in terms of increasing number of depositional episodes. The records were examined for pattern with the use for d_s-values of (i) a runs test and a turning points test (Miller & Kahn 1962, pp. 351, 341) and (ii) Fourier analysis; and for drape development of (iii) a three-element non-parametric runs test. The power of these techniques is strongly affected by (i) the length of the data sequence, and (ii) the number of periodic elements combining to produce the sequence. Consider in figure 20 the pattern in time of the height of high water at Manila (Philippine Islands) during March 1980. Both the runs test and the turning points test applied to this sequence of values lead at the 5% significance level to the rejection of the hypothesis that the data are patterned, and only the Fourier analysis gives any strong (but incomplete) indication of periodicity. As some of the data sequences described below are comparatively short, and may contain random as well as periodic elements, the results of the tests described cannot therefore be regarded as completely conclusive.

Two further statistics help in comparing cross-bedding units in the Folkestone Beds and

---

PLATE 1. GENERAL FEATURES OF CROSS-BEDDED UNITS

1. Part of the first few metres of unit A, Hog's Back Sandpit. Note lack of drapes, reactivation surfaces (shown by arrows), and locally acute basal contact. Scale is marked in decimetres.
2. The first few metres of unit A, West Heath Common Sandpit. Hammer 0.38 m long rests on reactivation surface within episode 6. Note lengthy drapes among bottomsets.
3. Unit B, West Heath Common Sandpit, approximately 12–16 m from the start. Note drape-covered counter-current ripples at unit base. Scale is marked in decimetres.
4. Unit C, West Heath Common Sandpit, approximately 15 m along its length. Note drape clusters and drape-covered ripple marks at unit base and on bottomsets. Spade handle (0.45 m visible) is for scale.
5. The first few metres of unit D, West Heath Common Sandpit. Note lack of reactivation, and poor development of drapes and bottomsets. Scales are marked in decimetres.

PLATE 2. GENERAL FEATURES OF CROSS-BEDDED UNITS

1. Slightly oblique view of middle portion of unit A, Pendean Sandpit. Note drape clusters and the extensive mud drapes amongst the well developed bottomsets. Scale is marked in decimetres.
2. Unit B, Pendean Sandpit, between approximately 6 and 13 m from the start. Dark iron-stained zones occur above the principal drapes. Scales are marked in decimetres.
3. Unit C, Pendean Sandpit, between approximately 3 and 7 m from the downcurrent end. Note reactivation structures (shown by arrows) and thick bottomset deposits exposed in shallow pit near left-hand scale. Scales are marked in decimetres.
4. Unit D (north), Pendean Sandpit, between approximately 8 and 12 m from the start of the measured section. Note lack of reactivation, long drapes, and conspicuous bottomset zone. Scales are marked in decimetres.
5. Unit D (south), Pendean Sandpit, between approximately 20 and 24 m from the downstream end. The bottomset zone includes many extensive mud drapes (in clusters) and forms almost one half of the preserved thickness of the unit. Scales are marked in decimetres.

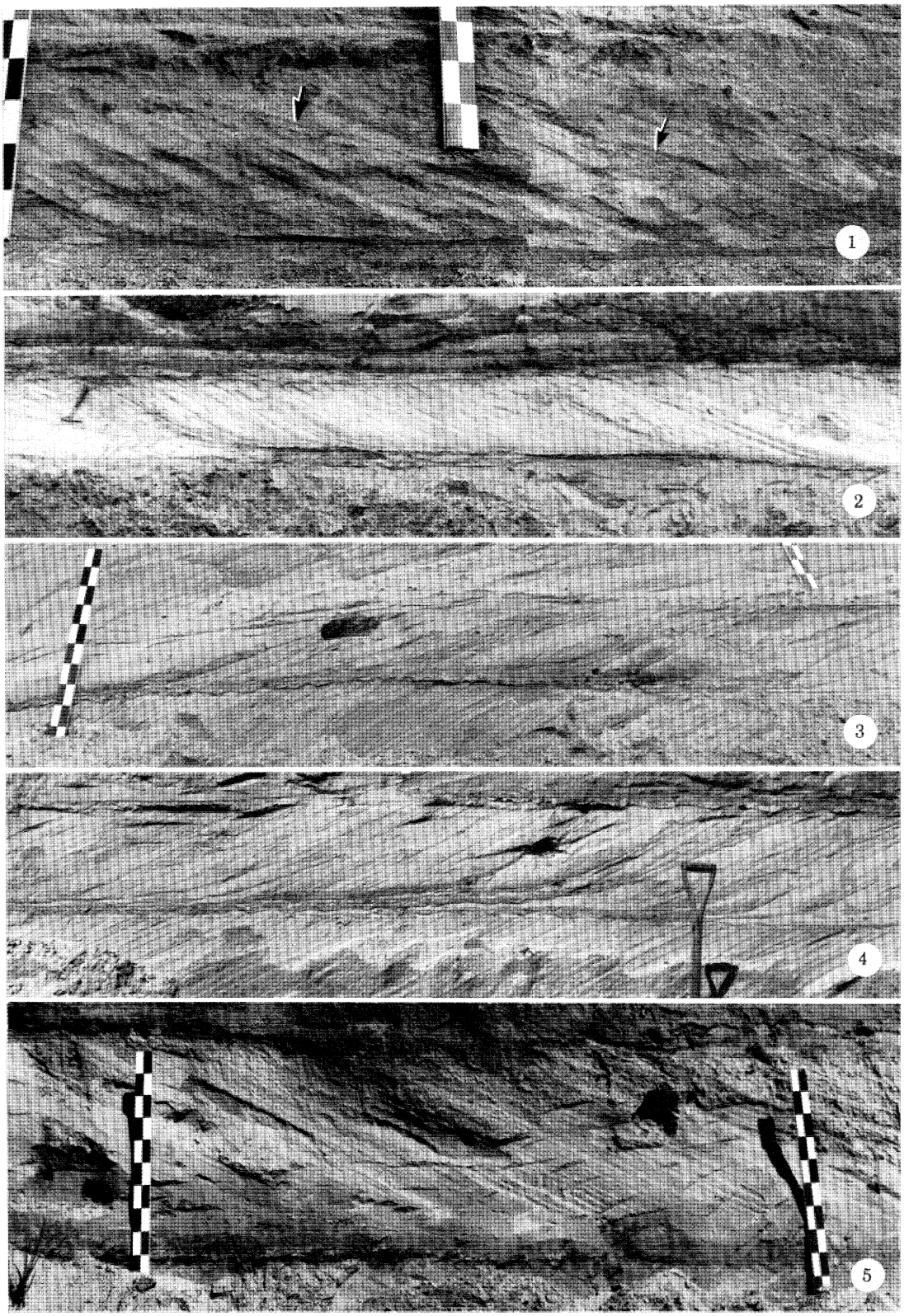

For description see opposite.

(*Facing p.* 322)

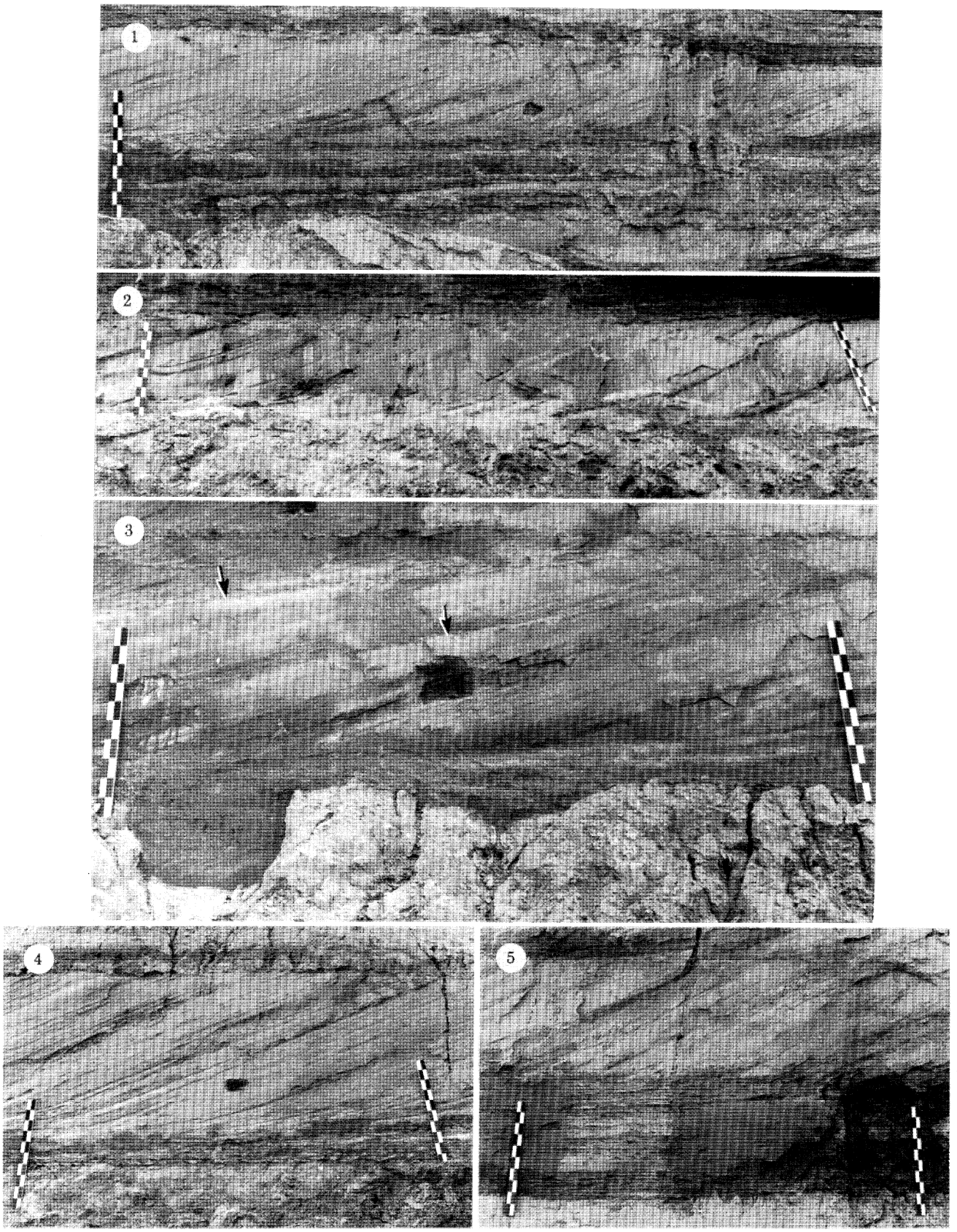

For description see p. 322.

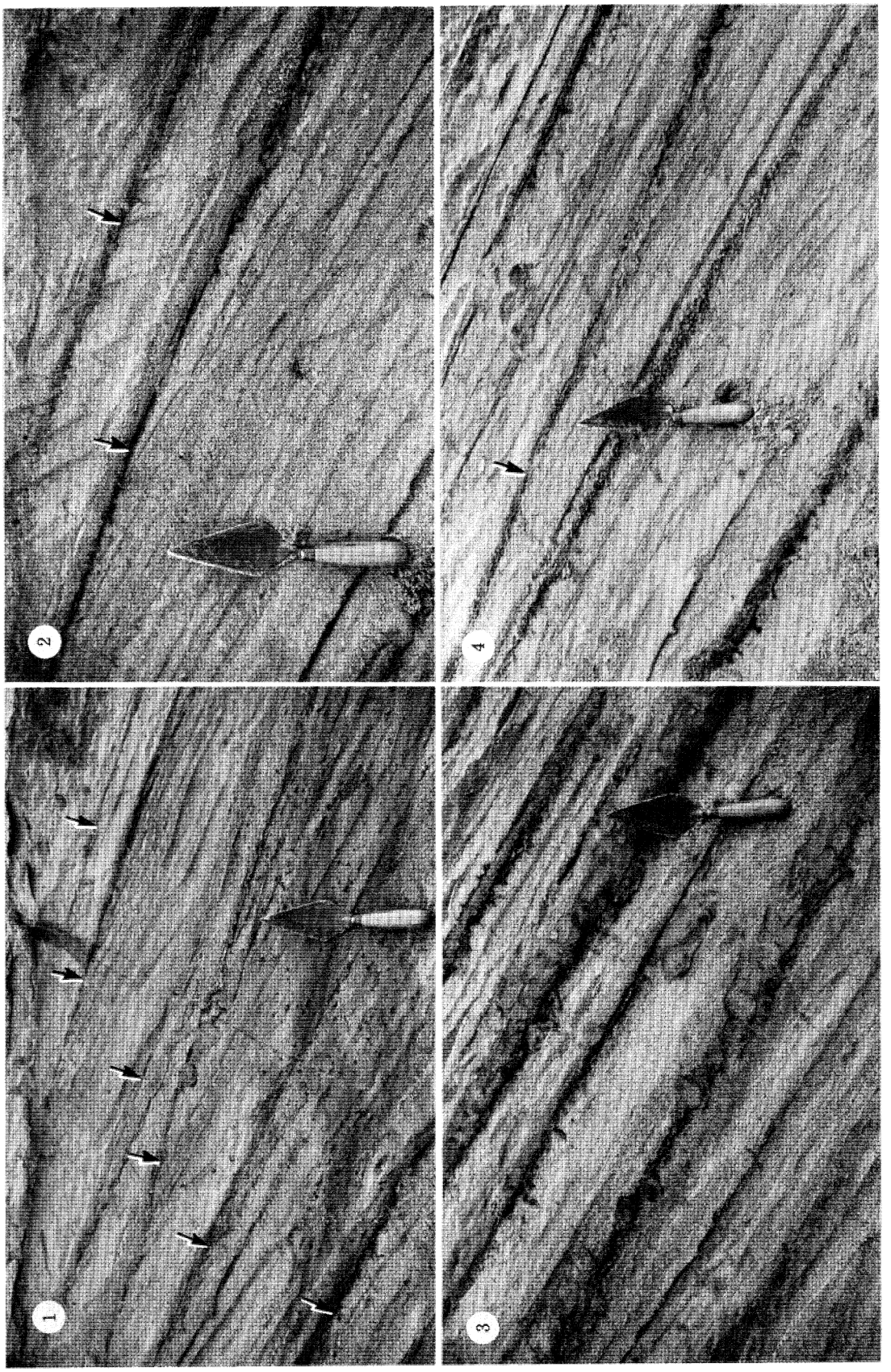

For description see p. 323.

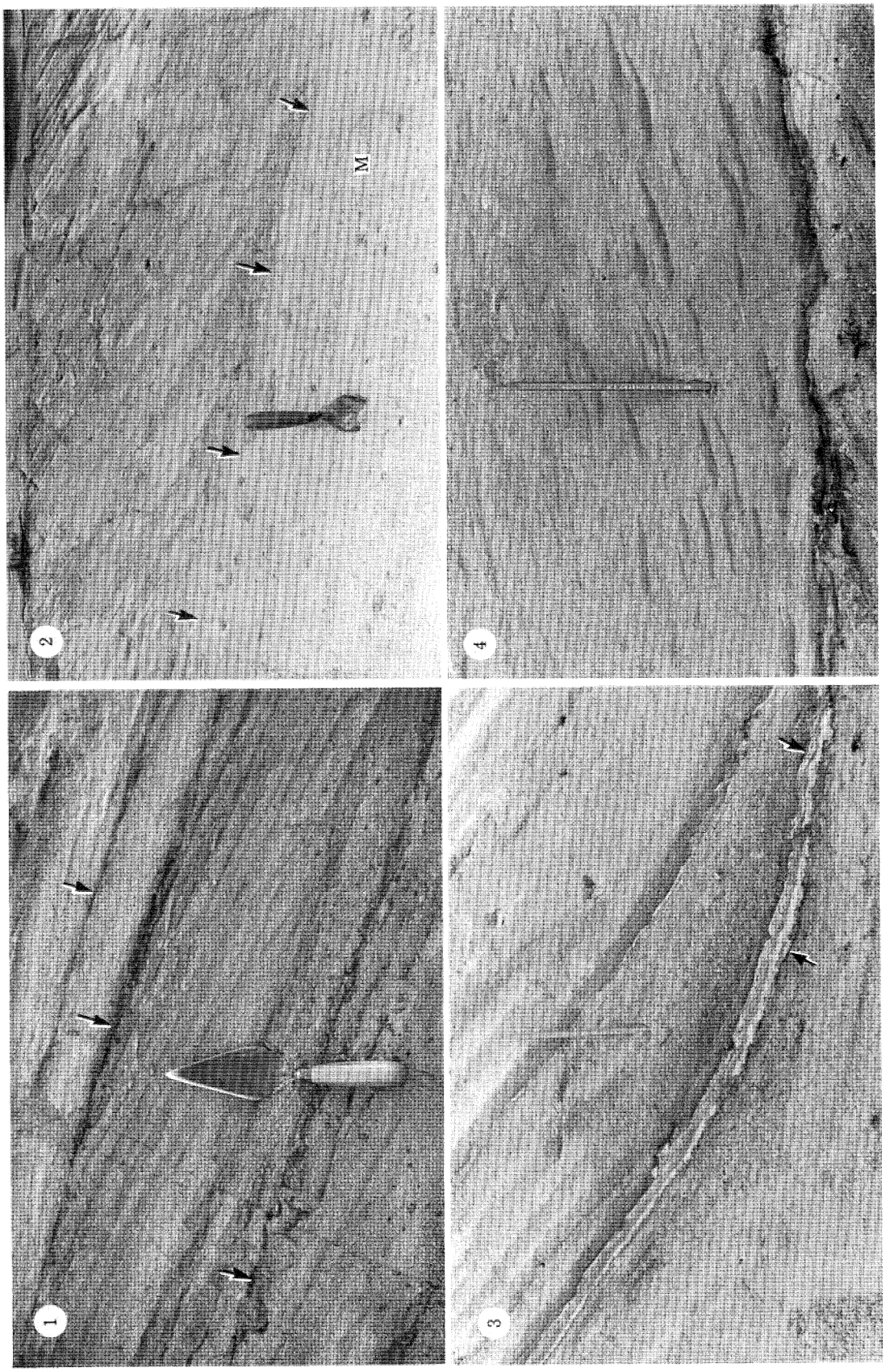

For description see opposite.

may in future be useful in regional studies. These are the *mean unit activity* $X_{11} = \bar{d}_s\bar{H}$ corresponding to the sand-wave activity, in which $\bar{d}_s$ is the mean streamwise horizontal separation distance between drapes and $\bar{H}$ is the average unit thickness, and the *drape development ratio* $X_{12} = (\Sigma M + \Sigma L)/\Sigma S$, in which ΣS, ΣM and ΣL are respectively the numbers of short, medium and long drapes encountered.

8. Hog's Back Sandpit

(*a*) *Unit* A

This medium- to coarse-grade unit lies close to the extreme of thinness for cross-bedding sets in the Folkestone Beds and is of low activity (see table 1). Reversely graded foresets pass locally into short thin bottomsets (see 1 of plate 1) and drapes of silty kaolinitic mud are, on the whole, poorly developed (see table 1 and figures 21*a*, 22). There is little sign of a negative correlation between drape length and spacing (sand thickness) (see figure 21*a*). Reactivation surfaces are restricted to the younger parts of the set, but bioturbation structures are locally plentiful, including vague mottles, 'Milford type' burrows (Middlemiss 1962), short stout sand- and pellet-filled tunnels, and narrow upright cylindrical tubes.

Time series for drape spacing and drape length appear in figure 24*a*. The runs and turning points tests (long-term trend removed) are against the occurrence of any pattern (see table 1), but the Fourier analysis (see figure 23*a*) points to the occurrence of depositional cycles (bundles) on periods of about 6 and 20 episodes. Bundle boundaries are tentatively recognized at episodes 8, 12, 18, 24 and 36, affording lengths of respectively 6, 6, 6 and 12 espiodes. The total drape spacing Σd_s is positively correlated with bundle size N but the bundling strength $d_{s,\max}/d_{s,\min}$ shows no obvious trend (see figure 24*b*, *c*).

Plate 3. Small-scale features of cross-bedded units, unit B, Hog's Back Sandpit. (Trowel is 0.28 m long.)

1. A sequence of six convex-up reactivation surfaces (shown by arrows) near the top of the unit, emphasized by concentrations of limonite grains. Several concentrations are bioturbated, and note the dispersed mottles just below the second reactivation surface from the top.
2. Two reactivation surfaces (shown by arrows) marked by limonite-rich sand, the lower being capped by up-slope-facing cross-lamination (about 0.3 m to the right of the trowel point). Note dispersed mottles below this surface.
3. Limonite-rich foresets with mainly large mottles in several cases including menisci, perhaps due to echinoderms.
4. Small mottles in a foreset (behind trowel) rich in limonite grains. Reactivation surface is shown by arrow.

Plate 4. Small-scale features of cross-bedded units

1. Dispersed small mottles within and below a reactivation surface (the middle of the three shown by arrows), unit B, Hog's Back Sandpit. Trowel is 0.28 m long.
2. Reactivation surface (marked by arrows) within episode 46, West Heath Common Sandpit. The sand below the surface is fine grained and intensely mottled, particularly at M, retaining traces of cross-lamination. Above the surface are foresets of medium to coarse sand. Trowel is 0.28 m long.
3. Three mud drapes (partings visible in photograph indicated by arrows), each capped by a dark zone of iron-stained sand, episodes 6–15 in unit A, West Heath Common Sandpit. Pencil is 0.16 m long.
4. Thin mud films capped by dark, iron-stained sand in rippled and cross-laminated bottomsets, episode 34, unit B, West Heath Common Sandpit. Pencil is 0.16 long.

(*b*) *Unit* B

This bed, lying about 8 m stratigraphically above unit A, is also of medium to coarse sand, but is of greater activity and presents a longer record (see table 1). It is dominated by reversely graded foresets 0.02–0.05 m thick passing down into bottomsets forming a zone 0.35 m in maximum thickness. The drape development ratio is relatively small (see table 1 and figure 22) and there is only a weak negative correlation between drape length and spacing (see figure 21*b*). Several medium and long drapes are up to 0.04 m thick and include numerous boldly developed silt or sand partings, in some instances ripple marked. The bottomsets contain many mud clasts.

Sand-size limonite grains are concentrated along particular foresets, creating conspicuous dark bands. These occur at streamwise intervals between 0.1 and 0.3 m and become narrower and fainter downward, many having petered out by mid-way down. None were recognized among the bottomsets. A few of the bands mark slightly convex-up reactivation surfaces confined to the topmost of the unit (see 1 of plate 3), and in one case (see 2 of plate 3), the dark sand above the surface is cross-laminated, an up-slope current being indicated. Four limonite-defined reactivation surfaces are draped lower down by mud (as in 2 of plate 3), but a comparable number of reactivation surfaces lie within foreset groups and lack a drape.

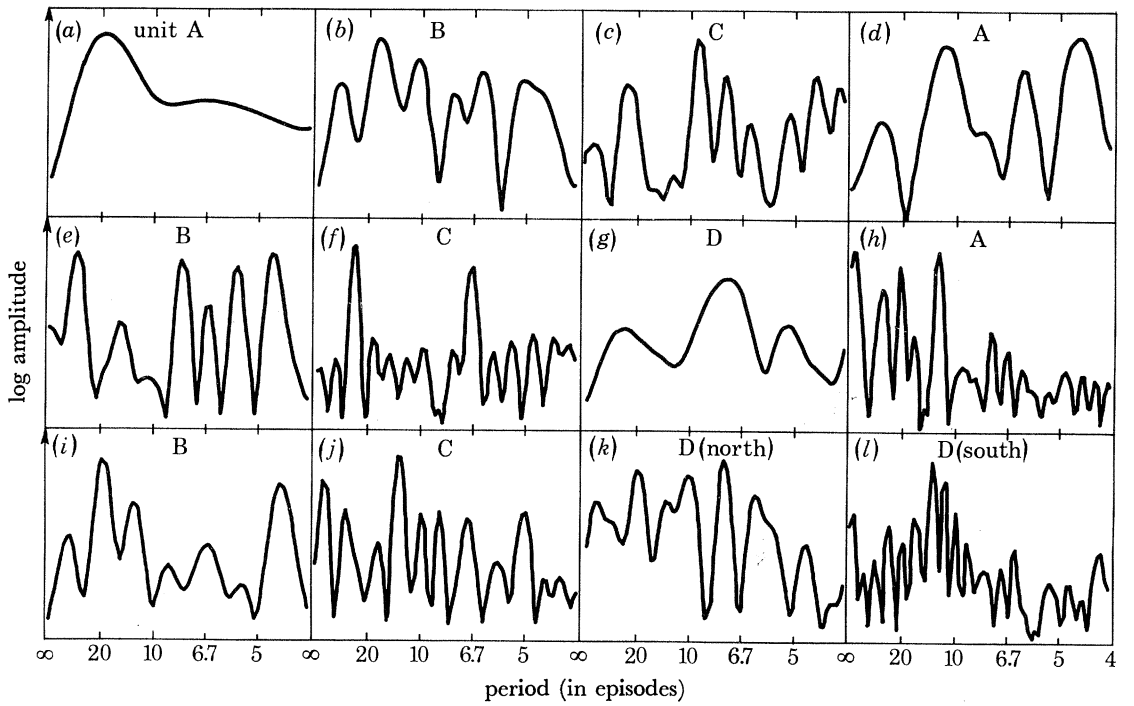

FIGURE 23. Wavelength spectra established by Fourier analysis of time-series for drape spacing. (*a*)–(*c*) Hog's Back Sandpit. (*d*)–(*g*) West Heath Common Sandpit. (*h*)–(*l*) Pendean Sandpit.

The limonite concentrations pick out a wide variety of bioturbation: (i) circular to oval burrows up to 0.06 m diameter and with occasional menisci (see 3 of plate 3), (ii) clustered oval to circular vague mottles or distinct traces up to 0.015 m across (see 4 of plate 3), (iii) occasional small upright tubes, and (iv) infrequent stout pellet-filled burrows. Mottling is often conspicuous at and just below the reactivation surfaces (see 1 of plate 4).

The time-series of drape spacings (see figure 24*d*) is random in terms of the runs and turning points tests (see table 1) but appears nonetheless to comprise irregular cycles (see figure 23*b*). Boundaries between depositional bundles are tentatively drawn at episodes 4, 20, 30, 38, 52, 60, 68, 78 and 96, yielding bundle lengths of 16, 10, 8, 14, 8, 8, 10 and 18 episodes. Among them the total drape spacing and bundling strength are positively correlated with size (see figure 24*e*,*f*). The sequence of drape lengths (see figure 24*d*) is significantly different from random almost at the 1% level (see table 1), figure 24*d* revealing two unequal clusters of medium and long drapes.

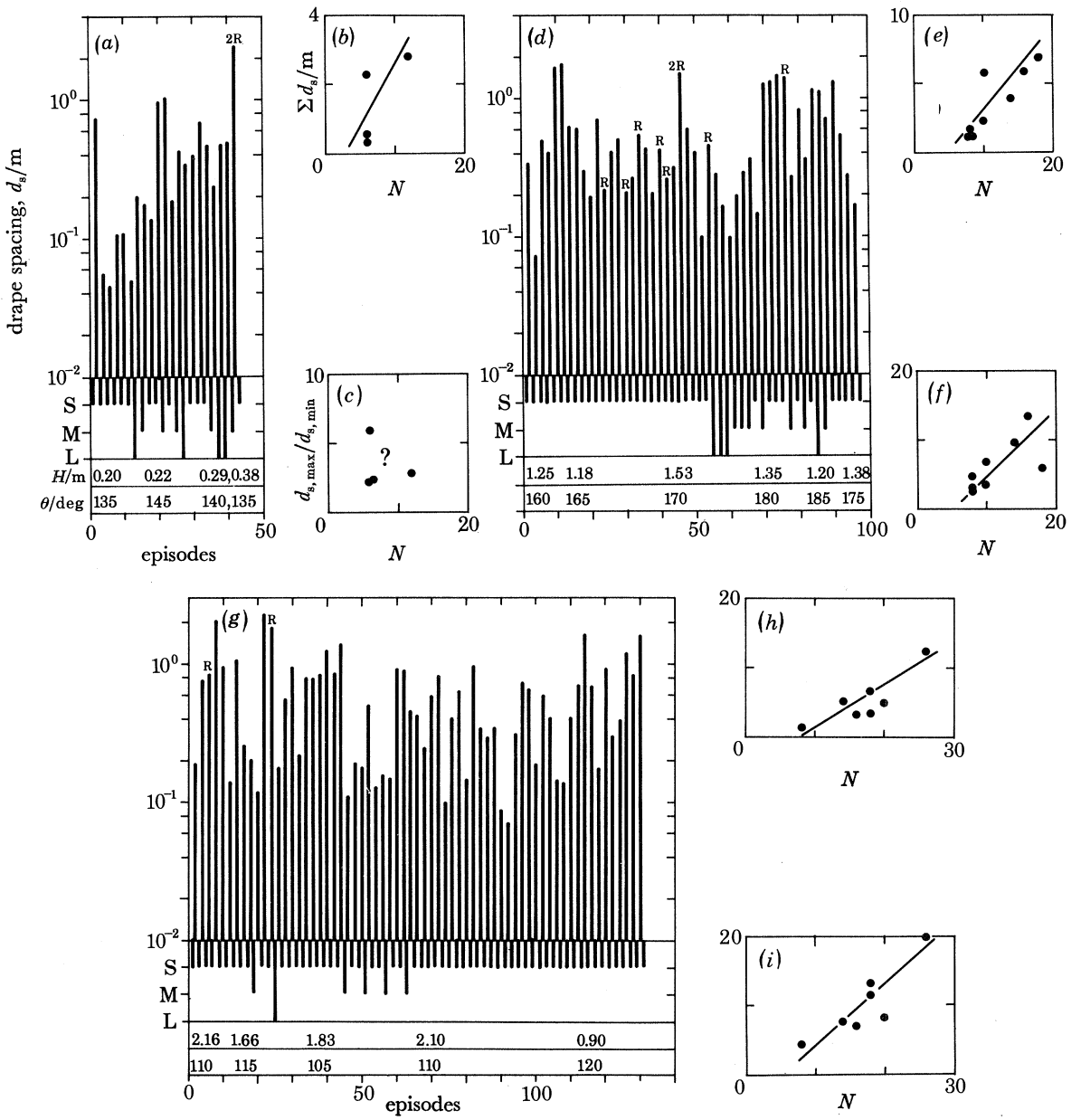

FIGURE 24. Properties of cross-bedded units with mud drapes, Hog's Back Sandpit: (*a*)–(*c*) unit A; (*d*)–(*f*) unit B; (*g*)–(*i*) unit C. (*a*), (*d*), (*g*) Time-series for drape spacing and development. (*b*), (*e*), (*h*) Total drape spacing in a depositional cycle (bundle) as a function of bundle length in episodes. (*c*), (*f*), (*i*) Bundling strength of a depositional cycle as a function of bundle length in episodes. S, short drapes; M, medium drapes; L, long drapes; *H*, local unit thickness; *θ*, local foreset dip azimuth; R, reactivation (numeral denotes number if more than one).

(*c*) *Unit* C

This bed, located a few metres higher stratigraphically than unit B, affords one of the thicker and lengthier records from the Folkestone Beds (see table 1) as well as extreme values for the activity and drape development ratio (see figure 22). The drapes of silty kaolinitic mud are overwhelmingly short and thin (one is, exceptionally, 0.04 m thick with a single bold rippled parting) (see also figure 21*c*) and the bottomset zone is nowhere thicker than 0.2 m. Only two

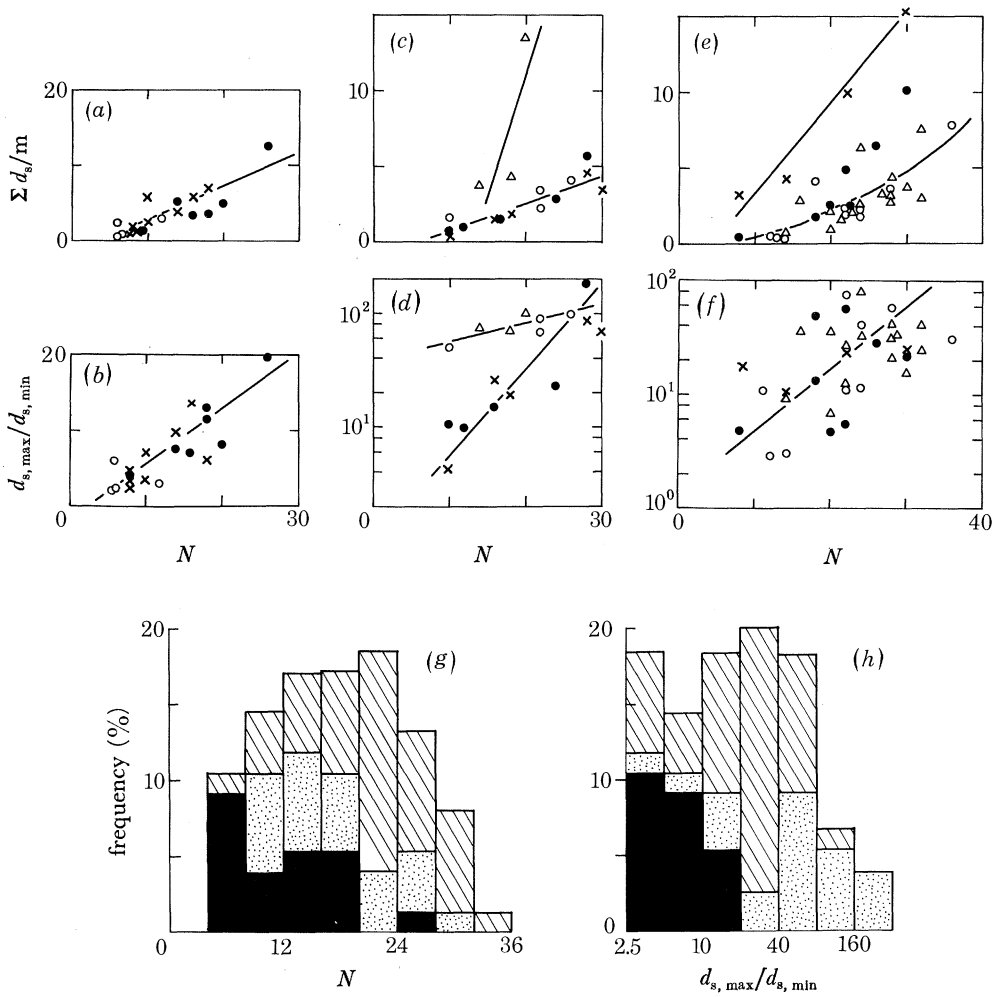

FIGURE 25. Summary of properties of cross-bedded units with mud drapes, (*a*), (*b*) Hog's Back Sandpit, (*c*), (*d*) West Heath Common Sandpit, (*e*), (*f*) Pendean Sandpit. Key to graphs: ○, unit A; ×, unit B; ●, unit C; △, unit D. (*g*) Frequency of depositional cycle (bundle) length; (*h*) frequency of bundling strength. Key to localities; solid black, Hog's Back Sandpit; stippled, West Heath Common Sandpit; hatched, Pendean Sandpit.

FIGURE 26. Properties of cross-bedded units with mud drapes, West Heath Common Sandpit: (*a*), (*e*), (*i*) unit A; (*b*), (*f*), (*j*) unit B; (*c*), (*g*), (*k*) unit C; (*d*), (*h*), (*l*), unit D. (*a*)–(*d*) Time-series for drape spacing and development. (*e*)–(*h*) Total drape spacing in a depositional cycle (bundle) as a function of bundle length in episodes. (*i*)–(*l*) Bundling strength of a depositional cycle as a function of bundle length in episodes. R, reactivation (numeral denotes number if more than one); F, mud film (numeral denotes number if more than one). For further details see figure 24.

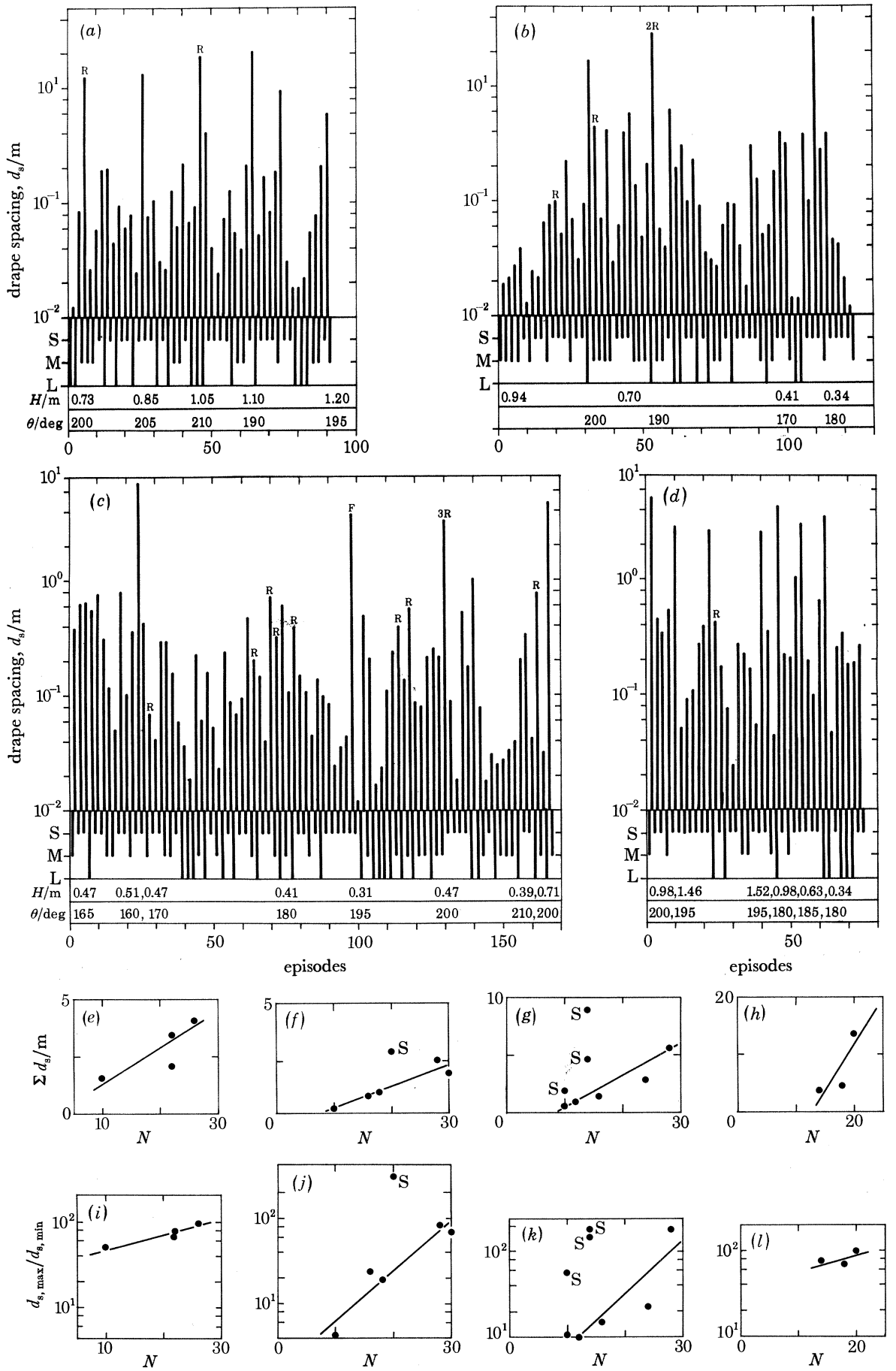

FIGURE 26. For description see opposite.

reactivation structures were recorded among the reversely graded foresets of commonly limonite-rich medium and some coarse sand. Bioturbation is common, however, and groups of siliceous sponges are found locally among the bottomsets sands.

The sequence of drape spacings (see figure 24*g*) lacks pattern on the basis of the turning points and runs tests and the drapes are not significantly clustered as regards length (see table 1). There are distinct periodicities at broadly 10 and 20 episodes (see figures 23*c*), and bundle boundaries are tentatively drawn at episodes 2, 20, 46, 54, 74, 92, 108, 122 (bundle lengths respectively 18, 26, 8, 20, 18, 16 and 14 episodes). Both Σd_s and the bundling strength are

TABLE 2.

locality	mean unit activity $\overline{m^2}$	mean bundle length (episodes)	mean bundle length, $\overline{\Sigma d_s}/m$	mean bundle bundling strength, $\overline{d_{s,max}/d_{s,min}}$
Hog's Back Sandpit				
unit A	0.129	7.5	1.50	3.38
unit B	0.777	11.5	3.60	6.25
unit C	1.07	17.1	5.25	10.2
West Heath Common Sandpit				
unit A	0.262	20.0	2.82	73.6
unit B	0.168	17.3	2.82	85.3
unit C	0.207	16.0	3.36	55.7
unit D	0.853	17.3	7.20	81.1
Pendean Sandpit				
unit A	0.171	21.6	2.28	27.2
unit B	0.595	18.5	8.08	19.2
unit C	0.429	20.5	10.10	21.7
unit D (north)	0.622	26.5	4.62	26.8
unit D (south)	0.573	21.6	2.63	31.0

PLATE 5. SMALL-SCALE FEATURES OF CROSS-BEDDED UNITS

1. Countercurrent ripples preserved by a mud drape and drape-rich bottomsets, approximately episodes 95–100, unit B, West Heath Common Sandpit. Pencil is 0.16 m long.
2. Ripple-like sand lens in parting within mud drape, episode 31, unit B, West Heath Common Sandpit. Pencil is 0.16 m long.
3. Clusters of drapes in unit C, West Heath Common Sandpit. Spade is 0.92 m long.
4. Weakly convex-up reactivation structure (marked by arrows), top of episode 28, unit C, West Heath Common Sandpit. The foresets overlying the structure are coarser grained than the sand below. Trowel is 0.28 m long.

PLATE 6. SMALL-SCALE FEATURES OF CROSS-BEDDED UNITS

1. Reactivation structure (marked by arrows) within episode 70, unit C, West Heath Common Sandpit. There is little sign of erosion but a marked coarsening of grain size occurs upward across the structure. Trowel is 0.28m long.
2. Reversely graded foresets several centimetres thick, unit A, Pendean Sandpit. Pencil is 0.15 m long.
3. Mud drapes in unit B, Pendean Sandpit. The lowest drape (episode 47) has up to six silty or sandy partings, and more than one parting is visible in some of the other drapes shown. Trowel is 0.28 m long.
4. Bottomset zone in unit D (South), Pendean Sandpit, approximately 22 m from the downstream end. Mud drapes occur throughout the zone, in at least twelve recognizable clusters (most shown by arrows), seen on cleaned (left) and naturally weathered (right) vertical faces. Trowel is 0.28 m long.

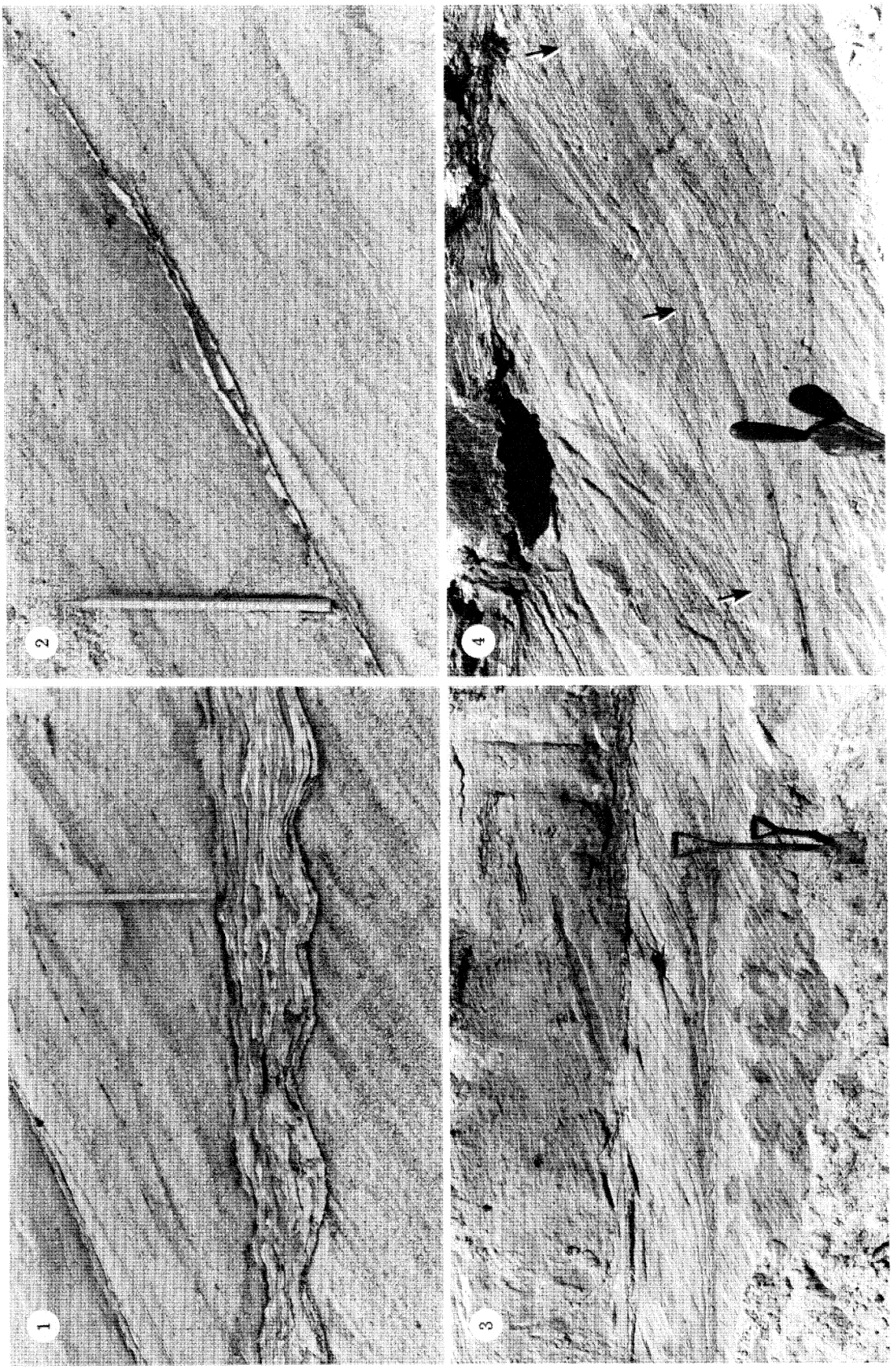

For description see opposite.

(*Facing p.* 328)

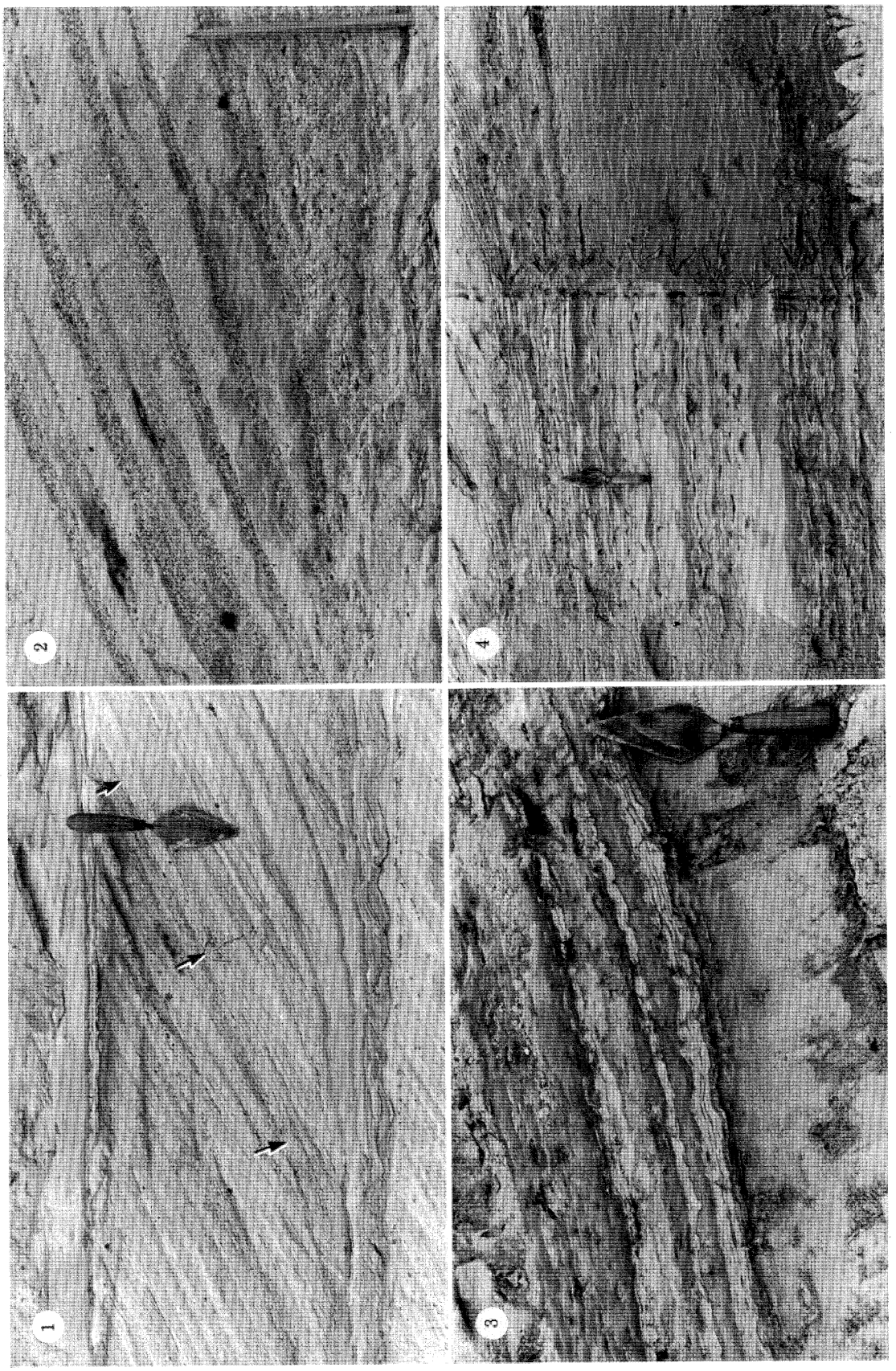

For description see p. 328.

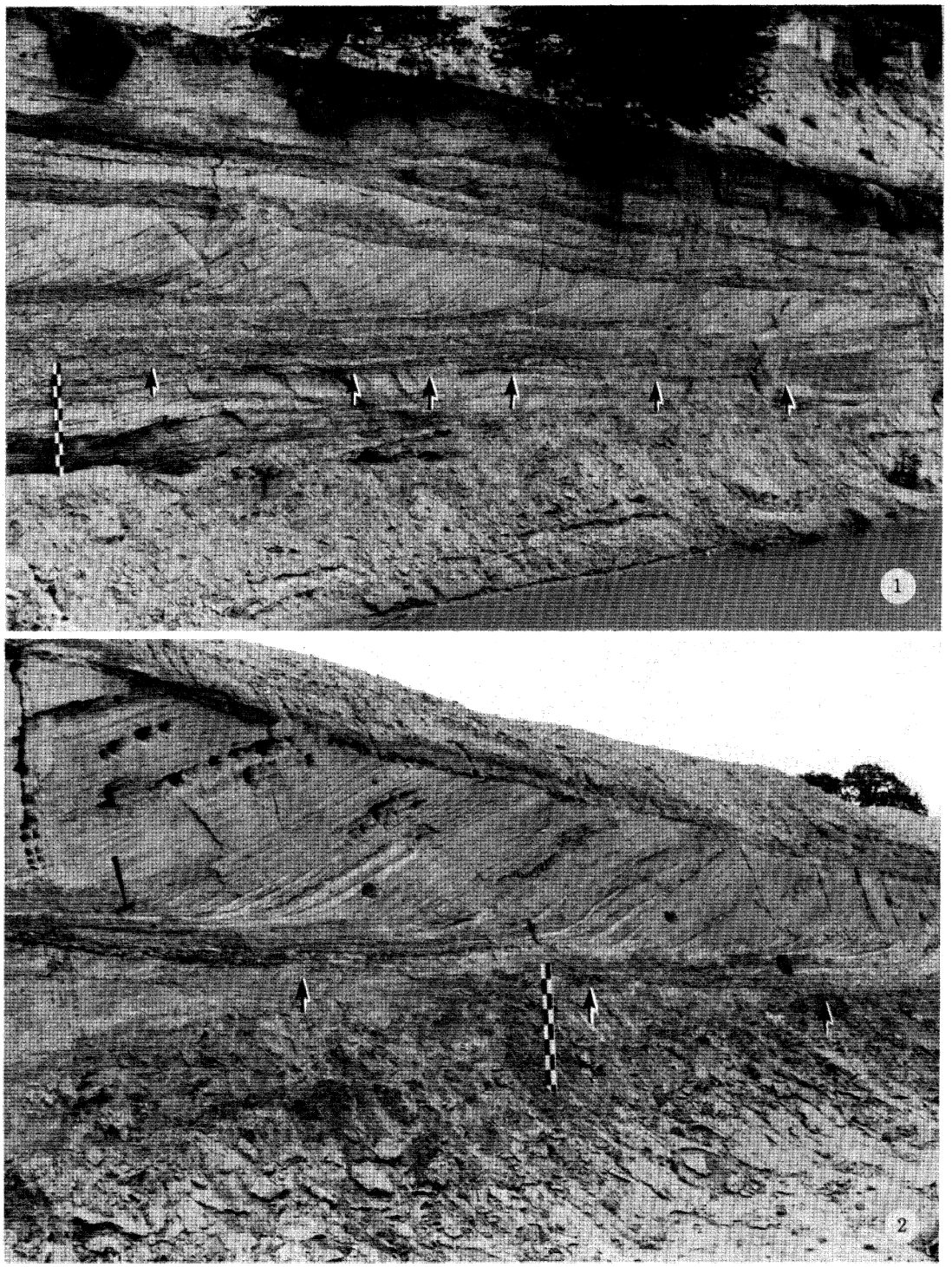

For description see p. 329.

For description see opposite.

positively correlated with N (see figure 24*h*, *i*). There is a weak long-term trend in drape spacing, the sand thickness drifting gradually downward up to episode 92 but subsequently increasing.

(*d*) *Comparison of units*

These three units form a homogeneous group in terms of grain size and trend in relation to mean unit activity. The bundling strength and Σd_s for the three plot each on a single trend (see figure 25*a*, *b*) and, with ascending activity, the unit mean bundle length, mean Σd_s, and mean bundling strength also increase (see table 2). The bundle length and bundling strength take comparatively low values (see figure 25*g*, *h*).

9. West Heath Common Sandpit

(*a*) *Unit* A

This set (see 2 of plate 1) is of medium and some coarse sand, and covers a long sequence of events (see table 1). It has a low activity and a rather high drape development ratio (see figure 22), drape length and spacing varying inversely (see figure 21*d*). Reversely graded foresets 0.02–0.04 m thick dominate the unit, the bottomset zone being nowhere thicker than 0.23 m. Sand episodes 6 and 46 each include a gently inclined reactivation surface (see 2 of plate 4), below which occurs cross-laminated mainly fine sand, whereas above come foresets of coarse sand. The mud drapes, characteristically overlain by iron-stained sand and in some cases with more than one parting (see 3 in plate 4), are generally well developed and commonly reach for several metres ahead of the foresets. They are silty and kaolinitic. Apart from the intense mottling below the reactivation structures, bioturbation is limited to a few upright cylindrical tubes and several large burrows with menisci.

The time-series (see figure 26*a*) is not significantly different from random in both drape spacing and length (see table 1). The drapes are noticeably clustered in the field, however, and bundle boundaries are largely on this evidence drawn at episodes 2, 24, 34, 52 and 78 (depositional cycle lengths respectively 22, 10, 22 and 26 episodes) (see also figure 23*d*). The bundling strength and Σd_s both increase with bundle size (see figure 26*e*, *i*).

(*b*) *Unit* B

This set (see 3 of plate 1) is exposed several hundred metres away from unit A and at about the same stratigraphical level. It is thinner and of lower activity and drape development ratio than unit A, but yields a significantly longer record (see table 1 and figure 22). Drapes of silty kaolinitic mud are well developed, showing no correlation between length and spacing (see figure

---

Plate 7. Clustering of drapes in cross-bedded units

1. Conspicuous clusters of dark-coloured mud drapes (above arrows) in unit A, Pendean Sandpit, as seen in an oblique view. Scale is marked in decimetres.
2. Clusters of pale-coloured drapes (above arrows) in unit D (north), Pendean Sandpit, as seen in an oblique view. Scale is marked in decimetres.

Plate 8. Closely spaced mud drapes in the lower part of the foreset zone, unit D (south), Pendean Sandpit

Sand–silt partings, often lenticular, are visible in the photograph within many of the drapes. Others have partings too thin to be photographed. Pencil, 0.15m long, for scale rests on episode 57 and points upward.

21*e*). The foresets, of fine to medium sand, overlie bottomsets in a zone up to 0.15 m thick, among which the troughs of ripple marks (rarely the crests) are partly coated with mud films each supporting a lens of iron-stained sand (see 4 of plate 4). Some of the drapes crowded into the bottomset zone overlie countercurrent ripples (see 1 of plate 5) and reach as far as 2.5 m ahead of the foresets they cover. Internal partings are present in nearly every case and conspicuous in some (see 1 of plate 5), swelling up locally, in a manner suggestive of incomplete ripple marks (see 2 of plate 5). Toward the younger end of the set, where the bottomsets fade out, the foresets end acutely on a level, pebble-strewn (lagged) erosion surface. Reactivation in the form of a slight steepening and coarsening of the foresets occurs within three groups of sand layers; in one of these (episode 54) the discontinuity is underlain by greatly expanded cross-laminated bottomsets.

Drape clustering is strikingly evident in the field, and the runs and turning points tests reveal the spacing to differ from random at better than the 5% level (see table 1). The drapes are significantly grouped in terms of length at better than the 10% level. In the light of the field evidence, and the indications from Fourier analysis (see figure 23*e*) of bundle lengths of approximately 17 and roughly 30 episodes, bundle boundaries are tentatively drawn at episodes 10, 40, 58, 86, 102 and 122 (bundle lengths respectively 30, 28, 18, 10, 16 and 20 episodes). The bundling strength and Σd_s are positively correlated with N (see figure 26*f,j*), except for one bundle (episodes 102–122) of anomalously large ratio and total spacing (labelled S in graphs). This bundle includes one foreset group 4.04 m long, unbroken by detectable reactivation structures.

(*c*) *Unit* C

This bed (see 4 of plate 1) follows unit B directly and on the same face, presenting the longest record of all from the pit (see table 1). The set comprises medium to coarse sand and is of moderate drape development ratio and activity (see figure 22), the longer drapes tending to accompany the thinner foreset groups (see figure 21*f*). Reversely graded foresets are dominant, either grading from a bottomset zone up to 0.15 m thick, or lying acutely on a mud drape in some places and a lagged erosion surface in others. The drapes are conspicuously grouped (see 3 of plate 5), clusters of layers reaching as much as 2–3 m ahead of the foresets. Several drapes bury countercurrent ripples and, locally, wave-current ripple marks. Mud films occur high up on many foresets in episode 98. Bioturbation is restricted to a few upright cylinders reaching down from the set top.

Two kinds of reactivation structure abound: (i) a slightly convex-up erosional disturbance followed by foresets steeper and coarser-grained than below (see 4 of plate 5), and (ii) foresets steeper and coarser-grained than below, but seldom coupled with an erosion surface, and never one that is convex-up (see 1 of plate 6).

Although drape-clustering is clearly visible in the field, the runs test applied to the series of spacings and lengths (see figure 26*c*) fails to show a significant difference from randomness (see table 1). The turning points test, however, reveals a significant contrast almost at the 5 % level. Using the field evidence, and the indication (ssee figure 23*f*) of a periodicity in excess of 20 episodes, boundaries between depositional bundles are tentatively placed at episodes 16, 30, 42, 52, 68, 92, 106, 134 and 144 (bundle lengths respectively 14, 12, 10, 16, 24, 14, 28 and 10 episodes). Two kinds of bundle are suggested by the total spacing and bundling strength plots (see figure 26*g, k*). One kind affords a graph similar to unit B (see figure 26*f, j*). The other (episodes 16–30, 92–106, 134–144) shows an exceptionally large bundling strength and total spacing (labelled S in graphs).

(*d*) *Unit* D

This set (see 5 of plate 1) could be a continuation of unit A, separated from it by an extent of covered ground (see table 1). The bed is of high activity but low drape development ratio (see figure 22), drape length being unrelated to spacing (see figure 21*g*). The foresets are reversely graded and consist of medium, coarse and some very coarse sand, either resting acutely on a granule- and pebble-strewn erosion surface or grading down into bottomsets in a zone up to 0.2 m thick. The drapes comprise silty kaolinitic mud. Reactivation and bioturbation are little in evidence.

The sequence of drape spacings (see figures 23*g*, 26*d*) differs significantly from randomness only under the runs test, and there is no significant drape clustering in terms of length (see table 1). Bundles are tentatively separated at episodes 12, 30, 44 and 64 (bundle lengths respectively 18, 14 and 20 episodes). Both the bundling strength and the total drape spacing seem to increase with N (see figure 26*h*, *l*).

(*e*) *Comparison of units*

The sets are distinguished by their low activity and generally high drape development ratio (see figure 22) but form a less homogeneous group than the beds at the Hog's Back Sandpit (see table 2). Unit D plots on a different and steeper trend than units A–C in terms of the total drape spacing and bundle length (see figure 25*c*). The bundling strength is relatively high (see figure 25*h*) and also positively correlated with bundle length (see figure 25*d*), with in this case units A and D plotting differently from units B and C. Moderate values typify the bundle length (see figure 25*g*).

10. Pendean Sandpit

(*a*) *Unit* A

This set (see 1 of plate 2), of low activity but moderate drape development ratio (see figure 22), consists of fine to medium and some coarse sand, and is dominated by foresets 0.02–0.06 m thick with a strong reverse grading (see 2 of plate 6). The ripple-marked and cross-laminated bottomset zone, crowded with mud drapes, reaches 0.42 m in thickness. Films of silty kaolinitic mud abound and the drapes are thick and well developed, with distinct silty to sandy partings; short, medium and long forms occur about equally (see figure 21*h*). Bioturbation is restricted to rare mottles and upright cylinders, and reactivation is altogether lacking.

The grouping of drapes evident in the field (see 1 of plate 7) is confirmed by the statistical tests (see figure 27*a* and table 1) and by the indications from Fourier analysis (see figure 23*h*) of periodicities ranging between about 15 and 35 episodes. The drapes are significantly clustered in terms of length (see table 1). Depositional bundles seem to be present with limits suggested to occur at episodes 20, 44, 56, 70, 94, 116, 138, 174, 186 and 214 (bundle lengths respectively 24, 12, 14, 24, 22, 22, 36, 12 and 28 episodes). This choice (there is some latitude) afforded the closest correlations of Σd_s and $d_{s,\max}/d_{s,\min}$ on the bundle length N (see figure 27*b*, *c*).

(*b*) *Unit* B

This set (see 2 of plate 2) lies about 15 m stratigraphically above unit A. It is of moderate activity and large drape development ratio (see figure 22), being dominated by foresets of medium sand which pass down into 0.25–0.35 m of bottomsets composed of fine to medium sand

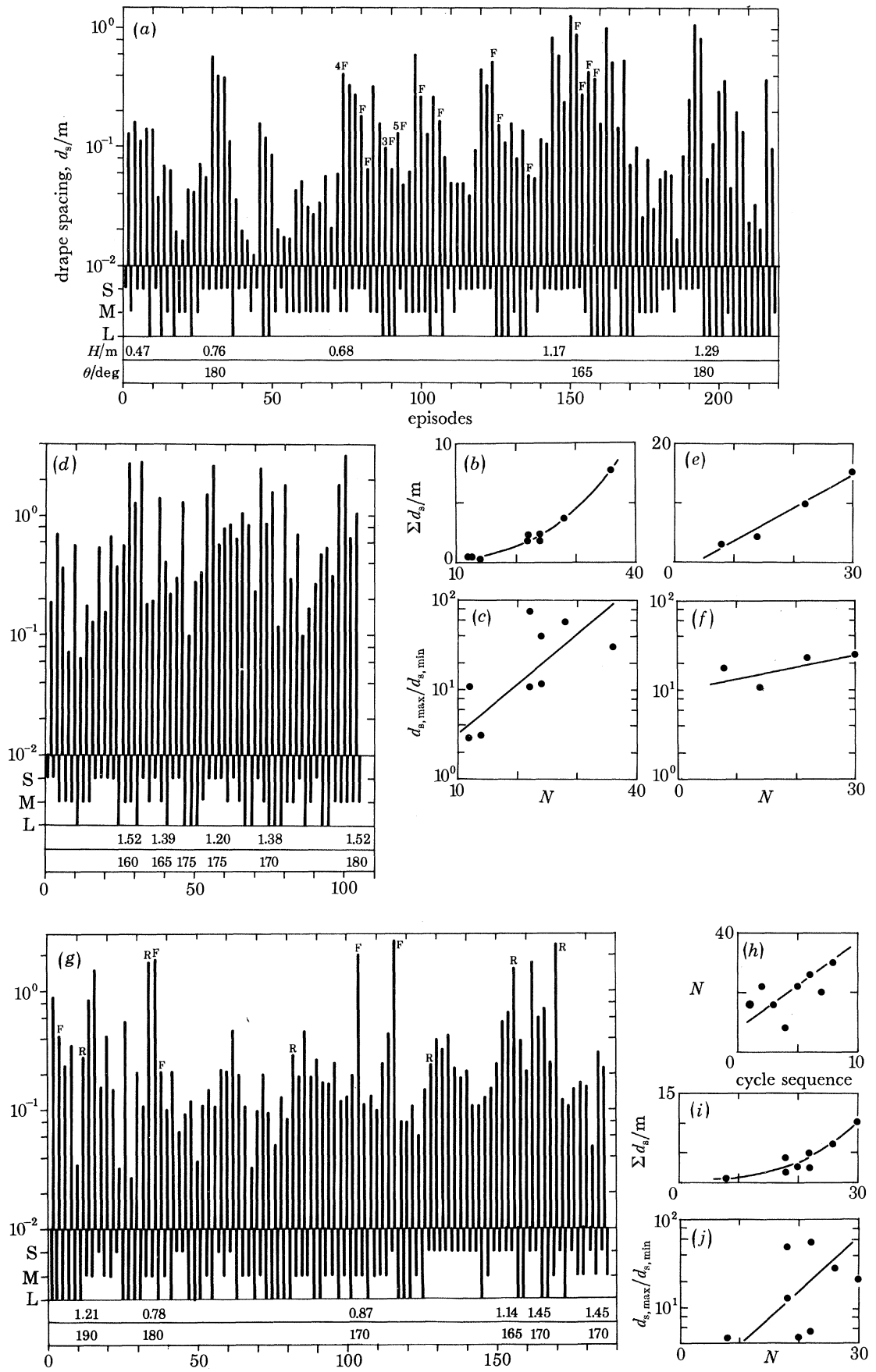

FIGURE 27. For description see opposite.

with numerous lengthy drapes of silty kaolinitic mud. The drapes are comparatively thick but shown no dependence of length on spacing (see figure 21*i*). Internal silty to sandy partings are well developed and many in the bottomset are ripple-marked. The parting in one long drape (episode 51) reveals up-slope-facing current ripples over the full vertical range of the set. In two cases (episodes 63 and 67), the drape mantles up-slope-facing cross-laminated ripple marks developed over the top of the foreset immediately beneath. There is no discordance of bedding, but reactivation may be suggested. One drape (episode 47) is 0.04 m thick with no fewer than five to six laterally extensive and largely ripple-marked sandy partings (see 3 of plate 6).

Some grouping of medium and long drapes is evident in the field, and the runs test points to a significant drape clustering at the 10% level (see table 1). Drape spacing is random according to the runs and turning points tests (see figure 27*d* and table 1), but the Fourier analysis points to several large groupings (see figure 23*i*). Depositional cycle boundaries are tentatively placed at episodes 12, 34, 48 (thick and possibly complex drape at episode 47), 78 and 86 (bundle lengths respectively 22, 14, 30 and 8 episodes). The bundling strength and total drape spacing are well correlated positively with N (see figure 27*e*,*f*).

(*c*) *Unit* C

This lies 5–10 m stratigraphically below unit A and in another part of the pit, consisting of reversely graded foresets of fine to medium and some coarse sand which pass down into fine-grained bottomsets in a zone 0.15–0.40 m thick (see 3 of plate 2). Reactivation takes the form mainly of an abrupt coarsening and slight steepening of the foresets first to overlie a mud drape, without any accompanying erosion. The activity is moderate and the drape development ratio high (see table 1 and figure 22). Mud films abound. Drapes of white to grey kaolinitic silt are very well developed, with long, medium and short forms occurring in that order of declining abundance, and drape spacing is negatively correlated with length (see figure 21*j*). All the medium and long drapes, and most short ones, have at least one silt–sand parting, and two to four partings, locally ripple-marked, occur in several of the lengthier examples. Bioturbation is limited to a few mottles, occasional stout burrows amongst the bottomsets, and rare upright cylinders.

A marked grouping of drapes is evident in the field (see 3 of plate 2) and the runs test applied to the spacings (see figure 27*g*) indicates a significant difference from randomness at better than the 1% level (see also table 1). The drapes in terms of length are also significantly clustered (see table 1). The field evidence, together with the indications from Fourier analysis (see figure 23*j*) of important groupings of 12 episodes and longer, permit depositional cycles to be separated at episodes 10, 28, 50, 68, 76, 98, 124, 174 (bundle lengths 18, 22, 18, 8, 22, 26, 20 and 30 episodes). This tabulation, together with figures 27*g* and 27*h*, suggest that drape spacing and bundle size increase from the older to younger parts of the set. The bundling strength and total drape spacing each increase with bundle length (see figure 27*i*,*j*).

FIGURE 27. Properties of cross-bedded units with sand drapes, Pendean Sandpit: (*a*)–(*c*) unit A; (*d*)–(*f*) unit B; (*g*)–(*j*) unit C. (*a*), (*d*), (*g*) Time-series for drape spacing and development. (*b*), (*e*), (*i*) Total drape spacing in depositional cycle (bundle) as a function of bundle length in episodes. (*c*), (*f*) (*j*) Bundling strength of a depositional cycle as a function of bundle length in episodes. (*h*) Bundle length as a function of position in sequence of bundles. R, reactivation F, mud film (numeral denotes number if more than one). For further details see figure 24.

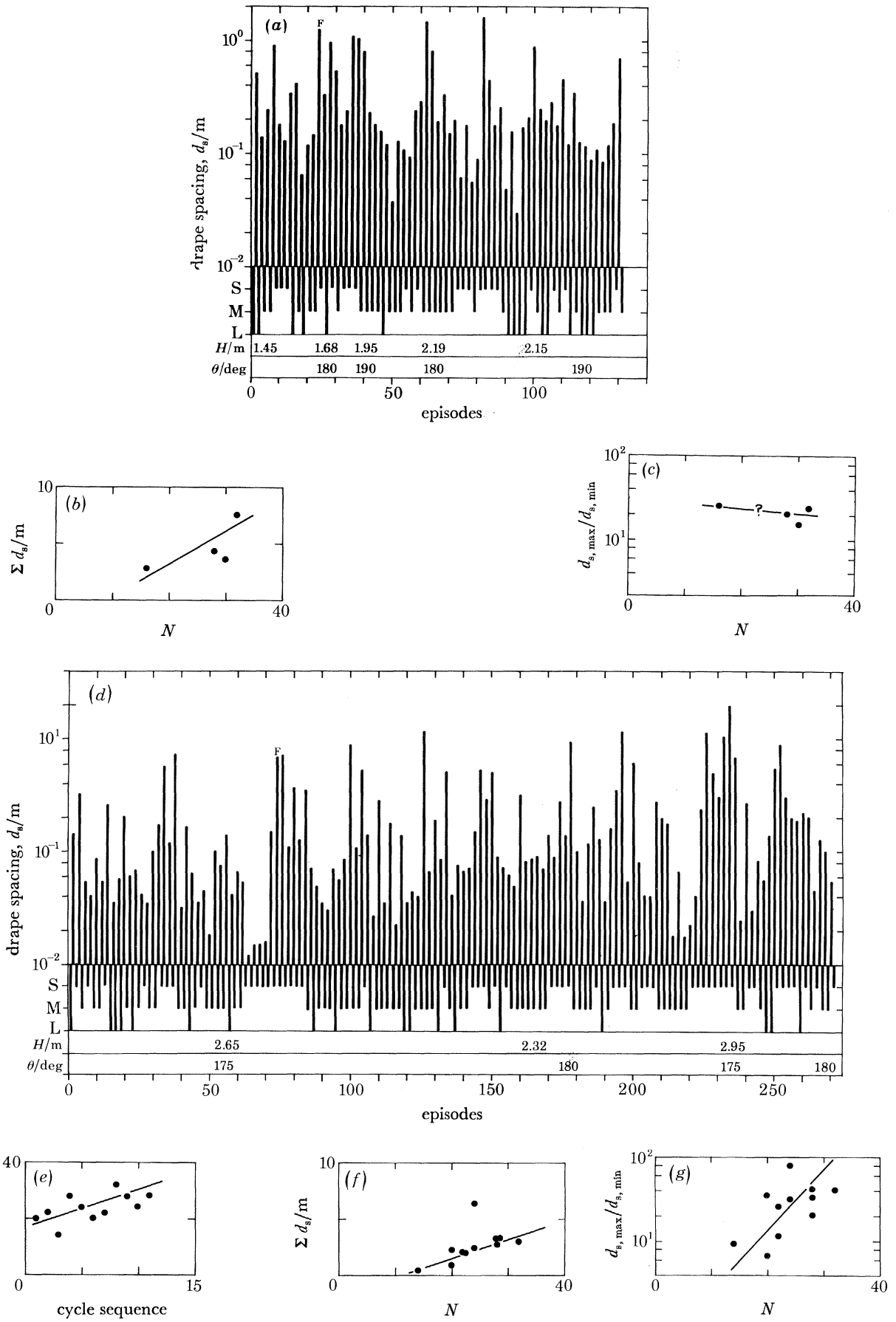

FIGURE 28. For description see opposite.

(*d*) *Unit* D (*north and south*)

Unit D lies a few metres above unit C on the same quarry face. The exposed extent exceeds 100 m, but only the northern (unit D (north), 5 bundles) and southern (unit D (south), 11 bundles) parts are directly accessible. Fourteen bundles were counted between the two accessible portions and a further four were estimated to lie in a covered interval.

Unit D (north) (see 4 of plate 2) is of low activity but high mud drape development ratio (see table 1 and figure 22). Foresets of fine to medium and considerable coarse sand pass down into locally rippled and cross-laminated fine-grained bottomset sands up to 0.45 m thick. Medium, short and long drapes occur in that order of declining abundance, and their spacing and length are negatively correlated (see figure 21*k*). As many as four internal silt–sand partings are present in some of the thicker and longer drapes. Bioturbation is rare and reactivation absent. The drapes are strikingly clustered (see 2 of plate 7), both drape spacing and length being distributed in a manner significantly different from random (see table 1). The time series (see figures 23*k* and 28*a*) reveals a distinct grouping of drapes matching that visible in the field, and bundles can be tentatively distinguished at episodes 18, 50, 78, 94 and 123 (bundle lengths respectively 32, 28, 16 and 30 episodes). The bundling strength ratio is apparently independent of N but the Σd_s-value increases with bundle size (see figure 28*b*, *c*).

Unit D gradually thickens as it youngs southward, at first by the strengthening of the bottomsets (see 5 of plate 2), but toward the extreme southern end by foreset expansion. Unit D (south) is of low activity but high drape development ratio (see table 1 and figure 22). Reversely graded foresets of fine to medium and some coarse sand overlie bottomsets up to 1.1 m thick composed of ripple-marked and cross-laminated fine sands profusely interbedded with lengthy clustered drapes of kaolinitic silty mud. Medium, short and long drapes occur in that order of decreasing abundance, the longer drapes accompanying the thinner foreset groups (see figure 21*l*). The drapes (see plate 8) are 0.001–0.03 m thick and almost invariably show a bold and commonly ripple-marked parting of clean quartz silt or sand. The marked ordering evident in the northern part of the bed persists in unit D (south). Not only are the drapes visibly grouped amongst the foresets (see 5 of plate 2) but also clusters of mud layers are separable within the bottomset zone (see 4 of plate 6). The series of drape spacings (see figures 23*l* and 28*d*) is significantly different from random under the runs test (see table 1) and shows important groupings longer than ten episodes or so. Drape length shows a highly significantly clustering (see table 1), the thicker drapes accompanying the thinner groups of foresets. It is suggested that bundles of foresets and drapes can be divided off at episodes 8, 28, 50, 64, 92, 116, 136, 158, 190, 218, 242 and 270 (bundle lengths respectively 20, 22, 14, 28, 24, 20, 22, 32, 38, 24 and 28 episodes). Drape spacing (see figure 28*d*) and bundle size (see figure 28*e*) gradually increase from older to younger parts of the set. Both the bundling strength and total spacing increase with bundle size (see figure 28*f*, *g*).

FIGURE 28. Properties of cross-bedded units with mud drapes, Pendean Sandpit: (*a*)–(*c*) unit D (north); (*d*)–(*g*) unit D. (south). (*a*), (*d*) Time-series for drape spacing and development. (*b*), (*f*) Total drape spacing in a depositional cycle (bundle) as a function of bundle length in episodes. (*c*), (*g*) Bundling strength of a depositional cycle as a function of bundle length in episodes. F, mud film (numeral denotes number if more than one). For further details see figure 24.

(*e*) *Comparison of units*

The sets form a homogeneous group typified by a high drape development ratio but low activity, and by a bundle length on average greater than at either the Hog's Back or West Heath Common Sandpits (see table 2 and figures 22, 25*e–h*). The bundling strength scatters widely but increases with bundle size. The Σd_s-value also grows with increasing N, unit B plotting on a steeper trend than units A, C and D.

11. Interpretation of cross-bedded units with mud drapes

(*a*) *Tidal origin*

Could the sets be of tidal origin? What seems incontestable faunally is the shallow-marine deposition of the Lower Greensand as a whole and of its French correlatives (Casey 1961; Mégnien & Mégnien 1980). Depths possibly never exceeded several tens of metres and could locally and at times have been significantly less. Land was nearby, to judge from the drifted timber – in some cases large logs – in the Folkestone Beds and the more delicate fossil plants detected at neighbouring levels (see also Casey 1961). A tidal origin therefore cannot be excluded.

Regional mappings of cross-bedding azimuths from the Folkestone Beds and its correlatives indicate a very strong net sand transport toward points between southwest and southeast (Schwarzacher 1953; Narayan 1963, 1971), except in the southern Bas Boulonnais, where the evidence suggests a northwesterly drift up to a possible local bedload convergence (Narayan 1971). The presence at most localities of occasional northerly dipping cross-bedding sets, however, means that tidal currents, albeit asymmetrical, could still have fashioned the deposits. As the source of asymmetry, ebb-flood evasion can be discounted, for under this régime there is areally a zero net bedload transport, unidirectional drifts beneath either flood or ebb dominant streams being purely local. The coupling of a tide with a substantial one-way river, thermohaline, or meteorological (including wind-drift) current better accounts for the regionally uniform sand transport system.

The close alternation of mud drapes with sandy foresets along the sets points to very many and rapid changes of current speed if not direction. Sandy foresets denote speeds in excess of several decimetres per second, while mud layers indicate slack waters drifting no faster than a few centimetres per second. Is the time-scale of this rhythm consistent with a tide? In answer we evaluate equation (8), given a value for d_s representative of the Folkestone Beds and plausible values for k, H, and U_{ces}, under the assumption that $U(t)$ is simple-harmonic and that the sand-driving stream runs for 12.4 hours. The described cross-bedding sets afford an overall mean drape spacing of 0.4 m and an overall mean set thickness after erosion of 1.2 m. Experimentally, equilibrium current ripples yield sets preserved to the extent of broadly one-half the ripple height (Jopling 1967; Allen 1973; Jopling & Forbes 1979), whence $H = 2.4$ m, and at 35% porosity $\gamma = 2070\,\mathrm{kg\,m^{-3}}$. We take $k = 0.83\,\mathrm{kg\,s^2\,m^{-4}}$ as suggested by river data (Colby 1964; Allen 1980*b*). Hence the tidal current peaked at approximately $0.95\,\mathrm{m\,s^{-1}}$ (*ca.* 1.75 knots), a value consistent with known shallow seas with sand waves (Stride 1963; Belderson *et al.* 1971; McCave 1971; Dalrymple *et al.* 1978). The implied scale of the foreset-drape couplets is thus significantly smaller than if mud was deposited only at neaps, or the sand was moved only when a river seasonally flooded an estuary. It is also significantly less than the time-scale on which major wind-drift and thermohaline currents (see for example Keller & Richards 1967; Boggs 1974), meteorological flows (see for example Wyrtki 1953, 1954*a*, 1954*b*), and storm currents

(see for example Murray 1970, 1972; Smith & Hopkins 1972; Gienapp 1973; Caston 1976; Forristall *et al.* 1976) seem to fluctuate.

Could an unsteady but essentially one-way river, wind-drift, thermohaline, or meterological current alone have shaped the sets? This seems most unlikely, merely on account of the complexity indicated by the drapes, with their silt–sand partings, and sandy foresets. Whatever currents fashioned the sets, their speed variation was doubly periodic, for the parting carried by almost every drape implies a second episode of bed-material transport, but much shorter and weaker than the dominant episode recorded by the foreset groups.

(*b*) *Nature of tidal régime*

The fundamental lithological rhythm in the Folkestone Beds just mentioned is fully stated as (i) mud drape (lower part), (ii) clean quartz silt or sand parting, commonly rippled, (iii) mud drape (upper portion), and (iv) sandy foresets. Two unequal semicycles (see plate 8) are implied. That defined by the lateral sequence mud drape (upper part) → sandy foresets → mud drape (lower portion) reflects a symmetrical but extreme change in current speed, from less than order 0.1 m s^{-1} to order 1 m s^{-1} and back. The other semicycle, from mud drape (lower part) → silt–sand parting → mud drape (upper portion), also denotes a symmetrical speed change but one much less extreme. Hence each parting records either a weak and short-lived remobilization of bed material, or the continued settling of coarse silt or sand, but at a flow speed between U_{cdm} and U_{ces} when mud is excluded. The implied current pattern is identical to those in figure 5, whence the drape–foreset rhythm could record a daily or twice-daily sequence of high and low waters accompanied by flow reversal. Supporting evidence is afforded by those drapes passing up to convex-up reactivation surfaces (for example unit B, Hog's Back Sandpit, see figure 24*d*), and by up-slope-facing cross-lamination and ripple marks on reactivation structures or within drapes (for example unit B, Hog's Back Sandpit, see 2 of plate 3, and unit B, Pendean Sandpit). The inferred strong sand-transport asymmetry is consistent with the conclusion, independently afforded by the regional palaeocurrents, that the tide was superimposed on a substantial one-way flow (see figure 4*b*,*c*), rather than made asymmetrical purely by wave distortion (see figure 4*a*). A final conclusion is that the Folkestone Beds sand waves were wholly subtidal, for mud drapes with partings cannot arise intertidally. The high sand-wave asymmetry implied by the Folkestone Beds sets was demonstrated elsewhere (Allen & Narayan 1964; Allen 1980*a*).

The grouping of foreset–drape couplets into bundles (see figures 23, 24, 26–28 and plate 7) suggests a spring–neap control. Do the bundles conform to the model (see figures 10–12), and is their length consistent with the early Cretaceous spring–neap cycle?. Various evidence (Rosenberg & Runcorn 1975; Lambeck 1977, 1980; Brosche & Sündermann, 1978; Scruton 1978) points to an early Cretaceous year of about 380 days with very nearly 30 days in the lunar month. That a spring–neap tide of diurnal kind fashioned the bundles is suggested by the following. (i) Few bundles (see figure 25*g*) violate the expectation of an early Cretaceous spring–neap cycle of roughly 15 diurnal or 30 semidiurnal tides (N.B. two episodes = one tidal cycle). (ii) Reference of bundle size to figure 10 points to a spring–neap cycle of diurnal or mixed predominantly diurnal type. (iii) Many bundles (for example unit D (north), Pendean Sandpit, see figure 28*a*) are asymmetrical in the manner suggested to result from mud armouring. (iv) As implied by figures 10 and 11 for spring–neap depositional cycles abbreviated through sand omission (see figure 16*a*), the bundling strength $d_{s,max}/d_{s,min}$ and total drape spacing Σd_s increase at each sandpit with bundle length (see figure 25*a*–*f*). (v) At Hog's Back (see figure 24*g*) and Pendean

(see figures 27*g*, 28*d*) Sandpits, there are cross-bedding units showing long-term trends in drape spacing and bundle length, consistent with an expected 'six-monthly' cycle of springs and neaps. (vi) In nine of the twelve units there is a weak negative correlation between drape spacing and length (see figure 21), and in several a marked clustering of drapes as to length (see table 1), both of which are consistent with a spring–neap cycle. (vii) In many of the thicker drapes, associated with the thinner foreset groups (see for example 3 of plate 6), there is more than one parting, pointing to sand omission perhaps during neaps, and to a dominant tidal stream which then peaked at less than U_{ces}.

There are no reliable means of estimating the spring–neap speed ratio $X_9 = U_{e,max}/U_{e,min}$ for the Folkestone Beds seas, but from the aforementioned characteristic peak stream of $0.95\,m\,s^{-1}$ and with $U_{ces} = 0.3\,m\,s^{-1}$, we obtain a characteristic spring–neap strength of $X_8 = (U_{e,max} - U_{ces})/U_{e,max} = 0.68$, pointing to a speed ratio of little greater than 3, on the basis of the lengthier bundles (see figure 10). Given that the dominant streams at neaps did not exceed $U_{ces} = 0.3\,m\,s^{-1}$, and that $U_{cdm} = 0.1\,m\,s^{-1}$ is the limiting value of any transverse component of tidal flow, the asymmetry of this characteristic tide becomes $X_1 > 0.52$ and the eccentricity $X_2 > 0.84$. With reference to the lengths of the depositional bundles, 0.3–1 could have been the range in neap–tide strength $X_7 = U_{e,min}/U_{ces}$.

Some aberrant features demand attention. The correlation and clustering of drapes recorded in figure 21 and table 1 are rarely strong, whence partly aperiodic non-tidal factors, for example storm depressions and river floods, may have strongly influenced drape production, perhaps to an extent through their control over mud concentration and wave action. Five of the 76 bundles described are not explicable by the sand-omission model, having either an exceptionally large bundling strength, or an unusually high total drape spacing, or both (see figure 26*f*, *j*, episodes 102–122; figure 26*g*, *k*, episodes 16–30, 92–106, 134–144; figure 28*f*, *g* episodes 218–242). Most include one or more exceptionally thick groups of foresets, and either they are candidates for abbreviation by mud suppression (see figure 16*b*), or they record unusual events, such as storms, which briefly enhanced sand transport.

Why do the three sites differ (see figure 25 and table 1)? Since from the relative textural uniformity of the sands U_{ces} varied little, it follows from figure 10 that $U_{e,max}$ could have been smaller at the Hog's Back than at either West Heath Common or Pendean. With reference to the bundle lengths, $U_{e,max}$ was possibly largest of all at Pendean. At Pendean and West Heath Common, where the bundles seem only moderately or not at all abbreviated, the sea may have been shallower than at the Hog's Back, where abbreviation is relatively severe. The prevalence of bioturbation at the Hog's Back, compared with West Heath Common and Pendean, also points to weaker currents and less sand transport there. Further proof that West Heath Common and Pendean saw the stronger currents lies in their strongly developed bottomsets (Allen 1968, p. 338). If the sea was shallowest at Pendean and West Heath Common, it might seem paradoxical that the drape development ratio there should generally be greater than at the Hog's Back (see figure 22). The mud-poor facies would have accumulated at a distance from land, however, beyond the influence of coast-hugging drifts. It is also conceivable that, lying further offshore than either West Heath Common or Pendean, the tidal ellipse at the Hog's Back was of only moderate eccentricity. Neither factor need be rejected, for in the southern North Sea (Houboult 1968; McCave 1971), depth increases with distance from land, while the tidal currents tend to decline in eccentricity and strength.

(*c*) *Time-scale of cross-bedded units*

What was the celerity of the Folkestone Beds sand waves? They advanced at the order of 100 m a^{-1}, judging from the distances covered (see table 1) and the numbers of inferred spring–neap bundles present (see figures 24, 26–28). The average is 81 m a^{-1} at the Hog's Back (range 47–120 m a^{-1}), 86 m a^{-1} at West Heath Common (range 49–193 m a^{-1}), and 102 m a^{-1} at Pendean (range 51–202 m a^{-1}, in agreement with the independent conclusion that the Hog's Back Sandpit saw the weakest flows. These comparatively high rates may reflect the relative importance of the one-way current thought to have accompanied the Folkestone Beds tide. North Sea and Irish Sea sand waves, admittedly probably taller and less asymmetrical than the Cretaceous examples, seem to travel at some 20 m a^{-1} (Jones *et al.* 1965; Langeraar 1966; McCave 1971; Terwindt 1971 *a*). Chesapeake Bay sand waves are about 2 m high and move at rates of 22.2–61.3 m a^{-1} (Ludwick 1971), thus just overlapping with the Folkestone Beds structures.

How much time is represented by erosion surfaces within the Folkestone Beds? The average

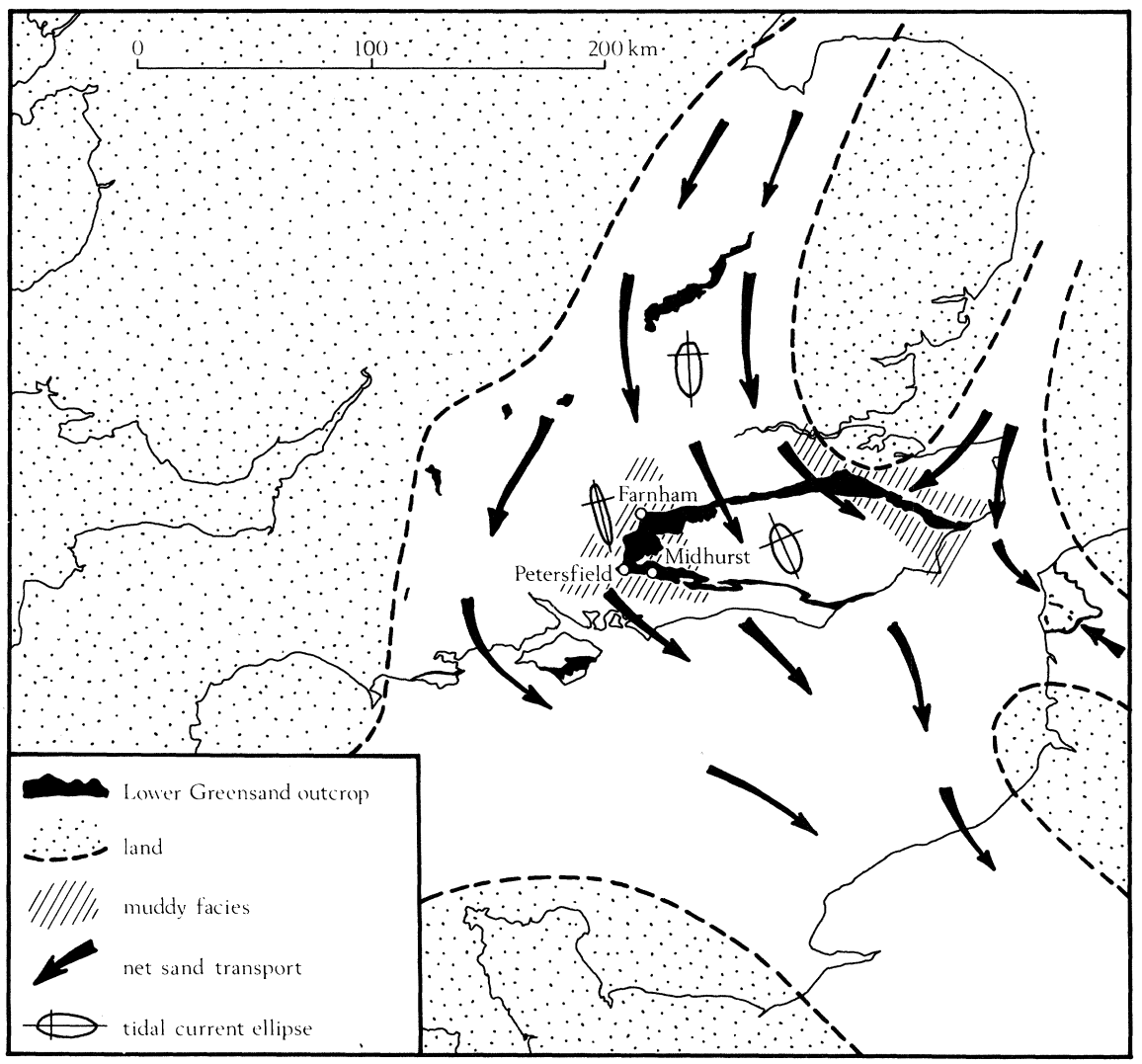

FIGURE 29. Tentative palaeogeography and sand dispersal system for the Folkestone Beds and its correlatives in southeast England and the Bas-Boulonnais.

cross-bedded unit in the Lower Greensand is only 1.05 m thick (Narayan 1971), yet the Folkestone Beds itself, to which this value also applies, is nowhere thicker than 80–90 m (see figure 17). A borehole through it would on average cut only 80 cross-bedding sets, representing a mere 80 years of sedimentation with the above rates of sand-wave travel! Hence most of the time represented by the Folkestone Beds must be expressed by the erosional surfaces between cross-bedded units. Attributing 10^5 years to the formation - plausible, but a guess - each erosional boundary would on average record 1.25×10^4 years of sedimentary activity, a period long enough for the creation and destruction of many sand waves and even large shoals.

(*d*) *Regional implications*

The tentative map (see figure 29) follows Anderton *et al.* (1979, fig 15.7) with modifications suggested by several sources (Schwarzacher 1953; Casey 1961; Narayan 1963, 1971; Middlemiss 1975). The Folkestone Beds and its correlatives apparently formed in a broad, shallow, island-studded strait connecting northern and southern seas. Sand waves existed widely on the sea floor, and there were many large and tall sand-wave-covered banks and shoals, to judge from the complex geometries sketched in figure 18. The muddiest water lay closest to shore. The strait was affected by a diurnal tide, least rotary near to land, and through it flowed a substantial one-way current, much as Sorby (1858) had deduced. Possible parallels are furnished by the Malacca Strait (Keller & Richards 1967) and the Taiwan Strait (Boggs 1974), each containing sand-wave fields influenced by the tide combined with either a meteorological (Malacca Strait) or thermohaline (Taiwan Strait) current.

12. General conclusions

The spatial distribution of mud drapes in subtidal sand waves is described quantitatively by using tidal theory, knowledge of real tides, and knowledge of sand and mud transport. Drape thickness and extent are enhanced by increasing tidal asymmetry and eccentricity, decreasing tidal current strength, and increasing sand-wave asymmetry. In the simple case of a strongly asymmetrical sand wave adjusted to a strongly asymmetrical tide (shallow-water effect or superimposed one-way current), a distinctive lithological couplet forms in response to each tidal cycle. Sandy foresets and bottomsets accumulate on the steeper face of the sand wave while the dominant tidal stream exceeds the sand threshold. Little or no sand transport occurs during the flow in the opposite direction of the subordinate stream, which either fails to reach the sand threshold or over-reaches it but little. Mud is deposited as a drape over the foresets and bottomsets during the times of slack water associated with much of this period of reduced flow. The drape is compound. It includes a central parting of clean quartz silt or sand which represents either bedload transport by the stronger currents of the subordinate stream, or the settlement of silt or sand where those currents fail to reach the sand threshold but over-reach the critical speed for mud deposition. The couplet therefore expresses a sand depositional episode and a complex mud depositional episode, one of each kind to a tidal cycle.

The waxing and waning of the tides from neaps to springs and back to neaps creates patterns in the spacing of drapes within sand waves. The character of these patterns depends on tidal régime and on the strength of the peak neap and peak spring streams compared with the sand threshold. The number of foreset–drape couplets in each spring–neap depositional cycle (bundle) equals the number of tides in the spring–neap cycle only when the neap-tide strength exceeds the sand

threshold. Otherwise the bundles become abbreviated through sand omission, there being fewer couplets as defined than tides. Drapes formed at neaps may then include more than one parting. Storm waves can cause abbreviation through the suppression of mud deposition, with groups of sandy foresets, which drapes would separate under normal conditions, becoming fused into one exceptionally thick and in practice indivisible group. The two kinds of abbreviation are distinguishable by reference to correlations between bundle characteristics.

Patterns of mud drapes in cross-bedded units conforming well to the model are widely preserved in the early Cretaceous shallow-marine Folkestone Beds of the Weald. The units commonly exceed 2 m in thickness and consist of medium to coarse sand with some fine sand and granules. Almost all the drapes include a silt–sand parting, and many possess several partings. Some drapes extend up into convex-up reactivation surfaces or cover lines of ripple marks indicating reversal of flow. A repeated grouping of drapes is visibly present in cross-bedded units from the muddier facies of the Folkestone Beds, the drapes varying from a few centimetres to as much as several metres apart. These groupings (bundles) afford a coherent body of data suggesting that tides affected the area and that the tidal currents were strongly asymmetrical, highly eccentric, spatially variable in strength, and diurnal. The asymmetry seems attributable to the presence of a substantial one-way current. The lengths of the bundles are consistent with an early Cretaceous day somewhat shorter than at present (Scruton 1978; Lambeck 1980). Many bundles are abbreviated, apparently in consequence of sand omission, and a few show signs of mud suppression.

Independently of reports of mud-drape bundles in the Folkestone Beds (Allen 1980*b*, 1981), a similar bundling was described by Visser (1980) from subfossil cross-bedded sands in the Oosterschelde, a large tidal waterway in the southwestern Netherlands, and by Homewood (1981) and Homewood & Allen (1981) from the Miocene Molasse of Switzerland. Visser also attributes the grouping to the spring–neap cycle, in his case strongly semidiurnal, but his model is qualitative and without the revealing explicit physical basis and quantitative outcomes described above. A reanalysis of Visser's data is fully consistent with the model here described, even to evidence for a diurnal inequality, but with fewer signs of sand omission, probably on account of the estuarine rather than open-water setting. Homewood & Allen (1981) claim evidence for both diurnal and semidiurnal tides. However, the mud drapes of the Folkestone Beds, the Oosterschelde, and the Miocene Molasse constitute but one possible kind of master bedding in large tidal bedforms. Patterns in all kinds of master bedding should be expected in tidal bedforms in response to spring–neap and other tidal periodicities (Allen 1980*b*).

I am most grateful to Mr A. S. Murray (Ebenezer Mears (Sand Producers) Limited), Mr S. E. Borrow (S. E. Borrow Limited), and Mr J. L. C. McIntyre (Hall Aggregates (South Coast) Limited) for their interest and for permission to work at their pits. Dr C. McCann gave helpful advice on statistical techniques and furnished the computer programme for Fourier analysis.

13. References

Allen, G. P., Bonnefille, R., Courtois, G. & Migniot, C. 1974 *Houille Blanche* **29**, 129–136.
Allen, J. R. L. 1965*a* *Bull. Am. Ass. Petrol. Geol.* **49**, 547–600.
Allen, J. R. L. 1965*b* *J. Geol.* **73**, 95–116.
Allen, J. R. L. 1968 *Current ripples.* Amsterdam: North-Holland.
Allen, J. R. L. 1970 *J. Geol.* **78**, 326–351.
Allen, J. R. L. 1973 *Sedimentology* **20**, 189–202.

Allen, J. R. L. 1980*a* *Sediment Geol.* **26**, 281–328.
Allen, J. R. L. 1980*b* *Geol. Mag.* **117**, 437–446.
Allen, J. R. L. 1980*c* *Sedimentology* **27**, 317–323.
Allen, J. R. L. 1981 *Nature, Lond.* **289**, 579–581.
Allen, J. R. L. & Friend, P. F. 1976 *Sedimentology* **23**, 329–346.
Allen, J. R. L. & Narayan, J. 1964 *Geologie Mijnb.* **43**, 451–461.
Anderton, R. 1976 *Sedimentology* **23**, 429–458.
Anderton, R., Bridges, P. H., Leeder, M. R. & Sellwood, B. W. 1976 *A dynamic stratigraphy of the British Isles.* London: George Allen & Unwin.
Anwar, H. O. & Atkins, R. 1980 *J. Hydraul. Div. Am. Soc. civ. Engrs* **106**, 1273–1289.
Bagnold, R. A. 1941 *The physics of blown sand and desert dunes.* London: Methuen.
Bagnold, R. A. 1956 *Phil. Trans. R. Soc., Lond.* A**249**, 236–297.
Bagnold, R. A. 1966 *Prof. Pap. U.S. geol. Surv.* **422-I.**
Banks. N. L. 1973 *J. Sedim. Petrol.* **43**, 423–427.
Belderson, R. H., Kenyon, N. H. & Stride, A. H. 1971 *Rep. Inst. geol. Sci. (Lond.)* **70/14**, 151–170.
Boersma, J. R. 1969 *Geologie Mijnb.* **48**, 409–414.
Boggs, S. 1974 *Geology* **2**, 251–253.
Bokuniewicz, H. J., Gordon, R. B. & Kastens, K. A. 1977 *Mar. Geol.* **24**, 184–199.
Boothroyd, J. C. & Hubbard, D. K. 1974 *Misc. Pap. U.S. Army Corps Engrs Coastal Engng Res. Centre* (Fort Belvoir. Virginia, U.S.A.) **1–74.**
Bouma, A. H., Hampton, M. A. & Orlando, R. C. 1977*a* *Mar. Geotechnol.* **2**, 291–308.
Bouma, A. H., Hampton,, M. A., Wennekens, M. P. & Dygas, J. A. 1977*b* *Proc. Ninth Offshore Technology Conf.* 79–84.
Bouma, A. H., Hampton, M. A., Rappeport, M. L., Whitney, J. W., Teleki, P. G., Orlando, R. C. & Torresan, M. E. 1978 *Proc. Tenth Offshore Technology Conf.*, 2271–2284.
Bowden, K. F., Fairbairn, L. A. & Hughes, P. 1959 *Geophys. Jl. R. astr. Soc.* **2**, 288–305.
Brookfield, M. E. 1977 *Sedimentology* **24**, 303–332.
Brookfield, M. E. 1979 *Scott. J. Geol.* **15**, 81–96.
Brosche, P. & Sündermann, J. (ed.) 1978 *Tidal friction and the Earth's rotation.* Berlin: Springer Verlag.
Button, A. & Vos, R. G. 1977 *Sediment. Geol.* **18**, 175–200.
Cartwright, D. E. 1959 *Proc. R. Soc. Lond.* A**253**, 218–241.
Casey, R. 1961 *Palaeontology* **3**, 487–621.
Caston, V. N. D. 1976 *Estuar. coast. mar. Sci.* **4**, 23–32.
Colby, B. R. 1964 *Prof. Pap. U.S. geol. Surv.* **426-A.**
Collinson, J. D. 1970 *Georg. Annlr* A**52**, 31–56.
Daboll, J. M. 1969 *Contr. Dept. Geol. Univ. Massachusetts* **3-CRG.**
Dalrymple, R. W., Knight, R. J. & Lambiase, J. J. 1978 *Nature, Lond.* **275**, 100–104.
Dalrymple, R. W., Knight, R. J. & Middleton, G. V. 1975 In *Estuarine research, vol. II, Geology and engineering* (ed. L. E. Cronin), pp. 293–307. New York: Academic Press.
De Raaf, J. F. M. & Boersma, J. R. 1971 *Geologie Mijnb.* **50**, 479–504.
Defant, A. 1958 *Ebb and flow.* Ann Arbor: Michigan University Press.
Delft Hydraulics Laboratory 1962 *Demerara coastal investigation.*
Dewey, H., Bromehead, C. E. N., Chatwin, C. P. & Dines, H. G. 1924 *The geology of the country around Dartford.* London: H.M.S.O.
Dines, H. G. & Edmunds, F. H. 1929 *The geology of the country around Aldershot and Guildford.* London: H.M.S.O.
Dines, H. G. & Edmunds, F. H. 1933 *The geology of the country around Reigate and Dorking.* London: H.M.S.O.
Dines, H. G., Holmes, S. C. A. & Robbie, J. A. 1954 *Geology of the country around Chatham.* London: H.M.S.O.
Dines, H. G., Buchan, S., Holmes, S. C. A. & Bristow, C. R. 1969 *Geology of the country around Sevenoaks and Tonbridge.* London: H.M.S.O.
Doodson, A. T. & Warburg, H. D. 1941 *Admiralty manual of tides.* London: H.M.S.O.
Drapeau, G. 1970 *Maritime sediments* **6**, 90–101.
Eisma, D. & Kalf, J. 1979 *Neth. J. Sea Res.* **13**, 298–324.
Falcon, N. L. & Kent, P. E. 1960 *Mem. geol. Soc. Lond.* **2.**
Farrell, S. C. 1970 *Contrib. Dep. Geol. Univ. Massachusetts* **6-CRG.**
Forristall, G. Z., Hamilton, R. C. & Cardone, V. J. 1977 *J. phys. Oceanogr.* **7**, 532–546.
Fukuda, M. K. & Lick, W. 1980 *J. geophys. Res.* **85**, 2813–2824.
Furnes, G. K. 1974 *Mar. Geol.* **16**, 145–160.
Gadd, P. E., Lavelle, J. W. & Swift, D. J. P. 1978 *J. sedim. Petrol.* **48**, 239–252.
Gallenne, B. 1974 *Estuar. coast. mar. Sci.* **2**, 261–272.
Gibson, W. M. 1951 *J. U.S. Cst. Geodetic Surv.* no. 4 (December 1951), 54–58.
Gienapp, H. 1973 *Senckenberg. maritima* **5**, 135–151.
Göhren, H. 1971 *Die Küste* **21**, 6–16.
Gordon, C. M. 1975 *Mar. Geol.* **18**, M57–M64.

Granat, M. A. & Ludwick, J. C. 1980 *Mar. Geol.* **36**, 307–323.
Guy, H. P., Simons, D. B. & Richardson, E. V. 1966 *Prof. Pap. U.S. geol. Surv.* **462-I.**
Hayward, H. A. 1932 *Peoc. Geol. Ass.* **43**, 1–31.
Hine, A. C. 1977 *J. sedim. Petrol.* **47**, 1554–1581.
Hobday, D. K. & Tankard, A. J. 1978 *Bull. geol. Soc. Am.* **89**, 1733–1744.
Homewood, P. 1981 *Eclog. geol. Helv.* **74**, 29–36.
Homewood, P. & Allen, P. 1981 *Bull. Am. Ass. Petrol. Geol.* **65**, 2534–2545.
Houbolt, J. J. H. C. 1968 *Geologie Mijnb.* **47**, 245–273.
Humphries, D. W. 1956 *Geol. Mag.* **93**, 491–503.
Humphries, D. W. 1964 *Proc. Geol. Ass.* **75**, 39–59.
Hunt, R. E., Swift, D. J. P. & Palmer, H. 1977 *Bull. geol. Soc. Am.* **88**, 299–311.
Hydrographer of the Navy 1979*a* *Admiralty tide tables, vol.* 1. *European waters.* Taunton: Hydrographer of the Navy.
Hydrographer of the Navy 1979*b* *Admiralty tide tables, vol.* 2. *Atlantic and Indian oceans.* Taunton: Hydrographer of the Navy.
Hydrographer of the Navy 1979*c* *Admiralty tide tables, vol.* 3. *Pacific ocean and adjacent areas.* Taunton: Hydrographer of the Navy.
Inglis, C. C. & Allen, F. H. 1957 *Proc. Instn civ. Engrs* **7**, 827–868.
Inglis, C. C. & Kestner, F. J. T. 1958 *Proc. Instn civ. Engrs* **11**, 435–466.
Johnson, H. D. 1975 *Sedimentology* **22**, 45–74.
Jones, N. S., Kain, J. M. & Stride, A. H. 1965 *Mar. Geol.* **3**, 329–336.
Jonsson, I. G. & Carlsen, M. A. 1976 *J. Hydraul. Res.* **14**, 45–60.
Jopling, A. V. 1967 *J. Geol.* **75**, 287–305.
Jopling, A. V. & Forbes, D. L. 1979 *Geogr. Annlr* **A61**, 67–85.
Jordan, G. F. 1962 *Science, Wash.* **136**, 839–848.
Joseph, J. 1954 *Arch. Met. Geophys. Bioklim.* **A7**, 482–501.
Kamphuis, J. W. 1975 *J. WatWays Harb. Div. Am. Soc. civ. Engrs* **101**, 135–144.
Karahan, M. E. & Peterson, A. W. 1980 *J. Hydraul. Div. Am. Soc. civ. Engrs* **106**, 1345–1352.
Keller, G. H. & Richards, A. F. 1967 *J. sedim. Petrol.* **37**, 102–127.
Kendrick, M. P. 1972 *Phil. Trans. R. Soc., Lond.* A **272**, 223–243.
Kennedy, J. F. 1969 *A. Rev. Fluid. Mech.* **1**, 147–168.
Kent, P. E. 1949 *Proc. Geol. Ass.* **60**, 87–104.
King, W. B. R. 1954 *Q. Jl geol. Soc. Lond.* **110**, 77–101.
Kirby, R. & Oele, E. 1975 *Phil. Trans. R. Soc., Lond.* A **279**, 257–267.
Klein, G. deV. 1970 *J. sedim. Petrol.* **40**, 1095–1127.
Klein, G. deV. & Whaley, M. L. 1972 *Bull. geol. Soc. Am.* **83**, 3465–3470.
Knight, D. W. 1978 *J. Hydraul. Div. Am. Soc. civ. Engrs* **104**, 839–855.
Kranck, K. 1972 *J. sedim. Petrol.* **42**, 596–601.
Krone, R. B. 1962 *Flume studies of the transport of sediment in esturial shoaling processes.* Berkeley: University of California Hydraulic Engineering Laboratory.
Lambeck, K. 1977 *Phil. Trans. R. Soc., Lond.* A **287**, 545–594.
Lambeck, K. 1980 *The Earth's variable rotation.* Cambridge University Press.
Langeraar, W. 1966 *Hydrogr. Newsletter* **1**, 243–246.
Langhorne, D. N. 1973 *Mar. Geol.* **14**, 129–143.
Levell, B. K. 1980 *Sedimentology* **27**, 539–557.
Lüders, K. 1929 *Senckenbergiana* **11**, 123–142.
Lüders, K. 1936 *Annln Hydrogr. Berl.* **8**, 335–342.
Ludwick, J. C. 1970 *Chesapeake Sc.* **11**, 98–110.
Ludwick, J. C. 1971 *Tech. Rep. Inst. Oceanogr. Old Dominion Univ. Norfolk, Virginia* **2.**
Ludwick, J. C. 1975 *Mar. Geol.* **19**, 19–28.
Ludwick, J. C. & Wells, J. T. 1974 *Tech. Rep. Inst. Oceanogr. Old Dominion Univ., Norfolk, Virginia* **12.**
Maddock, T. 1969 *Prof. Pap. U.S. geol. Surv.* **662-A.**
Marmer, H. A. 1926 *The tide.* New York: Appleton.
McCabe, P. J. & Jones, C. M. 1977 *J. sedim. Petrol.* **47**, 707–715.
McCave, I. N. 1970 *J. geophys. Res.* **75**, 4151–4159.
McCave, I. N. 1971 *Mar. Geol.* **10**, 199–225.
McCave, I. N. 1973 *Mem. Soc. r. Sci. Liège* (6)**6**, 187–206.
McCave, I. N. & Swift, D. J. P. 1976 *Bull. geol. Soc. Am.* **87**, 541–546.
McCave, I. N. 1978 *Oceanus* **21**, 27–33.
Mégnien, C. & Mégnien, F. 1980 *Bull. Bur. Rech. geol. Min.* **101.**
Middlemiss, F. A. 1962 *Geol. Mag.* **99**, 33–40.
Middlemiss, F. A. 1975 *Proc. Geol. Ass.* **86**, 457–473.
Migniot, C. 1968 *Houille Blanche* **23**, 591–620.

Migniot, C. 1974 *Houille Blanche* **29**, 137–147.
Miller, R. L. & Kahn, J. V. 1962 *Statistical analysis in the geological sciences.* New York: Wiley.
Murray, S. P. 1970 *J. geophys. Res.* **75**, 4579–4582.
Murray, S. P. 1972 In *Shelf sediment transport: process and pattern* (ed. D. J. P. Swift, D. B. Duane & J. O. Pilkey). Stroudsburg, Pennsylvania: Dowden, Hutchinson & Ross, 127–142.
Narayan, J. 1963 *Nature, Lond.* **199**, 1246–1247.
Narayan, J. 1971 *Sediment. Geol.* **6**, 73–109.
NEDECO (Netherlands Engineering Consultants) 1961 *The Waters of the Niger Delta.* The Hauge: NEDCO.
Nio, S. D. 1976 *Geologie Mijnb.* **55**, 18–40.
Nordin, C. F. 1971 *Prof. Pap. U.S. geol. Surv.* **562-F**.
Nordin, C. F. & Algert, J. H. 1966 *J. Hydraul. Div. Am. Soc. civ. Engrs* **92**, 95–114.
Odd, N. V. M. & Owen, M. W. 1972 *Proc. Inst. civ. Engrs, Suppl.* **9**, 175–205.
Owen, M. W. 1970 *Rep. Hydraulics Research Station Wallingford* **83**.
Owen, M. W. 1971 *Proc. Fourteenth Congr. Int. Ass. Hydraulic Res.* **4**, 27–32.
Ozasa, H. 1974 *Coastal Engng Japan* **17**, 155–184.
Partheniades, E., Cross, R. H. & Ayora, A. 1969 *Proc. Eleventh Conf. Coastal Engng* **1**, 723–742.
Parker, W. R., Smith, T. J., & Kirby, R. 1980 In *Stratified flows* (ed. T. Carstens & T. McClimans), vol. 2, pp. 955–966. Trondheim: Tapir.
Postma, H. 1954 *Archf Neerl. Zool.* **10**, 405–511.
Postma, H. 1961 *Neth. J. Sea Res.* **1**, 148–190.
Pryor, W. A. & Amaral, E. J. 1971 *Bull. geol. Soc. Am.* **82**, 239–244.
Raudkivi, A. J. 1976 *Loose boundary hydraulics* (2nd edn). Oxford: Pergamon.
Raudkivi, A. J. & Hutchinson, D. L. 1974 *Proc. R. Soc. Lond.*, A**337**, 537–554.
Reid, C. 1898 *The geology of the country around Eastbourne.* London: H.M.S.O.
Reid, C. 1903 *The geology of the country near Chichester.* London H.M.S.O.
Reineck, H.-E. 1963 *Abh. senckenb. naturfarsch. Ges.* **505**.
Reineck, H.-E. & Wunderlich, F. 1967 *Natur Mus., Frankf.* **97**, 193–197.
Reineck, H.-E. & Wunderlich, F. 1969 *Senckenberg. maritima* **50**, 79–84.
Robinson, A. H. W. 1956 *J. Inst. Navig.* **9**, 20–46.
Robinson, A. H. W. 1960 *Geography* **45**, 183–199.
Rosenberg, G. D. & Runcorn, S. K. (ed.) 1975 *Growth rhythms and the history of the Earth's rotation.* London: Wiley.
Sager, G. & Sammler, R. 1975 *Altas der Gezeitenströmme fur die Nordsee, den Kanal und die Irische See* (3rd edn). Rostock: Seehydrographische Dienst D.D.R.
Schubel, J. R. 1969 *Neth. J. Sea Res.* **4**, 283–309.
Schwarzacher, W. 1953 *Geol. Mag.* **90**, 322–330.
Scott, J. T. & Csanady, G. T. 1976 *J. geophys. Res.* **81**, 5401–5409.
Scruton, C. T. 1978 In *Tidal friction and the Earth's rotation* (ed. P. Brosche, & J. Sündermann,). pp. 154–196. Berlin: Springer-Verlag,
Sheldon, R. W. 1968 *Limnol. Oceanogr.* **13**, 72–83.
Sleath, J. F. A. 1974 *J. WatWays Harb. Div. Am. Soc. civ. Engrs* **100**, 105–122.
Sleath, J. F. A. 1975 *Proc. Instn civ. Engrs* **59**, 309–322.
Sleath, J. F. A. 1976 *J. Hydraul. Res.* **14**, 155–164.
Smart, J. G. O., Bisson, G. & Worssam, B. C. 1966 *Geology of the Country around Canterbury and Folkstone.* London: H.M.S.O.
Smith, J. D. & Hopkins, T. A. 1972 In *Shelf sediment transport: process and pattern* (ed. D. J. P. Swift, D. B. Duane & H. O. Pulkey), pp. 143–180. Stroudsburg: Dowden, Hutchinson & Ross.
So, C. L., Pierce, J. W. & Siegel, F. R. 1974 *Geogr. Annlr.* **A56**, 227–235.
Sorby, H. C. 1858 *Edinburgh New Philosophical Journal* **7**, 226–237.
Sternberg, R. W. 1968 *Mar. Geol.* **6**, 243–260.
Sternberg, R. W. 1972 In *Shelf sediment transport: process and pattern* (ed. D. J. P. Swift, D. B. Duane & H. O. Pilkey), pp. 61–82. Stroudsburg, Pennsylvania: Dowden, Hutchinson & Ross, 61–82.
Sternberg, R. W. & Marsden, M. A. H. 1979 *Earth Surf. Processes* **4**, 117–139.
Stride, A. H. 1963 *Q. Jl geol. Soc. Lond.* **119**, 175–197.
Stride, A. H. 1965 *Nature, Lond.* **206**, 498–499.
Stride, A. H. & Chesterman, W. D. 1974 *Mar. Geol.* **15**, M53–M58.
Taitt, A. H. & Kent, P. E. 1958 *Deep boreholes at Portsdown (Hants) and Benfield (Sussex).* London: British Petroleum Company.
Terwindt, J. H. J. 1967 *Neth. J. Sea. Res.* **3**, 505–531.
Terwindt, J. H. J. 1971*a* *Mar. Geol.* **10**, 51–67.
Terwindt, J. H. J. 1971*b* *Geologie Mijnb* **50**, 515–526.
Terwindt, J. H. J. & Breusers, H. N. C. 1972 *Sedimentology* **19**, 85–98.
Thurrell, R. G., Worssam, B. C. & Edmunds, E. A. 1968 *Geology of the country around Haslemere.* London: H.M.S.O.

Topley, W. 1875 *The geology of the Weald.* London: H.M.S.O.
Ulrich, J. 1972 *Die Küste* **23**, 112–121.
Van Andel, T. H. & Postma, H. 1954 *Verh. K. ned. Akad. Wet.* (1)**20**(5), 1–245.
Van Veen, J. 1935 *Hydrogr. Rev.* **12**, 21–29.
Van Veen, J. 1936 *Onderzoekingen in de Hoofden.* 'S-Gravenhage: Algemeene Landsdrukkerij.
Van Veen, J. 1950 *Tijdschr. Kon. ned. aardrijks Genoot.* **67**, 43–65.
Visser, M. J. 1980 *Geology* **8**, 543–546.
Visser, M. P. 1970 *Dt. hydrogr. Z.* **17**, 197–201.
Walton, F. D. & Goodell, H. G. 1972 *Mar. Geol.* **13**, 1–29.
Wells, J. T. & Coleman, J. M. 1977 *Mar. Geol.* **24**, M47–M54.
Wells, J. T. & Coleman, J. M. 1978 *Geologie Mijnb.* **57**, 353–359.
Werner, F. & Newton, R. S. 1970 *Meyniana* **20**, 83–90.
Werner, F. & Newton, R. S. 1975 *Mar. Geol.* **19**, 29–59.
Werner, F., Arntz, W. E. & Tauchgruppe Keil 1974 *Meyniana* **26**, 39–62.
White, H. J. O. 1913 *The Geology of the country near Fareham and Havant.* London: H.M.S.O.
White, H. O. 1924 *The Geology of the country near Brighton and Worthing.* London: H.M.S.O.
White, H. J. O. 1926 *The geology of the country near Lewes.* London: H.M.S.O.
White, H. J. O. 1928 *The geology of the country near Ramsgate and Dover.* London: H.M.S.O.
Wiegel, R. L. 1964 *Oceanographical engineering.* Engelwood Cliffs, New Jersey: Prentice-Hall.
Worssam, B. C. 1963 *Geology of the country around Maidstone.* London: H.M.S.O.
Wunderlich, F. 1969 *Senckenberg. maritima* **50**, 107–146.
Wunderlich, F. 1978 *Senckenberg. maritima* **10**, 257–267.
Wyrtki, K. 1953 *Kieler Meeresforsch.* **9**, 155–170.
Wyrtki, K. 1954*a* *Kieler Meeresforsch.* **10**, 19–25.
Wyrtki, K. 1954*b* *Kieler Meeresforsch.* **10**, 162–181.
Young, B. & Monkhouse, R. A. 1980 *Proc. Geol. Ass.* **91**, 307–313.
Zabawa, C. F. 1978 *Science, Wash.* **202**, 49–51.

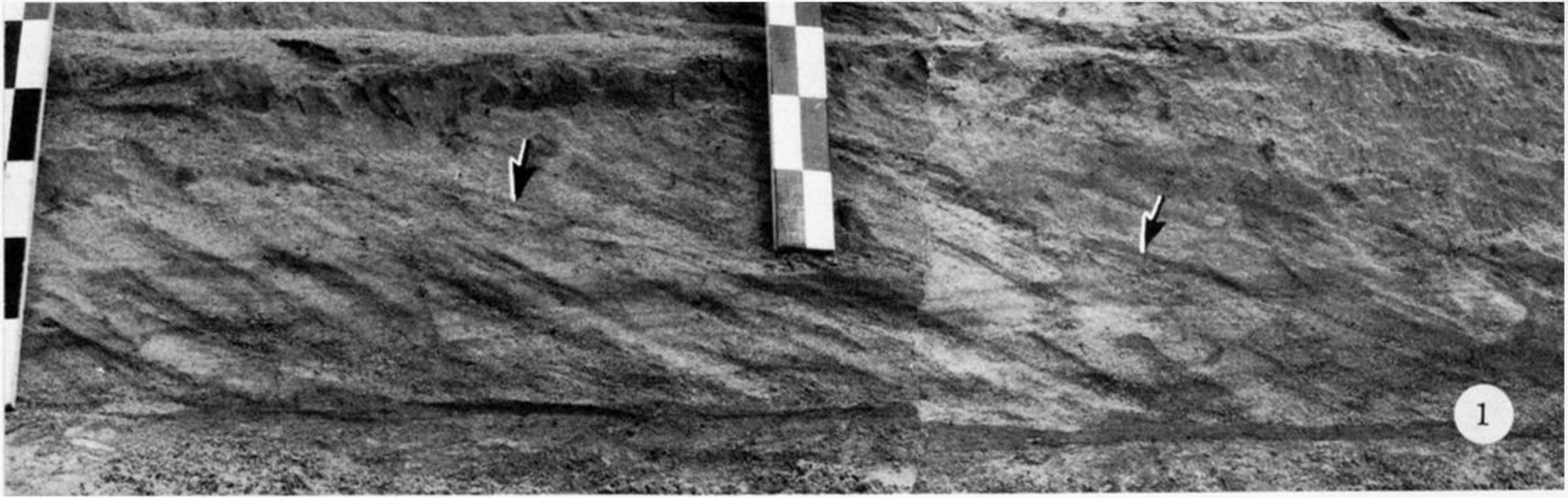

1. Part of the first few metres of unit A, Hog's Back Sandpit. Note lack of drapes, reactivation surfaces (shown by arrows), and locally acute basal contact. Scale is marked in decimetres.

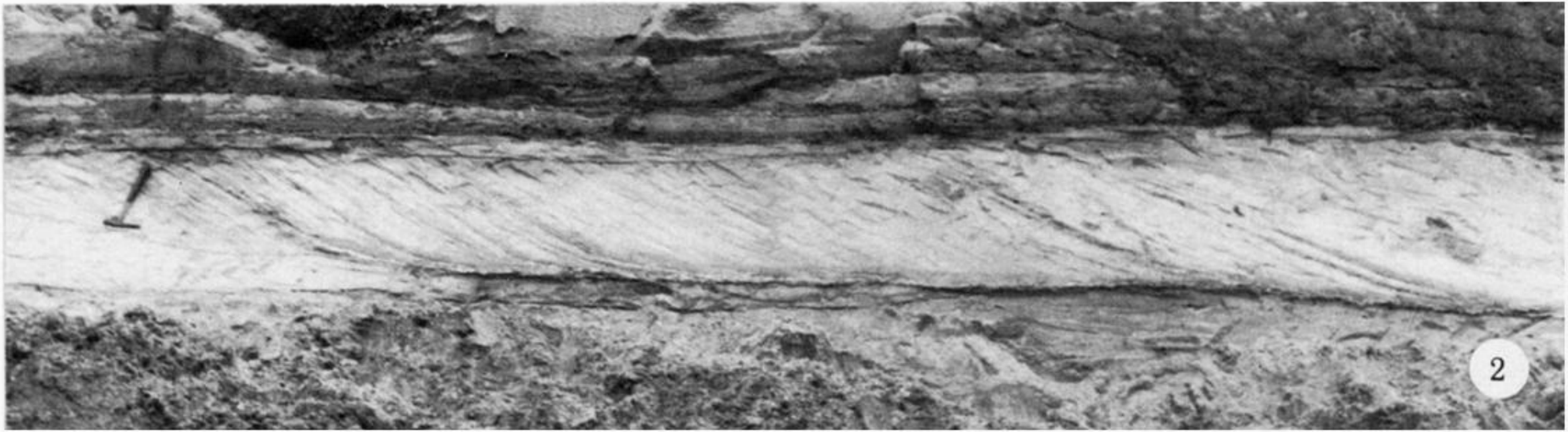

2. The first few metres of unit A, West Heath Common Sandpit. Hammer 0.38 m long rests on reactivation surface within episode 6. Note lengthy drapes among bottomsets.

3. Unit B, West Heath Common Sandpit, approximately 12–16 m from the start. Note drape-covered counter-current ripples at unit base. Scale is marked in decimetres.

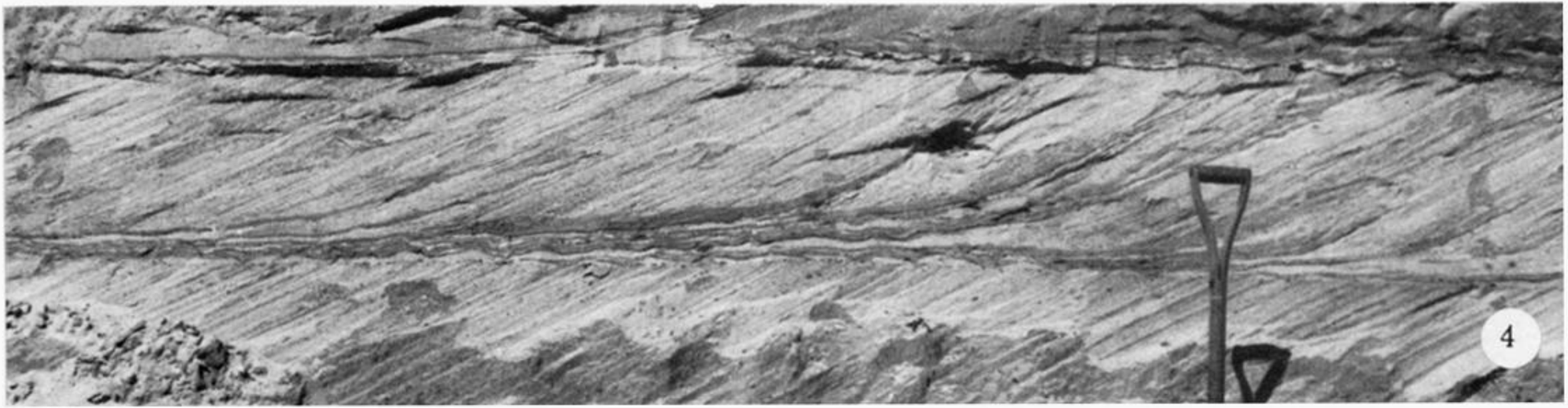

4. Unit C, West Heath Common Sandpit, approximately 15 m along its length. Note drape clusters and drape-covered ripple marks at unit base and on bottomsets. Spade handle (0.45 m visible) is for scale.

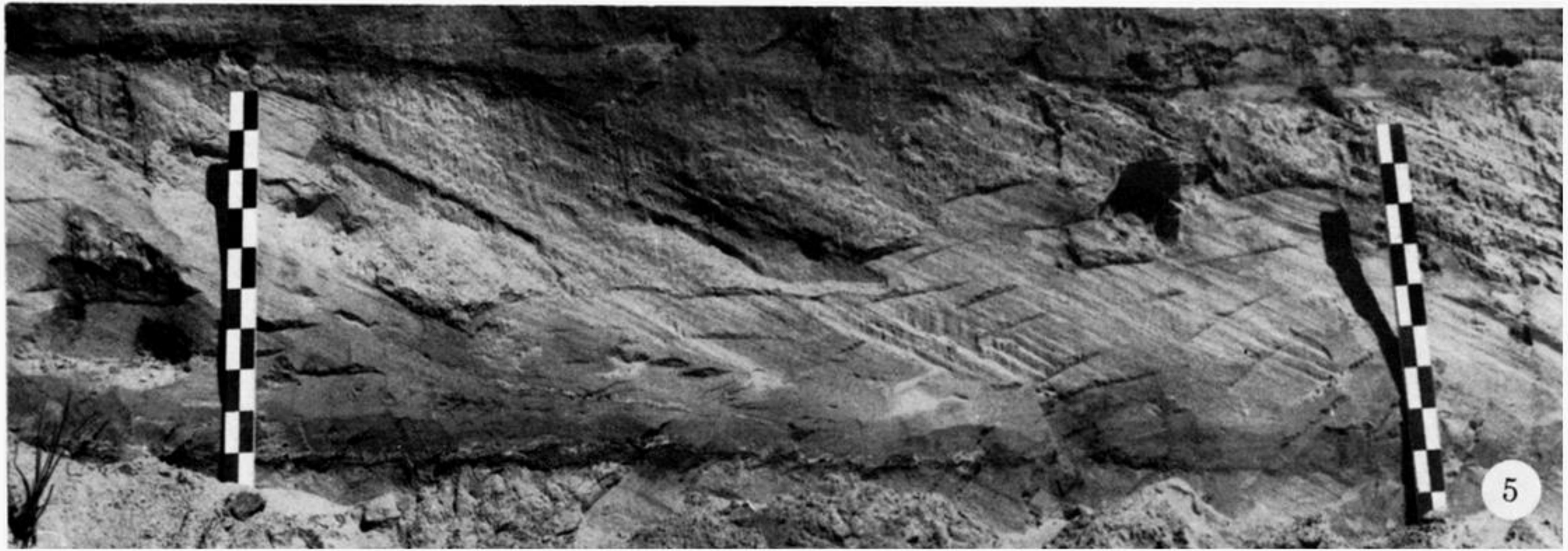

5. The first few metres of unit D, West Heath Common Sandpit. Note lack of reactivation, and poor development of drapes and bottomsets. Scales are marked in decimetres.

1. Slightly oblique view of middle portion of unit A, Pendean Sandpit. Note drape clusters and the extensive mud drapes amongst the well developed bottomsets. Scale is marked in decimetres.

2. Unit B, Pendean Sandpit, between approximately 6 and 13 m from the start. Dark iron-stained zones occur above the principal drapes. Scales are marked in decimetres.

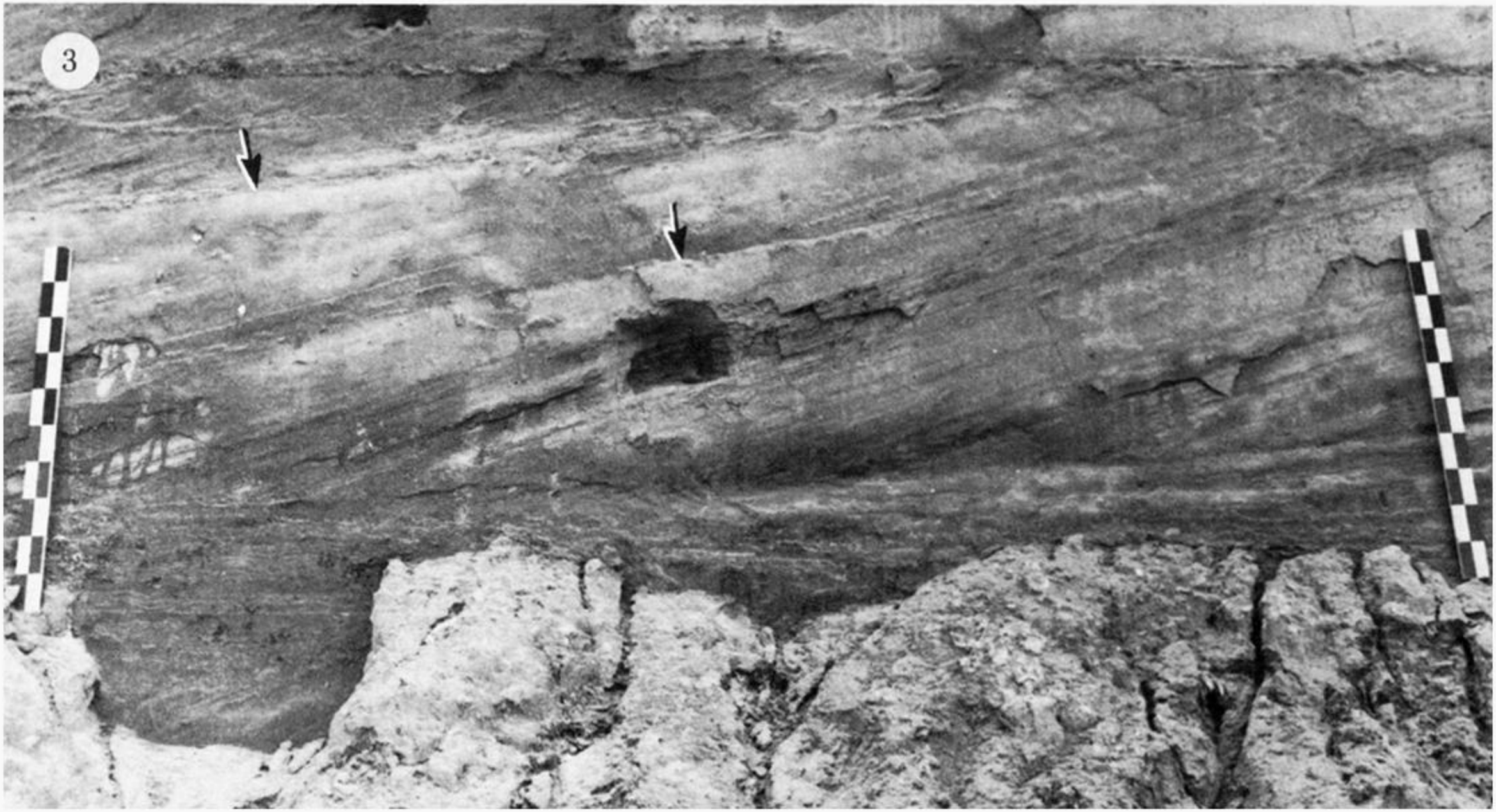

3. Unit C, Pendean Sandpit, between approximately 3 and 7 m from the downcurrent end. Note reactivation structures (shown by arrows) and thick bottomset deposits exposed in shallow pit near left-hand scale. Scales are marked in decimetres.

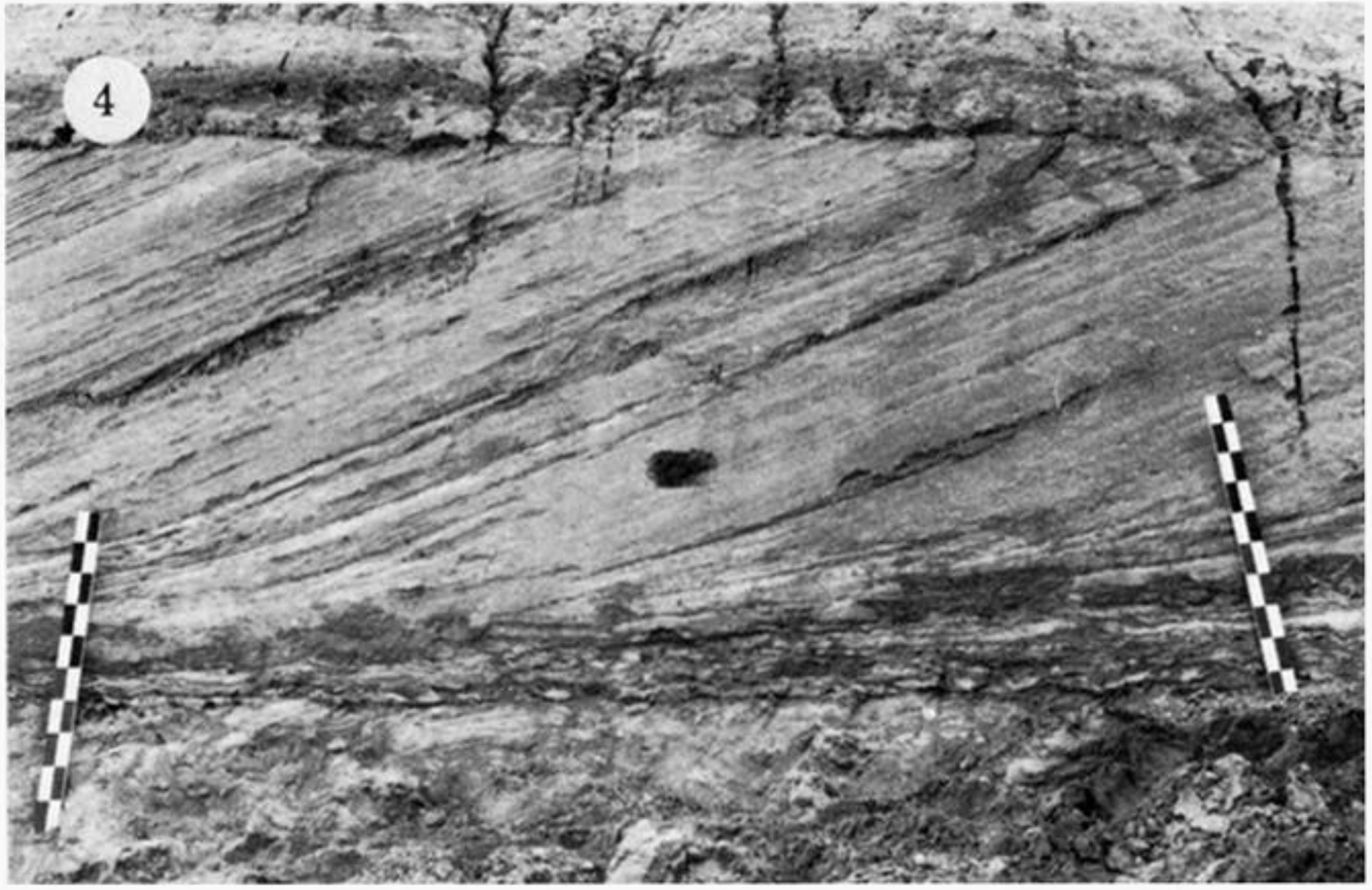

4. Unit D (north), Pendean Sandpit, between approximately 8 and 12 m from the start of the measured section. Note lack of reactivation, long drapes, and conspicuous bottomset zone. Scales are marked in decimetres.

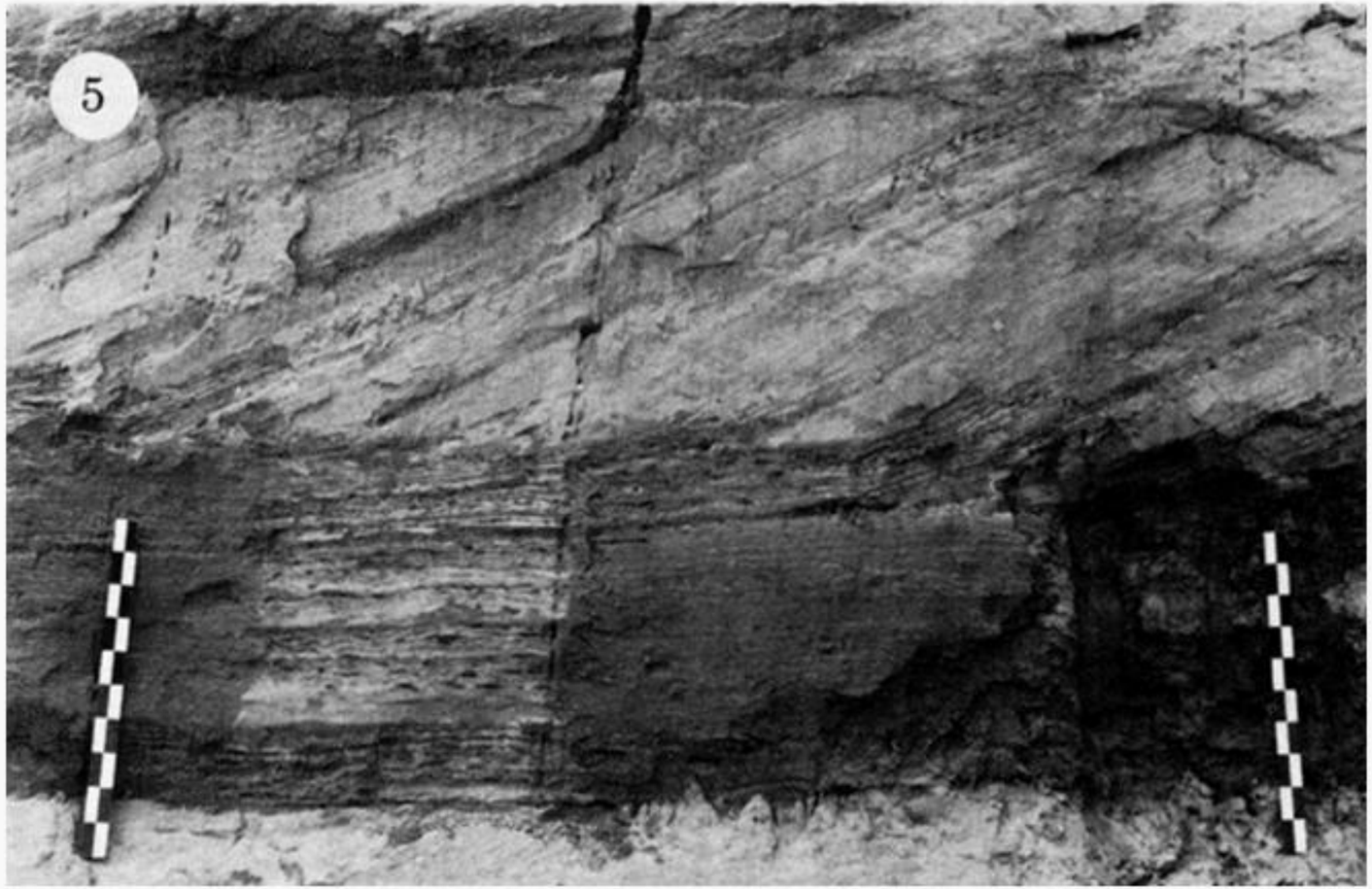

5. Unit D (south), Pendean Sandpit, between approximately 20 and 24 m from the downstream end. The bottom-set zone includes many extensive mud drapes (in clusters) and forms almost one half of the preserved thickness of the unit. Scales are marked in decimetres.

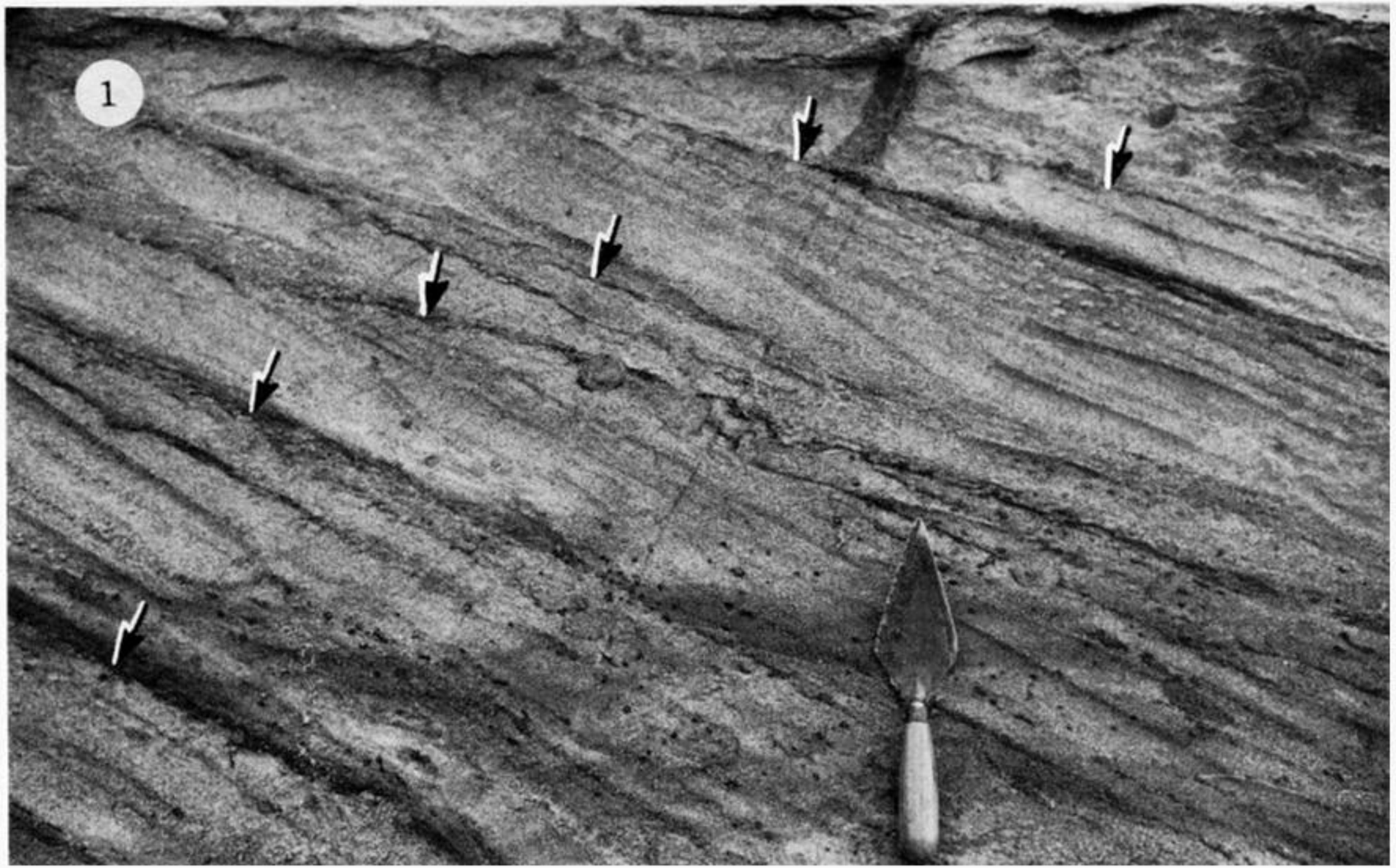

1. A sequence of six convex-up reactivation surfaces (shown by arrows) near the top of the unit, emphasized by concentrations of limonite grains. Several concentrations are bioturbated, and note the dispersed mottles just below the second reactivation surface from the top.

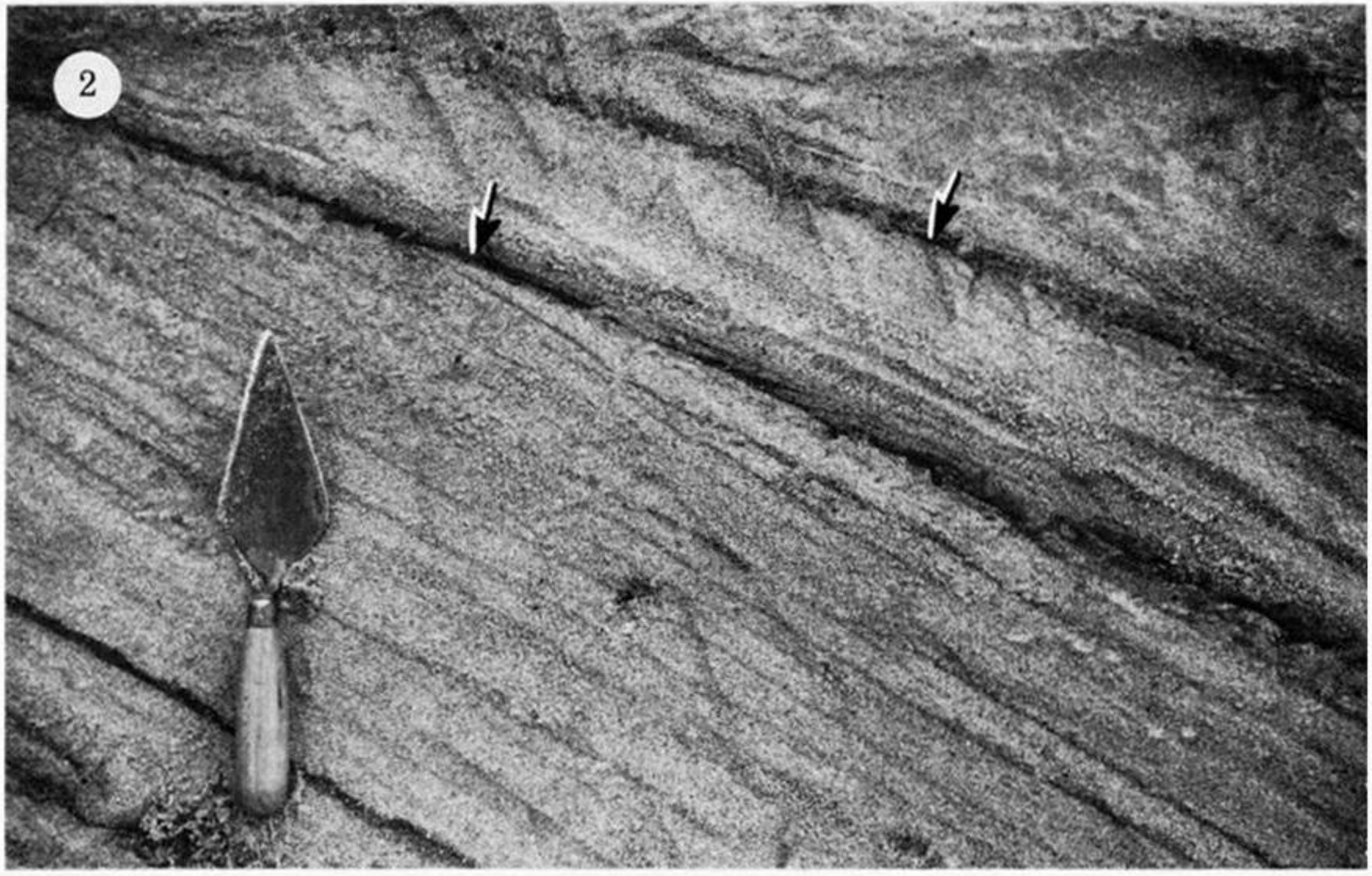

2. Two reactivation surfaces (shown by arrows) marked by limonite-rich sand, the lower being capped by up-slope-facing cross-lamination (about 0.3 m to the right of the trowel point). Note dispersed mottles below this surface.

3. Limonite-rich foresets with mainly large mottles in several cases including menisci, perhaps due to echinoderms.

4. Small mottles in a foreset (behind trowel) rich in limonite grains. Reactivation surface is shown by arrow.

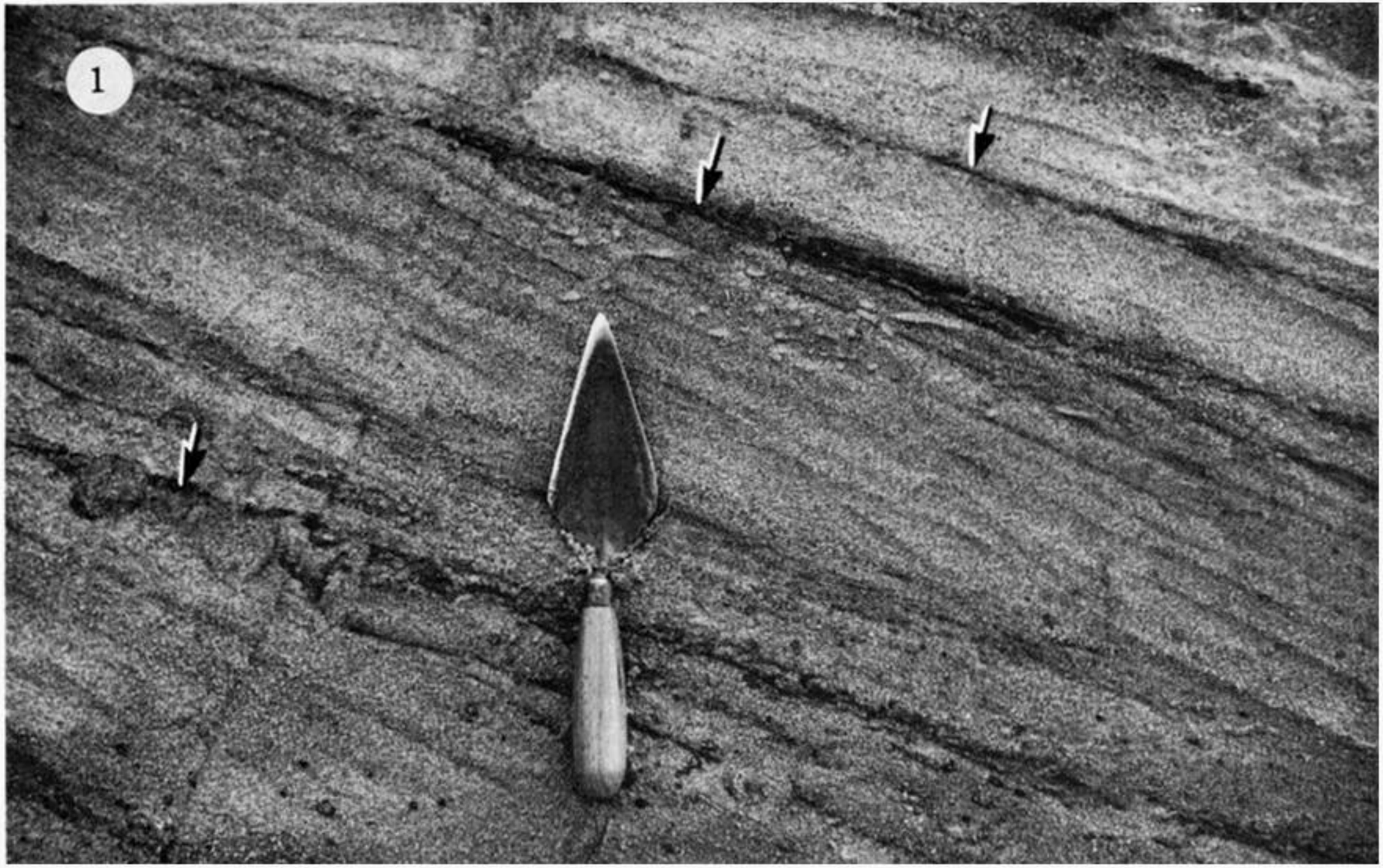

1. Dispersed small mottles within and below a reactivation surface (the middle of the three shown by arrows), unit B, Hog's Back Sandpit. Trowel is 0.28 m long.

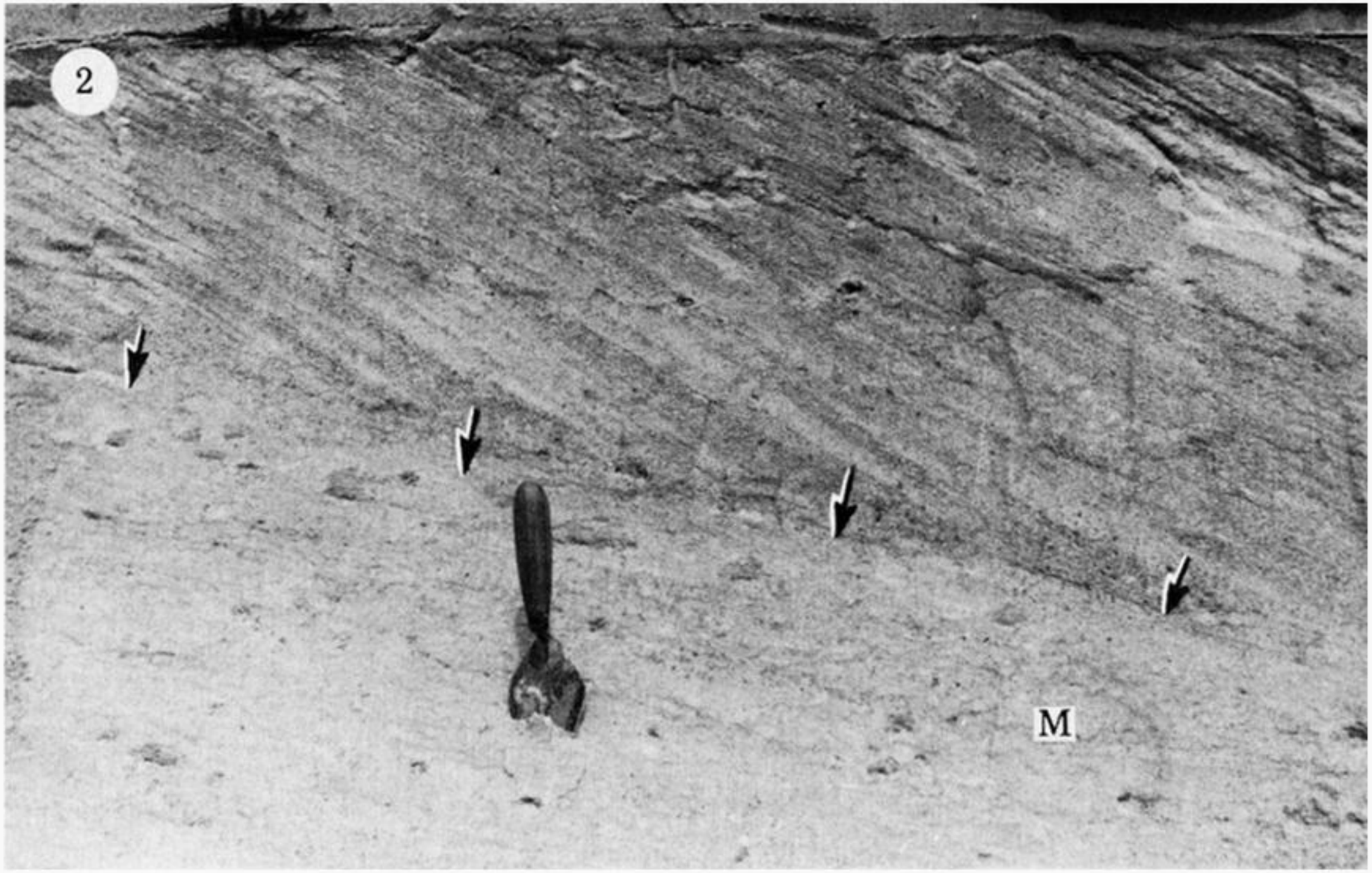

2. Reactivation surface (marked by arrows) within episode 46, West Heath Common Sandpit. The sand below the surface is fine grained and intensely mottled, particularly at M, retaining traces of cross-lamination. Above the surface are foresets of medium to coarse sand. Trowel is 0.28 m long.

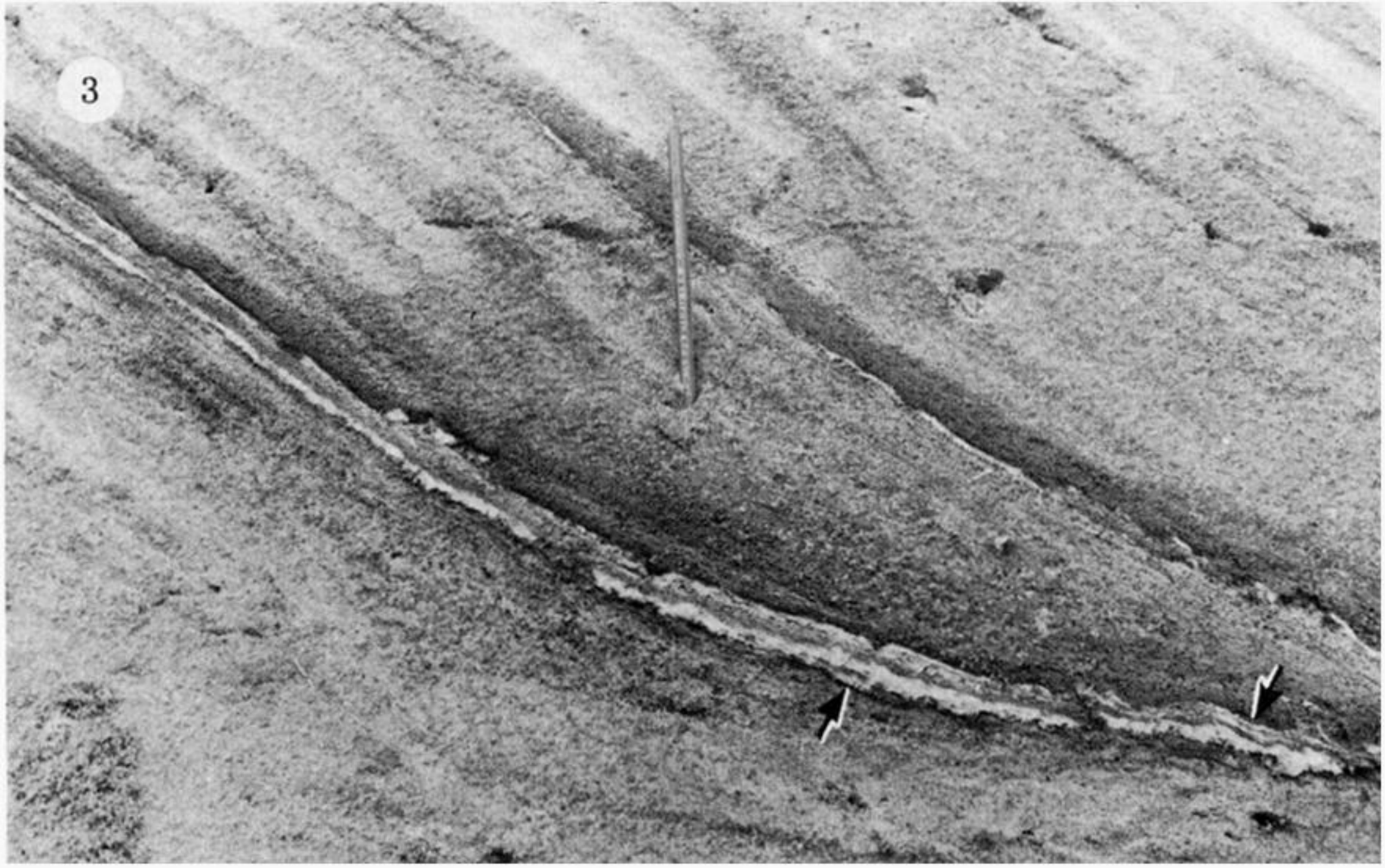

3. Three mud drapes (partings visible in photograph indicated by arrows), each capped by a dark zone of iron-stained sand, episodes 6–15 in unit A, West Heath Common Sandpit. Pencil is 0.16 m long.

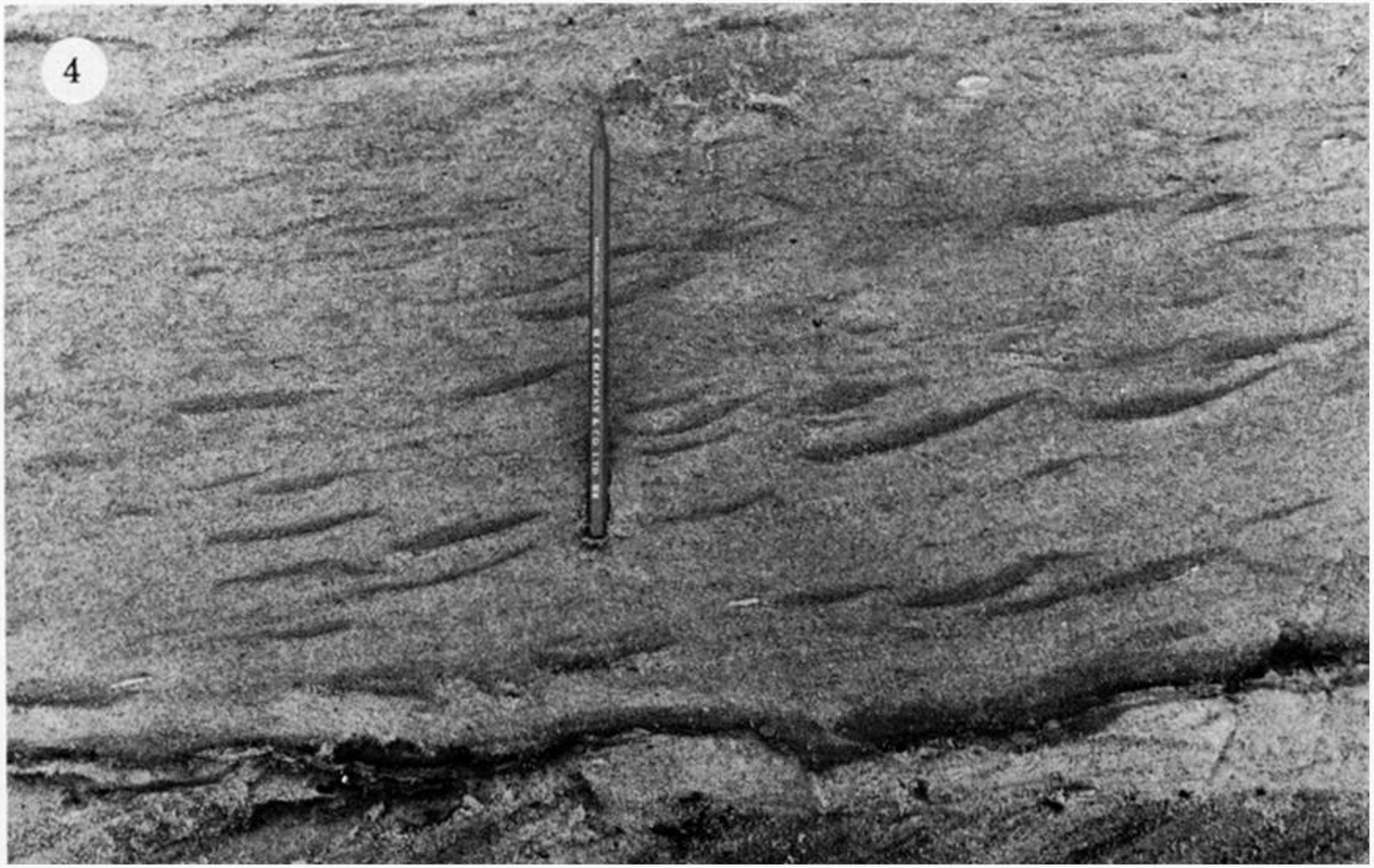

4. Thin mud films capped by dark, iron-stained sand in rippled and cross-laminated bottomsets, episode 34, unit B, West Heath Common Sandpit. Pencil is 0.16 long.

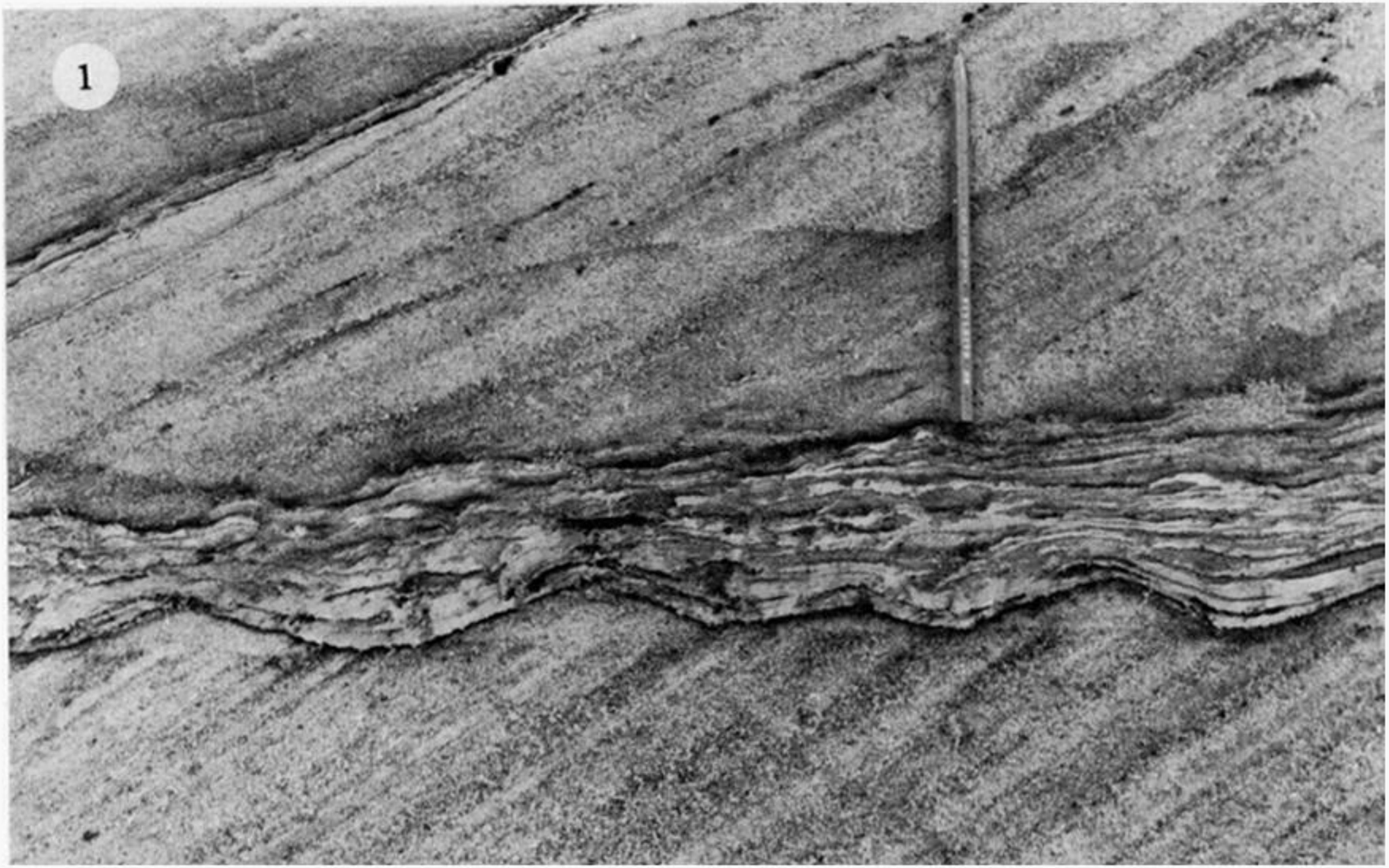

1. Countercurrent ripples preserved by a mud drape and drape-rich bottomsets, approximately episodes 95–100, unit B, West Heath Common Sandpit. Pencil is 0.16 m long.

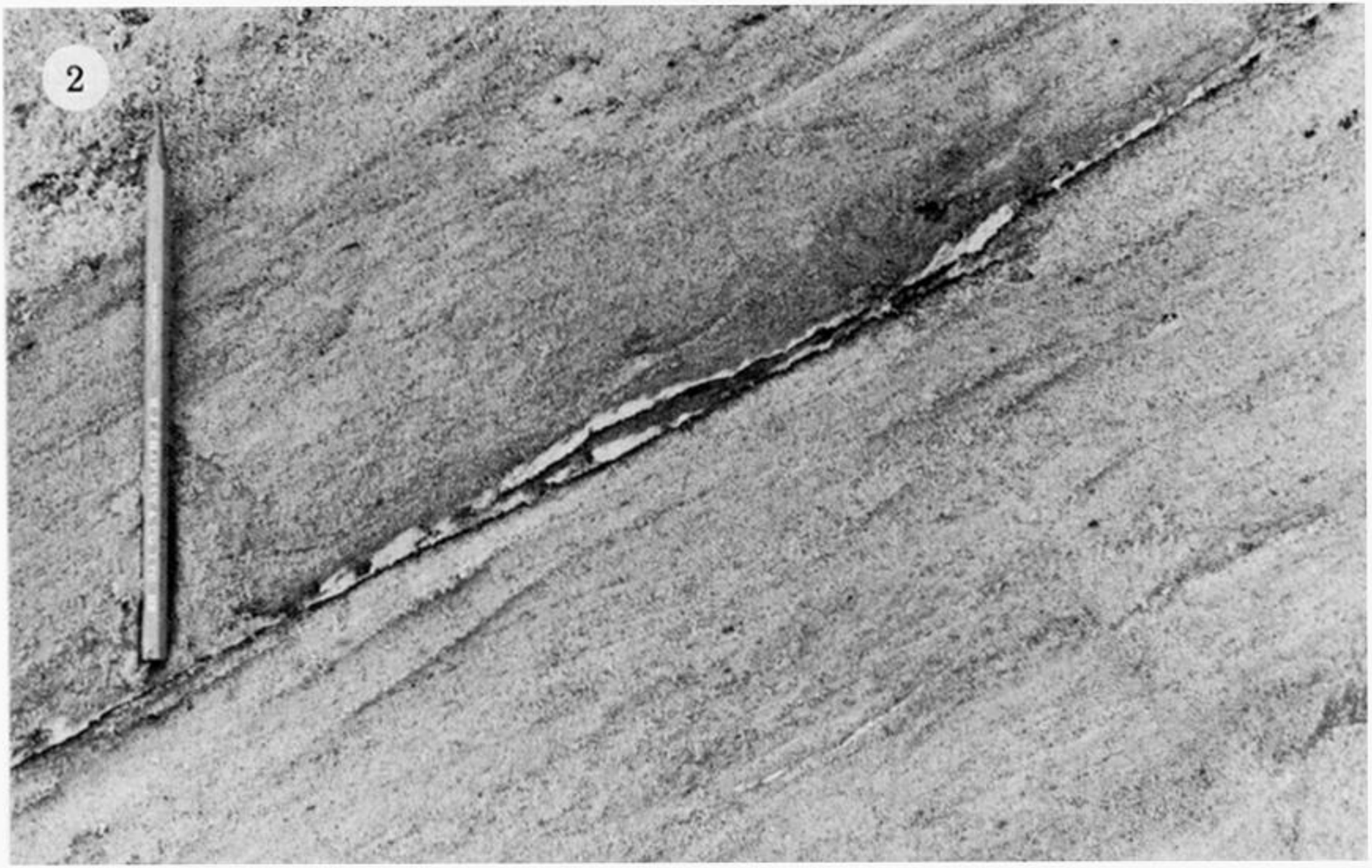

2. Ripple-like sand lens in parting within mud drape, episode 31, unit B, West Heath Common Sandpit. Pencil is 0.16 m long.

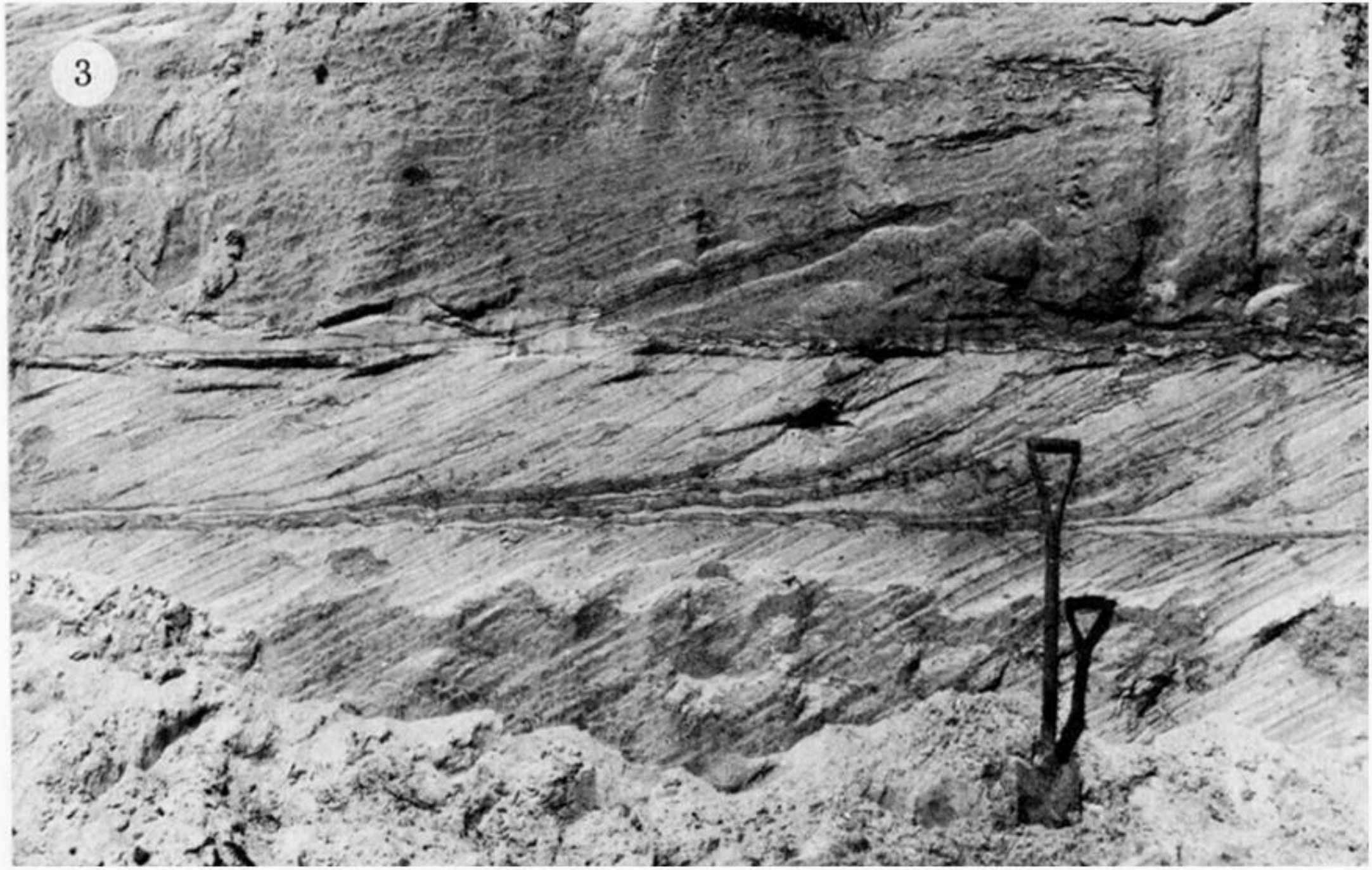

3. Clusters of drapes in unit C, West Heath Common Sandpit. Spade is 0.92 m long.

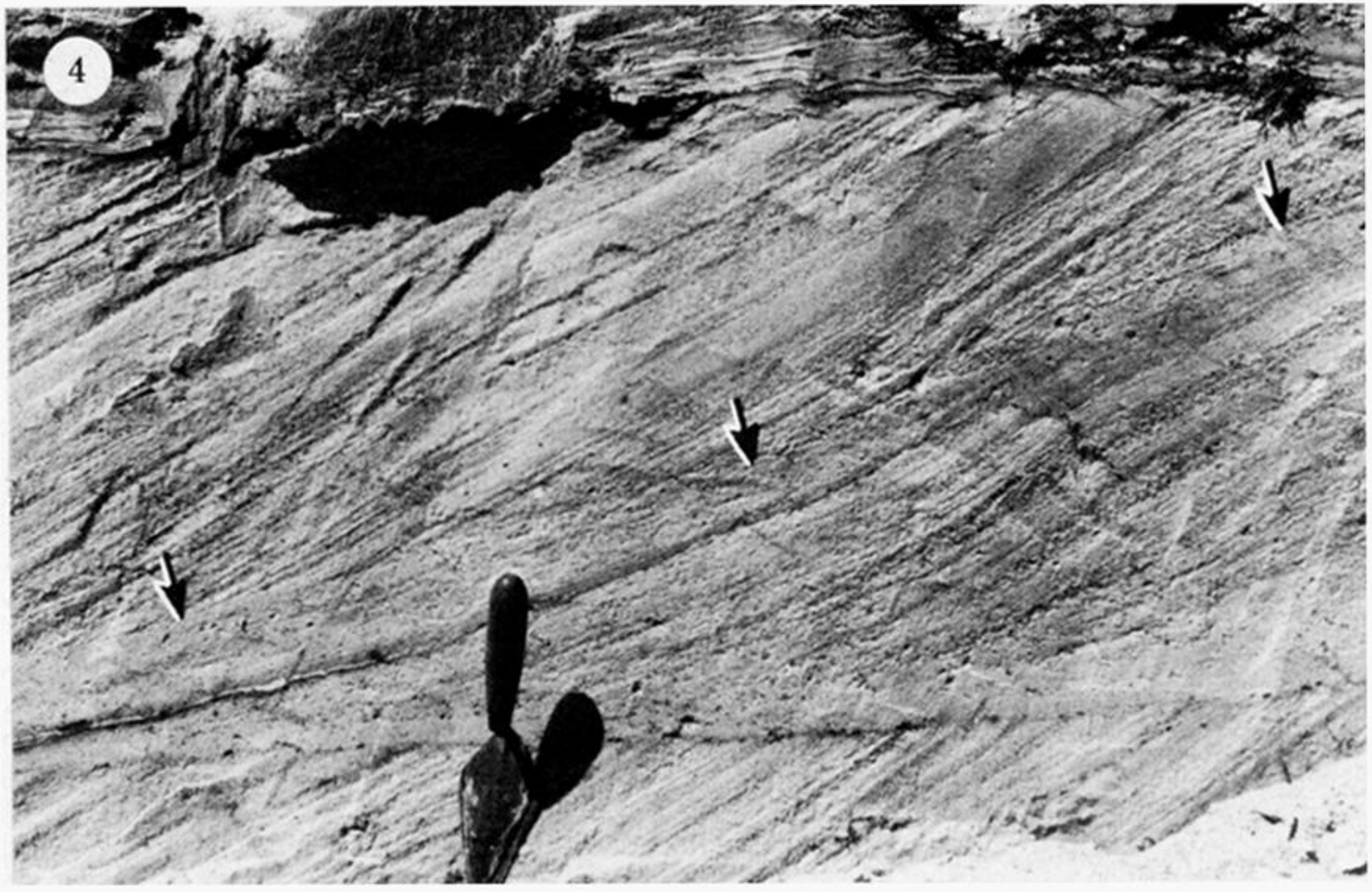

4. Weakly convex-up reactivation structure (marked by arrows), top of episode 28, unit C, West Heath Common Sandpit. The foresets overlying the structure are coarser grained than the sand below. Trowel is 0.28 m long.

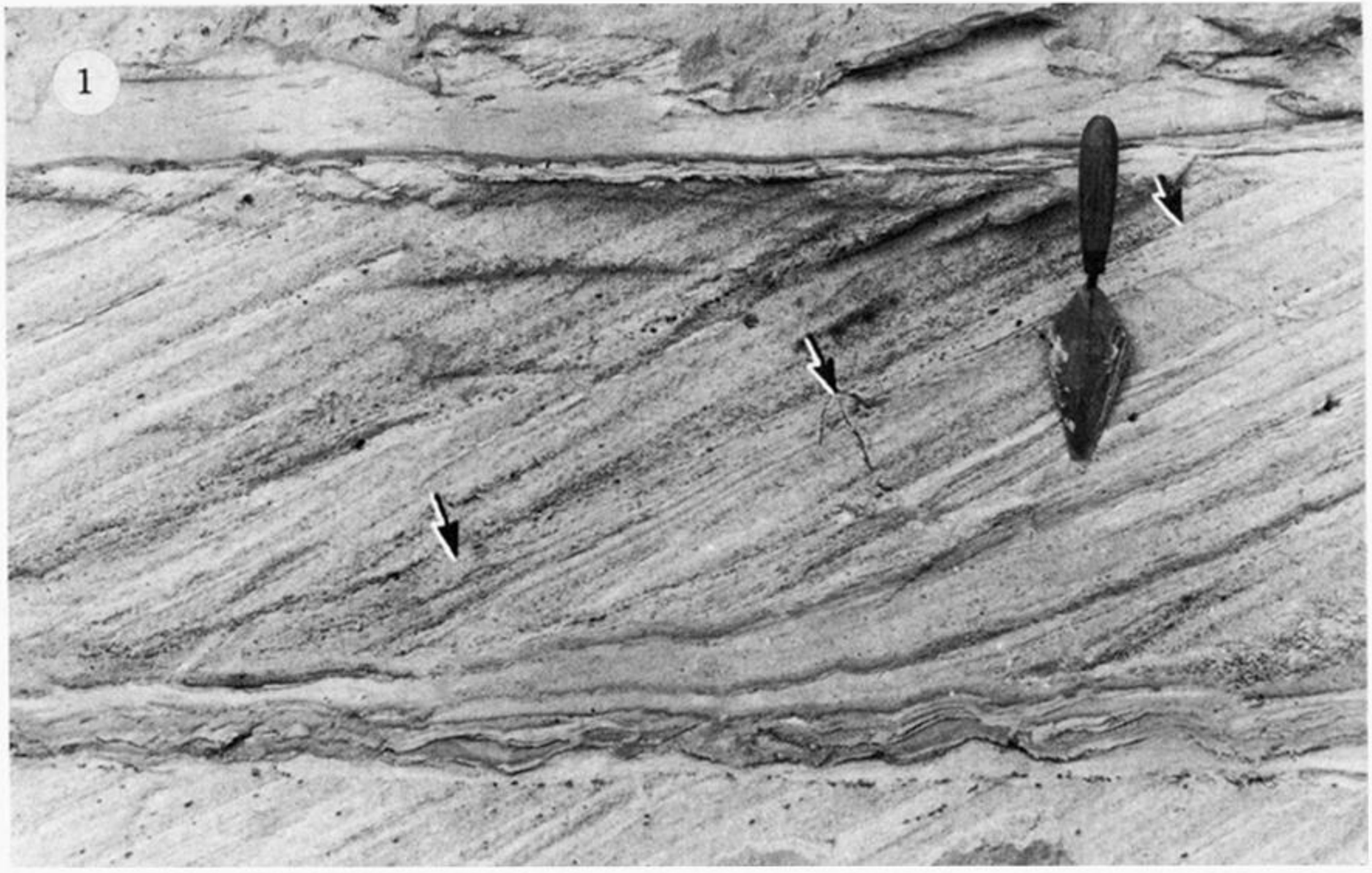

1. Reactivation structure (marked by arrows) within episode 70, unit C, West Heath Common Sandpit. There is little sign of erosion but a marked coarsening of grain size occurs upward across the structure. Trowel is 0.28m long.

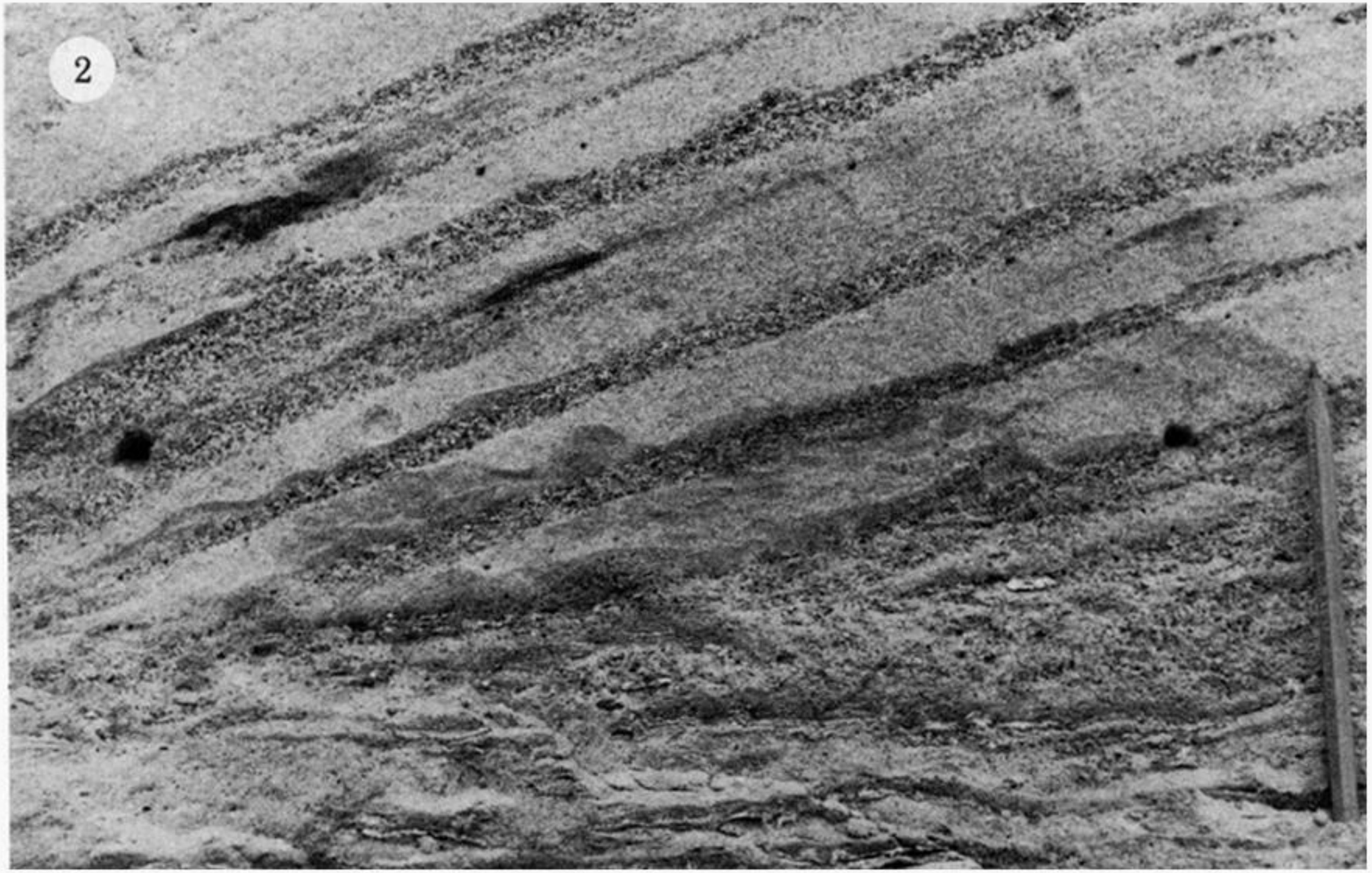

2. Reversely graded foresets several centimetres thick, unit A, Pendean Sandpit. Pencil is 0.15 m long.

3. Mud drapes in unit B, Pendean Sandpit. The lowest drape (episode 47) has up to six silty or sandy partings, and more than one parting is visible in some of the other drapes shown. Trowel is 0.28 m long.

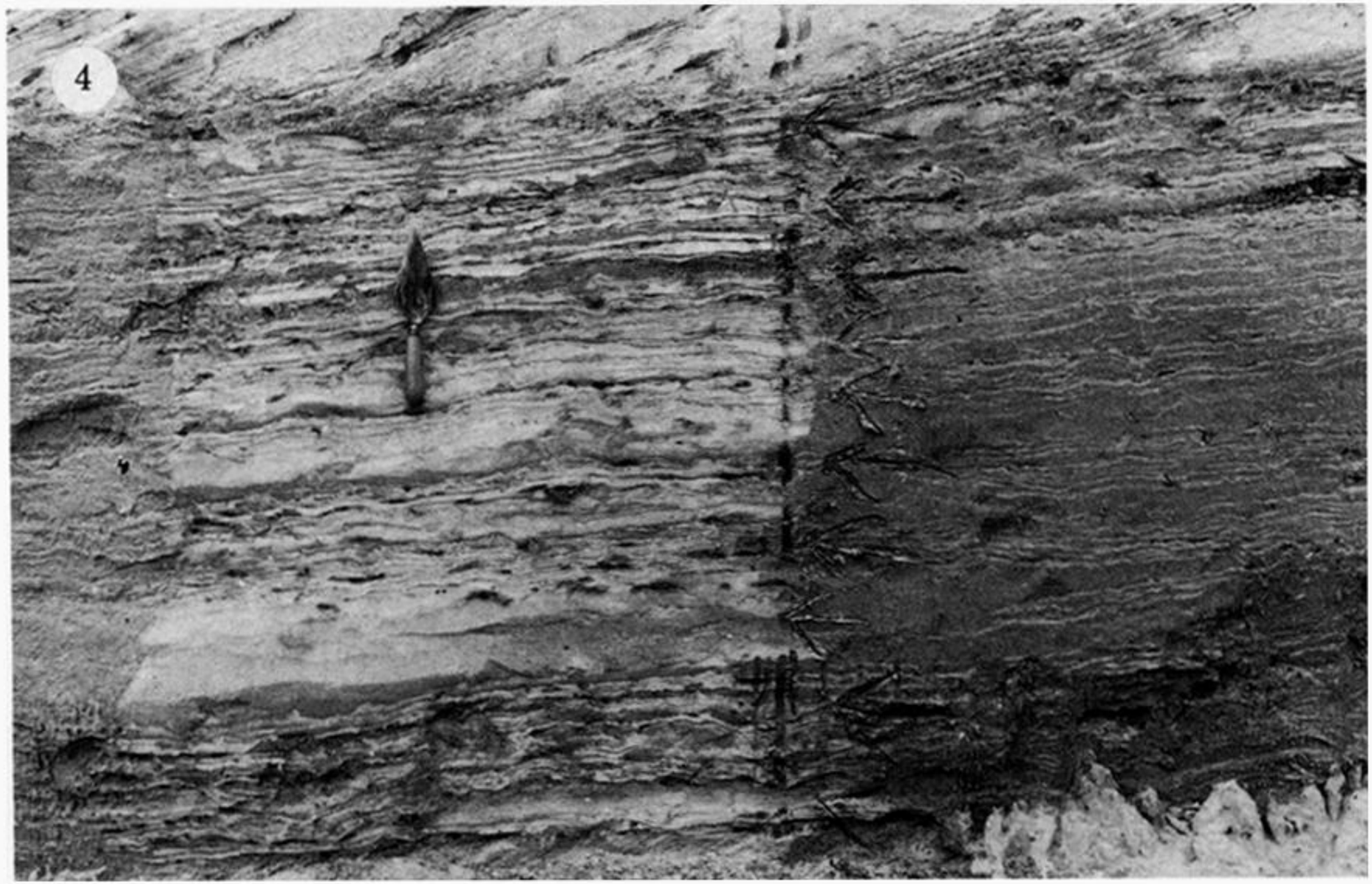

4. Bottomset zone in unit D (South), Pendean Sandpit, approximately 22 m from the downstream end. Mud drapes occur throughout the zone, in at least twelve recognizable clusters (most shown by arrows), seen on cleaned (left) and naturally weathered (right) vertical faces. Trowel is 0.28 m long.

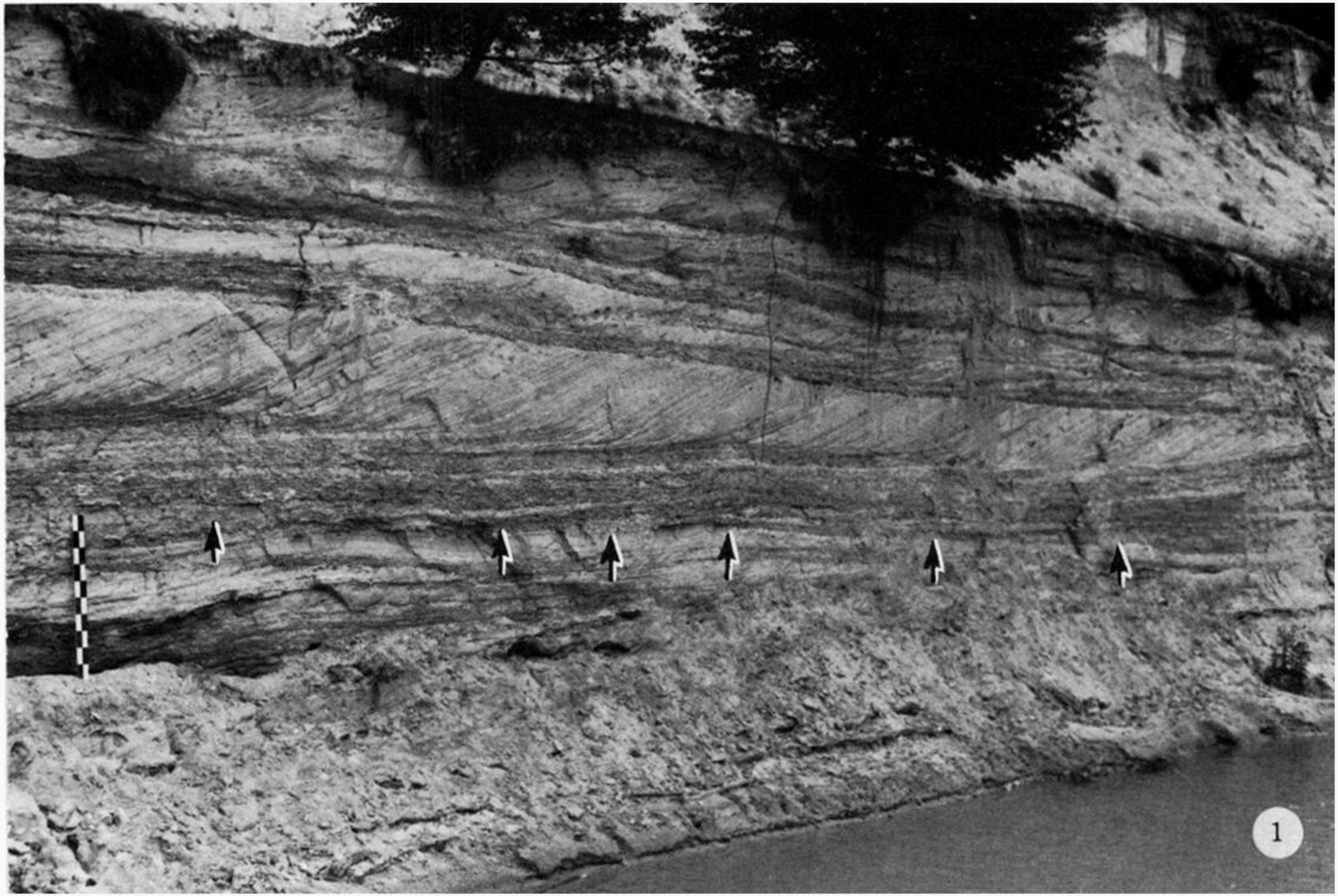

1. Conspicuous clusters of dark-coloured mud drapes (above arrows) in unit A, Pendean Sandpit, as seen in an oblique view. Scale is marked in decimetres.

2. Clusters of pale-coloured drapes (above arrows) in unit D (north), Pendean Sandpit, as seen in an oblique view. Scale is marked in decimetres.

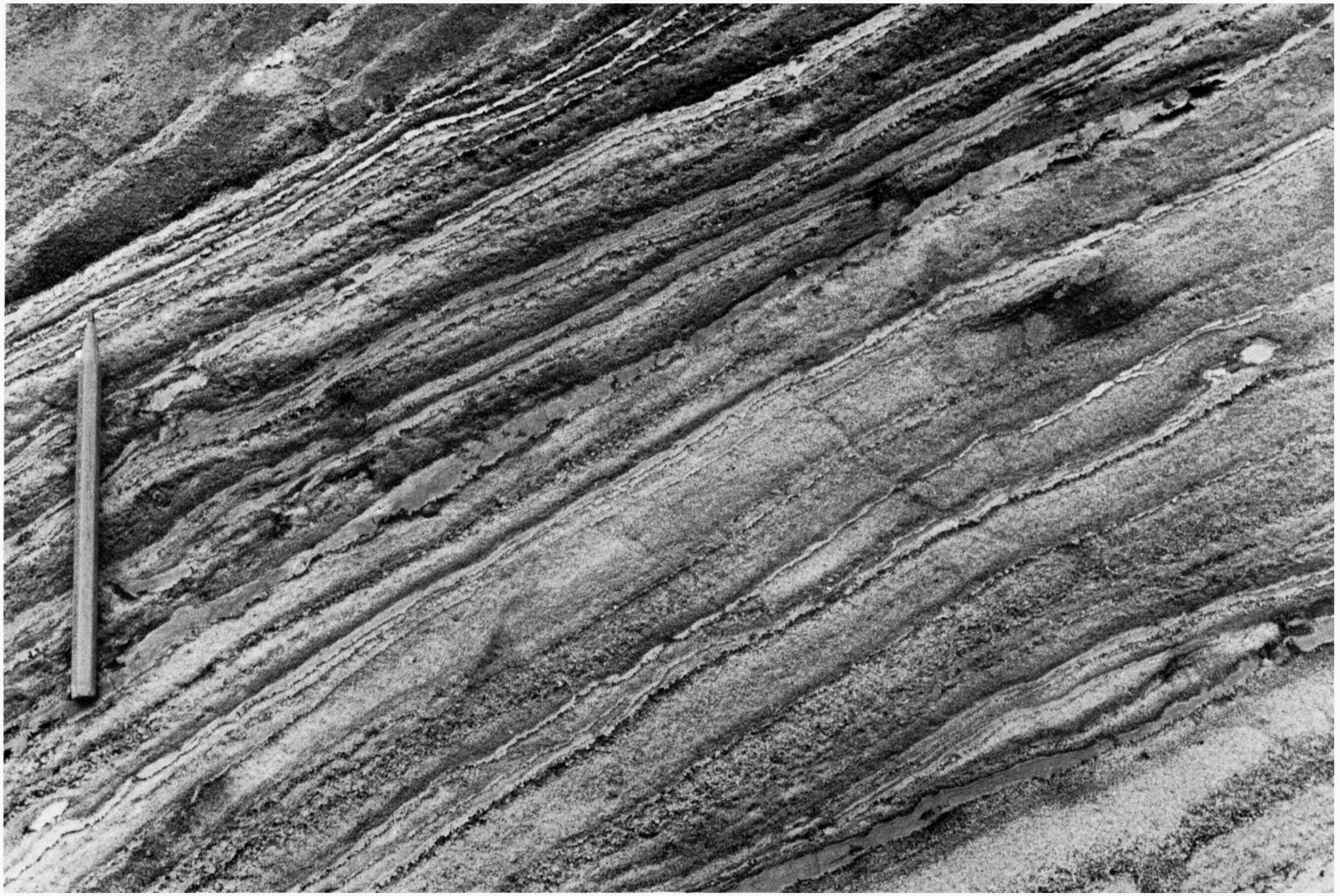

Sand–silt partings, often lenticular, are visible in the photograph within many of the drapes. Others have partings too thin to be photographed. Pencil, 0.15m long, for scale rests on episode 57 and points upward.